

THESIS

RESISTANCE COMPONENTS AND VELOCITY DISTRIBUTIONS
OF OPEN CHANNEL FLOWS OVER BEDFORMS

Submitted by

Henry Michael Fehlman

Department of Civil Engineering

In partial fulfillment of the requirements

for the Degree of Master of Science

Colorado State University

Fort Collins, Colorado

Summer 1985

TC
175
-F45
1985


COLORADO STATE UNIVERSITY

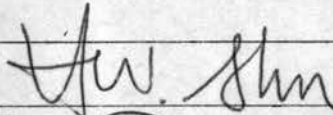
April 17 19 85

WE HEREBY RECOMMEND THAT THE THESIS PREPARED UNDER OUR SUPERVISION
BY Henry Michael Fehlman
ENTITLED RESISTANCE COMPONENTS AND VELOCITY DISTRIBUTIONS
OF OPEN CHANNEL FLOWS OVER BEDFORMS
BE ACCEPTED AS FULFILLING IN PART REQUIREMENTS FOR THE DEGREE OF
Master of Science

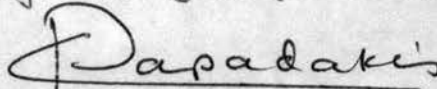
Committee on Graduate Work







Adviser



Department Head

COLORADO STATE UNIVERSITY

ABSTRACT OF THESIS

RESISTANCE COMPONENTS AND VELOCITY DISTRIBUTIONS OF OPEN CHANNEL FLOWS OVER BEDFORMS

The components of flow resistance and the velocity distributions of open-channel flows over bedforms were investigated by conducting idealized bedform experiments in a laboratory flume. Experiments involving uniform smooth, uniform rough, and nonuniform smooth bedform elements were performed. Local shear stress and pressure on the bedform surface was measured in order to determine the characteristics of skin and form resistance. Total flow resistance was measured directly and compared to the sum of the resistance components. Using the results of this study and published data, relations were developed to enable the prediction of each resistance component. Boundary layer velocity profiles were measured over the bedform surface in the region of reattached flow. An average velocity distribution was developed based on free stream velocity measurements made over the length of the modeled bedform. This average velocity distribution is in good agreement with the published data from alluvial bedform experiments.

Henry Michael Fehlman
Civil Engineering Department
Colorado State University
Fort Collins, Colorado 80523
Summer 1985

ACKNOWLEDGMENTS

The author wishes to express grateful appreciation to his major adviser, Dr. H. W. Shen, for his support and guidance throughout the development of this thesis. Deep gratitude is also extended to graduate committee members Dr. S. R. Abt and Dr. M. D. Harvey for their review of this thesis.

Special thanks are due to Cesar Mendoza for his valuable insight and suggestions. Grateful acknowledgment is expressed to the staff of the Hydraulics Laboratory and Technical Typing in the Engineering Research Center of Colorado State University.

Finally, the author wishes to express sincere thanks to his family and friends for their constant encouragement and understanding during investigation and preparation of this thesis.

This study was made possible by Grant No. ENG-7825054 from the National Science Foundation.

TABLE OF CONTENTS

<u>Chapter</u>		<u>Page</u>
1	INTRODUCTION	1
	1.1 General	1
	1.2 Objectives	2
2	LITERATURE REVIEW	4
	2.1 Introduction	4
	2.2 Flow Resistance in Open Channels	5
	2.3 Velocity Profiles in Open Channels	8
3	EXPERIMENTAL SET-UP AND PROCEDURE	10
	3.1 Introduction	10
	3.2 Flume and Accessories	10
	3.3 Bedform Model	11
	3.4 Experimental Procedures	16
4	CHARACTERISTICS OF OPEN CHANNEL FLOW OVER BEDFORMS	24
	4.1 Introduction	24
	4.2 Total Longitudinal Force	27
	4.3 Water Surface and Pressure Distribution Over Bedform	31
	4.4 Pressure Drag	56
	4.5 Skin Shear	71
	4.5.1 Uniform, Smooth Bedform Experiment	72
	4.5.2 Nonuniform, Smooth Bedform Experiment	87
	4.5.3 Uniform, Rough Bedform Experiment	99
	4.6 Velocity Distributions	123
	4.6.1 Boundary Layer Velocity Distribution Over Smooth Bedform	123
	4.6.2 Boundary Layer Velocity Distribution Over Rough Bedform	127
	4.6.3 Average Velocity Distribution Over Bedform	136
5	CONCLUSIONS	161
6	RECOMMENDATIONS FOR FUTURE STUDY	166
7	REFERENCES	167

LIST OF TABLES

<u>Table</u>	<u>Page</u>
3.1	Summary of Measurement Procedures 21
4.1	Summary of Flow Conditions 25
4.2	Total Resistance Parameters for Uniform Bedform Experimental Runs 28
4.3	Summary of Water Surface Profiles for the Uniform, Smooth Bedform Experiment 32
4.4	Summary of Water Surface Profiles for the Uniform, Rough Bedform Experiment 34
4.5	Summary of Water Surface Profiles for the Nonuniform, Smooth Bedform Experiment 35
4.6	Summary of Piezometric Head Distributions on Bedform Surface for the Uniform, Smooth Bedform Experiment . . . 38
4.7	Summary of Piezometric Head Distributions on Bedform Surface for the Uniform, Rough Bedform Experiment . . . 40
4.8	Summary of Piezometric Head Distributions on Bedform Surface for the Nonuniform, Smooth Bedform Experiment 41
4.9	Form Resistance Parameters for the Present Study 64
4.10	Summary of Shear Stress Distributions for Uniform, Smooth Bedform Experiment 73
4.11	Skin Resistance Parameters for the Uniform, Smooth Bedform Experiment 83
4.12	Summary of Shear Stress Distributions for Nonuniform, Smooth Bedform Experiment 88
4.13	Skin Resistance Parameters for Smooth Bedform Studies 98
4.14	Summary of Shear Probe Differential Head Measurements for the Uniform, Rough Bedform Experiment 100

<u>Table</u>	<u>Page</u>
4.15	Skin Resistance Parameters for Uniform, Rough Bedform Experiment 102
4.16	Boundary Layer Velocity Measurements for Uniform, Smooth Bedform Experiment: $x = 1.465$ and 1.240 ft . . . 124
4.17	Boundary Layer Velocity Measurements for Uniform, Smooth Bedform Experiment: $x = 1.690$ ft 125
4.18	Boundary Layer Velocity Measurements for Uniform, Smooth Bedform Experiment: $x = 2.190$ ft 126
4.19	Boundary Layer Velocity Measurements for Uniform, Rough Bedform Experiment: $x = 1.682$ ft 131
4.20	Boundary Layer Velocity Measurements for Uniform, Rough Bedform Experiment: $x = 2.182$ ft 132
4.21	Free Stream Velocity Measurements for Uniform, Smooth Bedform Experiment: $x = 0.00$ ft 137
4.22	Free Stream Velocity Measurements for Uniform, Smooth Bedform Experiment: $x = 0.446$ ft 138
4.23	Free Stream Velocity Measurements for Uniform, Smooth Bedform Experiment: $x = 0.890$ ft 139
4.24	Free Stream Velocity Measurements for Uniform, Smooth Bedform Experiment: $x = 1.465$ and 1.240 ft . . . 140
4.25	Free Stream Velocity Measurements for Uniform, Smooth Bedform Experiment: $x = 1.690$ ft 141
4.26	Free Stream Velocity Measurements for Uniform, Smooth Bedform Experiment: $x = 2.190$ ft 142
4.27	Free Stream Velocity Measurements for Uniform, Smooth Bedform Experiment: $x = 2.612$ ft 143
4.28	Free Stream Velocity Measurements for Uniform, Rough Bedform Experiment: $x = 1.182$ ft 146
4.29	Free Stream Velocity Measurements for Uniform, Rough Bedform Experiment: $x = 1.682$ ft 147
4.30	Free Stream Velocity Measurements for Uniform, Rough Bedform Experiment: $x = 2.182$ ft 148

LIST OF FIGURES

<u>Figure</u>		<u>Page</u>
3.1	Bedform Model	12
3.2	Test Bedform	14
3.3	Locations of Bedform Surface Pressure Taps	15
3.4	First Plastic Bedform Geometries Used in Nonuniform, Smooth Bedform Experiment	17
3.5	Size Distribution of Sand Used in Uniform, Rough Bedform Experiment	18
4.1	Comparison of the Measured Total Friction Factor with the Friction Factor Computed Using Vanoni and Brooks' (1957) Procedure	30
4.2	Relative Piezometric Head Distribution and Relative Water Surface Profile for Uniform, Smooth Bedform Experiment: Depth at Crest = 6 in	43
4.3	Relative Piezometric Head Distribution and Relative Water Surface Profile for Uniform, Smooth Bedform Experiment: Depth at Crest = 8 in	44
4.4	Relative Piezometric Head Distribution and Relative Water Surface Profile for Uniform, Smooth Bedform Experiment: Depth at Crest = 10 in	45
4.5	Relative Piezometric Head Distribution and Relative Water Surface Profile for Uniform, Rough Bedform Experiment: Depth at Crest = 6 in	46
4.6	Relative Piezometric Head Distribution and Relative Water Surface Profile for Uniform, Rough Bedform Experiment: Depth at Crest = 8 in	47
4.7	Relative Piezometric Head Distribution and Relative Water Surface Profile for Uniform, Rough Bedform Experiment: Depth at Crest = 10 in	48
4.8	Relative Piezometric Head Distribution and Relative Water Surface Profile for Nonuniform, Smooth Bedform Experiment: Runs 1S 1B, 7S, 7B	49

<u>Figure</u>		<u>Page</u>
4.9	Relative Piezometric Head Distribution and Relative Water Surface Profile for Nonuniform, Smooth Bedform Experiment: Runs 2S, 2B, 8S, 8B	50
4.10	Relative Piezometric Head Distribution and Relative Water Surface Profile for Nonuniform, Smooth Bedform Experiment: Runs 3S, 3B, 9S, 9B	51
4.11	Nondimensional Pressure Distribution for Uniform, Smooth Bedform Experiment: Depth at Crest = 6 in . . .	53
4.12	Nondimensional Pressure Distribution for Uniform, Smooth Bedform Experiment: Depth at Crest = 8 in . . .	54
4.13	Nondimensional Pressure Distribution for Uniform, Smooth Bedform Experiment: Depth at Crest = 10 in . . .	55
4.14	Definition Sketch Showing the Variables Used in the Calculation of Pressure Drag	57
4.15	Variation of Pressure Drag Coefficient with Relative Roughness	68
4.16	Variation of Average Pressure Drag Coefficient with Relative Roughness	70
4.17	Variation of Local Skin Shear Coefficient with Reynolds Number and Position for Uniform, Smooth Bedform Experiment	76
4.18	Variation of B with Position along the Bedform Surface for Uniform, Smooth Bedform Experiment	78
4.19	Shear Stress Distribution for Uniform, Smooth Bedform Experiment: Depth at Crest = 6 in	80
4.20	Shear Stress Distribution for Uniform, Smooth Bedform Experiment: Depth at Crest = 8 in	81
4.21	Shear Stress Distribution for Uniform, Smooth Bedform Experiment: Depth at Crest = 10 in	82
4.22	Comparison of Measured Bed Skin Friction Factor with Equation 4.60 for Uniform, Smooth Bedform Experiment . .	85
4.23	Comparison of Measured Total Force with the Sum of the Measured Skin Shear and Measured Form Drag for Uniform, Smooth Bedform Experiment	86
4.24	Variation of Skin Shear Coefficient with Reynolds Number and Position for Nonuniform, Smooth Bedform Experiment: Small Bedform Upstream	90

<u>Figure</u>		<u>Page</u>
4.25	Variation of Skin Shear Coefficient with Reynolds Number and Position for Nonuniform, Smooth Bedform Experiment: Large Bedform Upstream	91
4.26	Variation of B with Position Along the Bedform Surface for Uniform and Nonuniform, Smooth Bedform Experiments	92
4.27	Shear Stress Distribution for Nonuniform, Smooth Bedform Experiment: Runs 1S, 1B, 7S, 7B	95
4.28	Shear Stress Distribution for Nonuniform, Smooth Bedform Experiment: Runs 2S, 2B, 8S, 8B	96
4.29	Shear Stress Distribution for Nonuniform, Smooth Bedform Experiment: Runs 3S, 3B, 9S, 9B	97
4.30	Shear Stress Distribution for Uniform, Rough Bedform Experiment: Depth at Crest = 6 in	103
4.31	Shear Stress Distribution for Uniform, Rough Bedform Experiment: Depth at Crest = 8 in	104
4.32	Shear Stress Distribution for Uniform, Rough Bedform Experiment: Depth at Crest = 10 in	105
4.33	Variation of Local Skin Shear Coefficient with D_x/d_{50} Log R_e and Position for Uniform, Rough Bedform Experiment	107
4.34	Variation of B_R with Position along the Bedform Surface for Uniform, Rough Bedform Experiment	109
4.35	Variation of Bed Skin Friction Factor with R_b/d_{50} Log R_e for Uniform, Rough Bedform Experiment	111
4.36	Relation between $\frac{1}{\sqrt{f'}}$ and $R_b/d_{50} [A/L]^2$ Log R_e for Rough Modeled Bedform Data	113
4.37	Relation between $[\frac{1}{\sqrt{f'}} + 18.5A]$ and $R_b/d_{50} [A/L]^2$ Log R_e for Rough Modeled Bedform Data	114
4.38	Comparison of Equations 4.72 and 4.73 Using Reported Alluvial Data	116
4.39	Average Deviation of Predicted f' from f'_e for Different Ranges of Bedform Heights Using Reported Alluvial Data	118

<u>Figure</u>		<u>Page</u>
4.40	Variation of Bed Skin Friction Factor with d_{50}/A and Bedform Steepness Using Equation 4.72	120
4.41	Effect of R_b/d_{50} on Bed Skin Friction Factor Using Equation 4.72	121
4.42	Effect of Bedform Height on Bed Skin Friction Factor Computed Using Equation 4.72	122
4.43	Variation of yu_*'/v with u/u_*' for Uniform, Smooth Bedform Experiment: $x = 1.240$ and 1.465 ft	128
4.44	Variation of yu_*'/v with u/u_*' for Uniform, Smooth Bedform Experiment: $x = 1.690$ ft	129
4.45	Variation of yu_*'/v with u/u_*' for Uniform, Smooth Bedform Experiment: $x = 2.190$ ft	130
4.46	Nondimensional Boundary Layer Velocity Profiles for Uniform, Rough Bedform Experiment	133
4.47	Average Nondimensional Boundary Layer Velocity Profile for Uniform, Rough Bedform Experiment	135
4.48	Nondimensional Velocity Profiles for Uniform, Smooth Bedform Experiment	144
4.49	Nondimensional Velocity Profiles for Uniform, Rough Bedform Experiment	149
4.50	Comparison of Equation 4.80 with Data from Jonys (1973)	150
4.51	Comparison of Equation 4.80 with Data from Haque (1970)	151
4.52	Nondimensional Velocity Profiles for Uniform, Smooth Bedform Experiment: $x = 0.000$ ft	153
4.53	Nondimensional Velocity Profiles for Uniform, Smooth Bedform Experiment: $x = 0.446$ ft	154
4.54	Nondimensional Velocity Profiles for Uniform, Smooth Bedform Experiment: $x = 0.890$ ft	155
4.55	Nondimensional Velocity Profiles for Uniform, Smooth Bedform Experiment: $x = 1.240$ ft	156

UNIVERSITY OF CALIFORNIA

<u>Figure</u>		<u>Page</u>
4.56	Nondimensional Velocity Profiles for Uniform, Smooth Bedform Experiment: $x = 1.465$ ft	157
4.57	Nondimensional Velocity Profiles for Uniform, Smooth Bedform Experiment: $x = 1.690$ ft	158
4.58	Nondimensional Velocity Profiles for Uniform, Smooth Bedform Experiment: $x = 2.190$ ft	159
4.59	Nondimensional Velocity Profiles for Uniform, Smooth Bedform Experiment: $x = 2.612$ ft	160

LIST OF SYMBOLS

<u>Symbol</u>	<u>Definition</u>	<u>Unit</u>
A	Bedform height	ft
a	Coefficient in Eq. 2.1	
B	Local smooth skin shear variable	
B_R	Local rough skin shear variable	
b	Exponent in Eq. 2.1	
C_1	Coefficient in Eq. 4.64	
C_2	Coefficient in Eq. 4.65	
C_3	Coefficient in Eq. 4.79	
C_D	Pressure drag coefficient	
C_f	Local skin shear coefficient	
c	Exponent in Eq. 2.1	
D	Average flow depth defined as $D_c + A/2$	ft
D_c	Flow depth above bedform crest	ft
D_x	Local flow depth	ft
d_{50}	Median grain size	mm
F	Froude number	
F_b	Total force per unit width acting on bedform	lb/ft
F_p	Form drag force per unit width acting on bedform	lb/ft
F_s	Skin shear force per unit width acting on bedform	lb/ft
f'	Bed skin friction factor	

<u>Symbol</u>	<u>Definition</u>	<u>Unit</u>
f''	Bed form friction factor	
f_b	Total bed friction factor	
f'_x	Local skin friction factor	
g	Acceleration of gravity	ft/s ²
ΔH	Head difference in surface pressure measurement	ft
ΔH_x	Local differential head in skin shear measurement	ft
H_{REF}	Reference head in surface pressure measurement	ft
h_z	Piezometric head without channel slope effect	ft
h'_z	Piezometric head with channel slope effect	ft
Δh_z	Relative piezometric head without channel slope effect	ft
K	von Karman's constant	
k_s	Characteristic roughness size	mm
L	Bedform length	ft.
m	Coefficient in Eq. 4.40	
n	Coefficient in Eq. 4.64	
p	Local surface pressure	lb/ft ²
ΔP_r	Nondimensional relative pressure	
Q	Flume discharge	ft ³ /s
q	Flume specific discharge defined as Q/W	ft ² /s
R	Hydraulic radius	ft
R_b	Hydraulic radius of the bed	ft
R_e	Reynolds number defined as VR_b/ν	
R_n	Reynolds number defined as q/ν	
S_b	Flume slope	
S_e	Energy slope	

<u>Symbol</u>	<u>Definition</u>	<u>Unit</u>
s	Distance along bedform surface from upstream toe	ft
s_c	Value of s at bedform crest	ft
s_t	Value of s at downstream heel of bedform	ft
T	Fluid temperature	$^{\circ}\text{F}$
u	Point velocity	ft/s
U_*	Total shear velocity	ft/s
u_*'	Local shear velocity due to skin shear	ft/s
V	Average velocity defined as $Q/(WD)$	ft/s
V_c	Average velocity at crest defined as $Q/(WD_c)$	ft/s
V_x	Local average velocity defined as $Q/(WD_x)$	ft/s
W	Flume width	ft
x	Coordinate in longitudinal direction	ft
y	Coordinate in direction normal to the main flow direction, with bedform surface as origin	ft
y'	Value of y for $u = 0$	ft
y_b	Coordinate in direction normal to the main flow direction, with bedform base as origin	ft
y_m	Coordinate in direction normal to the main flow direction, with origin at $y_b = A/2$	ft
z	Elevation head from a given horizontal datum	ft
γ	Specific weight of fluid	lb/ft ³
θ	Angle of flume to a horizontal plane	degrees
θ_d	Downstream angle of bedform with respect to x direction	degrees
θ_u	Upstream angle of bedform with respect to x direction	degrees
ν	Kinematic viscosity of fluid	ft ² /s
ρ	Fluid density	slugs/ft ³

<u>Symbol</u>	<u>Definition</u>	<u>Unit</u>
τ_b	Total bed shear stress	lb/ft ²
τ'	Bed shear stress due to skin resistance	lb/ft ²
τ''	Bed shear stress due to form resistance	lb/ft ²
τ'_x	Local skin shear stress	lb/ft ²

Chapter 1
INTRODUCTION

1.1 General

Open channel flow over alluvial bedforms has been the subject of a great deal of study by researchers, particularly over the last thirty years. In order to predict sediment transport and channel capacity, the shape of the velocity profile and resistance factors for given conditions of flow and bedform geometry must be known. Hence, the flow resistance and the velocity profile are two important characteristics of flow in alluvial channels, and are the subjects of interest for the study presented herein.

The resistance to flow of alluvial bedforms is often divided into two parts: the skin resistance and the form resistance. The skin resistance, or skin shear, is caused by the viscous interaction of the flow with the surface material of the bedform. It is a local resistance, and is the main hydraulic force determining the sediment transport rate. The form resistance, or form drag, is caused by the nonuniform distribution of pressure on the bedform surface. For bedforms with large amplitude-to-length ratios, the form drag may constitute the major portion of the flow resistance, and have the greatest effect on channel capacity.

A variety of methods have been presented in the literature for separating the skin and form resistance. In evaluating the skin shear, investigators often assume that it is the same as for the case of open

channel flow over sand grains on a flat bed. An estimate of the skin shear is sometimes obtained using pipe-flow relations such as the Moody diagram. The skin resistance is then subtracted from the total resistance to determine the form drag. Other investigators have developed empirical relations to predict the form drag and skin shear, based on actual measurements of each component. These empirical relations may be valid in some cases, while differing significantly from other published data. Still other investigators reject the idea of separating the total resistance, and have developed curves for determining the total resistance to flow, based on bedform geometry and flow conditions. An experimental justification for the separation of flow resistance into form and skin components as well as a study of the effect of flow parameters and bedform geometry is deemed necessary. The value of theoretically sound, empirical relations which can predict each component of flow resistance and be valid over a wide range of flow situations, is without question.

The velocity profile and how it varies over the length of an alluvial bedform is a topic of continuing research and dispute. A number of procedures for predicting the variation of the velocity profile have been presented in the literature. However, the determination of a representative, or average, velocity profile has yet to be published to the author's knowledge. The practicality of such a representative profile merits further effort in its development.

1.2 Objectives

The objectives of the present study are as follows:

1. Determine the validity of separating total resistance to flow into skin and form resistance for the case of open channel

flow over idealized bedforms by measuring all three quantities in laboratory experiments.

2. Investigate the parameters affecting skin shear and form drag, and develop relations predicting each resistance component.
3. Develop a representative velocity profile for the case of open channel flow over alluvial bedforms.

Chapter 2

LITERATURE REVIEW

2.1 Introduction

It is commonly observed that erodible beds composed of granular material deform under the action of turbulent flows into arrays of wave shapes, or bedforms. The various configurations of bedforms have been classified by the ASCE Task Force on Bedforms in Alluvial Channels (1966). In the lower flow regime, defined as flows with Froude number less than one, flat bed, ripples, or dunes may characterize the channel floor, depending on the flow velocity and the properties of fluid and sediment. Ripples and dunes are out of phase with water waves, and are roughly triangular in shape, with a gentle sloping upstream face, and a steep downstream face. The angle the downstream face makes with the bed is approximately equal to the angle of repose of the bed material. Separation of flow occurs downstream of the crest of each bedform, and as the size of the bedform changes, the flow resistance and velocity profile over the length of the bedform is affected. The flow is resisted by the interaction of the fluid with the bed material making up the bedform, as well as by the bedform itself. These two types of flow resistance are termed skin resistance and form resistance, respectively.

This thesis concentrates on the resistances to flow of alluvial bedforms, and the effect of bedforms on the velocity profile, in lower

regime flow. In this chapter, a review of the literature on these topics is presented.

2.2 Flow Resistance in Open Channels

Early investigators in the hydraulics of open channel flow derived flow resistance formulas by equating the gravitational driving force acting on the flowing water to the resistance force acting on the flow boundary. Chezy proposed a flow-resistance formula in 1769, using flow velocity, hydraulic radius and energy slope as variables. Manning published a resistance formula of similar form, using the same flow variables, in 1891. The form of both relations is as follows:

$$V = a R^b S_e^c \quad (2.1)$$

where V is the average velocity, R is the hydraulic radius, S_e is the energy slope, b and c are dimensionless exponents and a is a coefficient of appropriate dimensions. The coefficient a has been found to change with flow area, boundary roughness, and the choice of constants b and c . These relations were derived for the case of uniform flow in rigid boundary channels. The conditions of uniform flow and rigid boundary are not characteristic to flow in alluvial channels.

The two types of flow resistance characteristic of flow in alluvial channels were identified by Einstein (1950). The total resistance may be separated into skin and form resistance, or skin shear and form drag. The division of the skin and form resistances is of practical importance in the hydraulics of sediment transport because the skin resistance corresponds to the shear acting on the sediment grains, and thus, is the major factor contributing to the bed-load motion of the sediment. According to Einstein (1950), the energy which corresponds

to form drag is transformed into turbulence at the interference between the wake and free stream, or at a considerable distance from the bed sediment, and, therefore, does not significantly contribute to the bed-load motion of sediment.

In order to separate the skin shear and form drag from the total resistance to flow of alluvial bedforms, a number of investigators have assumed that the skin resistance may be estimated from the friction for plane rigid-boundary pipe flow. Einstein and Barbarosa (1952) first proposed this procedure for estimating skin resistance, and based on this assumption, Shen (1962) and Simons and Richardson (1966) have published graphical relations to estimate the form drag for open channel flow over alluvial bedforms. Lovera and Kennedy (1969) developed a graphical method for estimating skin shear by analyzing the flow resistance data from laboratory and field flat bed channels in an active state of sediment transport. Alam and Kennedy (1969) used the results of this study to develop a graphical method for estimating the form resistance of dune bed channels.

Both of the above methods of estimating skin resistance assume that the skin resistance of a channel with bedforms is comparable to that for plane bed flow. When alluvial bedforms exist in lower regime flow, there is separation downstream of the crest, and hence, the surface shear stress is not uniformly distributed over the entire channel bed. A more direct approach in separating flow resistance into skin and form components is by actual measurement of each in laboratory studies. Raudkivi (1963), Vanoni and Hwang (1967), Rifai and Smith (1969), and Wang (1984) have published studies wherein the form and/or skin resistance of immobilized bedform elements was directly measured.

Vittal et al. (1977) measured the skin shear on artificial triangular bedforms, and found the skin resistance of plane bed flows is greater than that of flow over bedforms, and the deviation increases as the amplitude-to-length ratio of the bedform increases. Vittal et al. measured the skin and form resistance of a single element in a series of idealized bedforms, and arrived at relations enabling the prediction of each component. These relations, which work well for the data presented in their study, have not proved reliable in other studies, i.e. Engel and Lau (1980).

Two conclusions that can be drawn as a result of previous studies are that the surface shear stress increases from zero at the flow-reattachment point to a maximum at the crest; and the piezometric head decreases from a maximum near the flow reattachment point to a minimum at or slightly downstream of the crest.

A number of investigators have used numerical models to study the form drag of alluvial bedforms. Kikkawa and Ishikawa (1979), Haque and Mahmood (1983), and Wang (1984) have developed various numerical models, and all report that the computed form friction factor is a function of the bedform height, bedform length, and flow depth only. This agrees well with the results reported by Vanoni and Hwang (1967) and Vittal et al. (1977).

Although certain characteristics of skin shear and form drag may be identified from studies previously conducted, there is a need to analyze and consolidate, as well as verify, the published data in an effort to enable the prediction of each component of flow resistance for open channel flow over alluvial bedforms.

2.3 Velocity Profile in Open Channels

The velocity distribution is an important characteristic of open channel flow in alluvial channels. A knowledge of the velocity profile is necessary for the estimation of suspended load transport. While it is possible to predict the velocity distribution on plane and rigid boundaries fairly well, the same cannot be said for flow over large roughness elements such as alluvial bedforms.

In order to describe the velocity distribution for turbulent flow over rigid boundaries, the logarithmic law is frequently used by engineers. The logarithmic law can be obtained from Prandtl's mixing length theory or from von Karman's similarity law, by applying certain simplifying assumptions [see Schlichting (1980)], and can be stated as

$$\frac{u}{U_*} = \frac{1}{K} \ln \frac{y}{y'} \quad (2.2)$$

where u is the velocity at a distance y from the bed, U_* is the shear velocity, K is the von Karman constant, and y' is some length at which the velocity is zero.

Nikuradse [see Schlichting (1980)] conducted experiments with roughened pipes and found that for $U_* k_s / \nu$ less than 3.5, Eq. 2.2 takes the form

$$\frac{u}{U_*} = \frac{2.3}{K} \log \frac{U_* y}{\nu} + 8.5 \quad (2.3)$$

and for $U_* k_s / \nu$ less than 67

$$\frac{u}{U_*} = \frac{2.3}{K} \log \frac{y}{k_s} + 8.5 \quad (2.4)$$

where ν is the kinematic viscosity of the fluid and k_s is the characteristic roughness size. Keulegan (1938) showed that Eqs. 2.3 and 2.4 are also applicable to open channel flow.

Raudkivi (1963), Garde and Paintal (1964), Rifai and Smith (1971) and Vittal et al. (1977) have measured velocity distributions over natural and artificial bedform elements, and reported significant deviations in the profile described by Eq. 2.4 over the length of the bedform. Much study has gone into the prediction of the variation of the von Karman constant along the length of a bedform, and graphical methods for determining this variation have been published. However, the importance of the variation and practicality in using it are questioned by some authors [see Mahmood and Blinco (1972)].

It should be noted that previous studies have used the total resistance to flow in calculating the shear velocity for use in Eq. 2.4, and from this base have studied the variation of the von Karman constant. According to Einstein (1950), the velocity distribution at any point along the upstream face of a bedform is related to the flow resistance acting on the bed grains at that location. That is, the shear velocity U_* in Eq. 2.4 must be replaced by u_*' , the local shear velocity of the skin roughness, to establish the velocity distribution.

Another topic of question is that of the representative velocity profile. Which velocity profile is representative of the velocity distribution above alluvial bedforms, and what are the relevant parameters for regions upstream and downstream of the reattachment point?

A study is required in order to investigate and develop the following: the velocity profile in areas of reattached flow, using the local shear velocity to normalize the velocity in Eq. 2.4; and the representative velocity profile which characterizes the velocity distribution along the length of an alluvial bedform.

Chapter 3

EXPERIMENTAL SET-UP AND PROCEDURE

3.1 Introduction

In this chapter, the experimental set-up and procedure of the study is described. Three separate experiments using idealized bedforms were conducted: one with uniform, smooth elements; one with uniform, roughened elements; and one with nonuniform, smooth elements. These studies were performed in order to investigate the characteristics of open channel flow over idealized bedforms of fixed geometry and they concentrated on the topics of flow resistance and velocity distribution. All experimentation was conducted in the same flume in the hydraulics laboratory of the Engineering Research Center at Colorado State University.

3.2 Flume and Accessories

Each experiment was conducted in a recirculating flume which was 60 ft long, 2.0 ft wide, and 2.5 ft deep. The flume had clear plastic sidewalls. A constant speed 20-HP centrifugal pump circulated water from the tail sump to the head box through a cast-iron return pipe, 1.0 ft in diameter, located under the flume support structure. The flume was supported by hinges at the midsection and screw jacks at the upstream and downstream ends. The screw jacks were operated by a motor and allowed adjustment of the flume slope. A calibrated digital counter attached to the flume tilting device was used to determine the flume slope.

The discharge was measured using a calibrated orifice connected to a differential manometer. Flow depth was controlled by adjusting a tilt-gate at the flume exit. Flow depth was measured using a point gage mounted on a movable carriage. The carriage moved along rails installed on the tops of the flume sidewalls.

Tap water was used in the experiment, and between runs was stored in the tail sump and additional off-flume storage tanks. During an experimental run, the water level in the tail sump was held constant by continuously adding water and allowing overflow thereby reducing fluctuations in pump discharge.

3.3 Bedform Model

The bedform model consisted of 12 aluminum bedforms and three plastic bedforms. Six aluminum bedforms were positioned upstream and downstream of the plastic bedforms. Of the three plastic bedforms the first was of adjustable size, the second (hereafter called the test bedform) was used for measurement of flow resistances, and the third was used to verify the measurements made on the test bedform. The geometries of all 15 bedforms were the same for the uniform bedform experiments. The geometry of the first plastic bedform was varied for the nonuniform experiment.

As shown in Figure 3.1, the bedforms used in the uniform bedform experiments were triangular in shape and were 0.451 ft high, 3 ft long and 2 ft wide. Each bedform had a downstream face with a 30° incline and an upstream face with a 11.5° incline. Both the upstream and downstream faces were extended vertically at the ends to form a rectangular base, 0.667 ft high and 2 ft wide. The selection of the bedform geometries was based on the results of an alluvial bedform

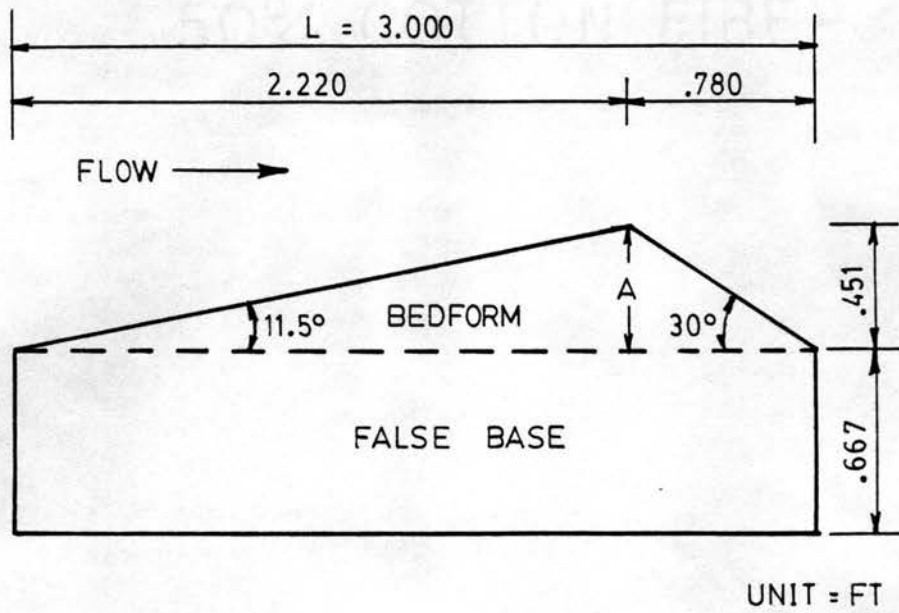


Figure 3.1. Bedform Model

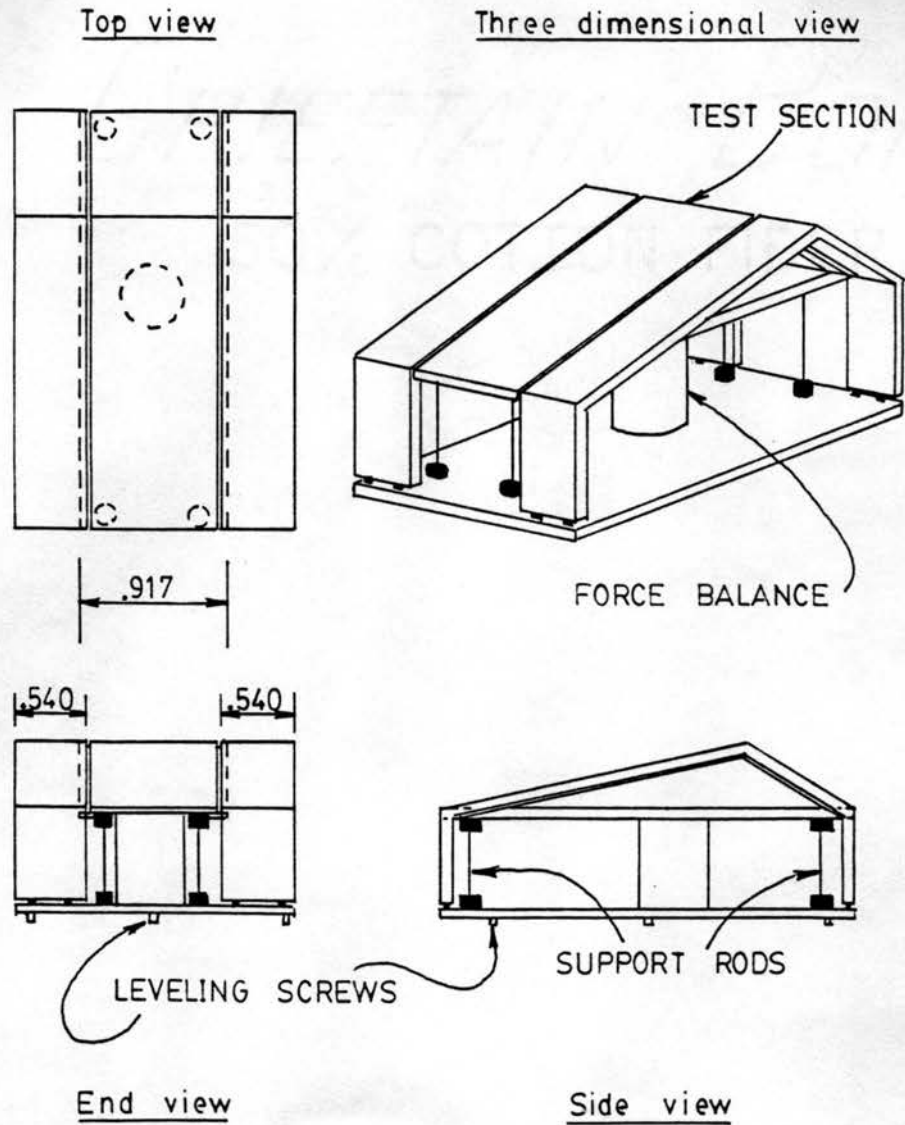
experiment conducted by Wang and Shen (1980), with proper adjustment to the flow conditions to be used in the present experiment. The bedform geometries were identical to those used in an idealized bedform experiment conducted by Wang (1984).

The test bedform was comprised of three parts as shown in Figure 3.2. The middle section was mounted on a total force measuring device (hereafter called the force balance), and was supported at its four corners by slender metal rods. The side sections were constructed entirely of plastic and were used to fill the rest of the width of the flume on each side of the middle section. The middle section was constructed in such a way as to allow its free movement without friction from the side sections, and yet restrict the flow of water through the necessary gaps between the sections. The total width of the middle section was 0.917 ft and each side section was 0.540 ft wide.

The force balance was constructed with small diameter metal rods to which strain gages were attached. After calibration under static water conditions at various flume slopes, the force balance was used to indicate the total longitudinal force applied to the middle section of the test bedform. For design details and additional information regarding the force balance, see Meyer (1985).

The test bedform and third bedform were installed with pressure taps which were staggered off the centerline of each bedform, as shown in Figure 3.3. The pressure taps were connected to a single pressure transducer through plastic tubes and a diaphragm arrangement which enabled the measurement of pressure at each individual tap.

In the nonuniform element experiment, the size of the first plastic bedform was varied, and the flow characteristics over the test



UNIT = FT

Figure 3.2. Test Bedform

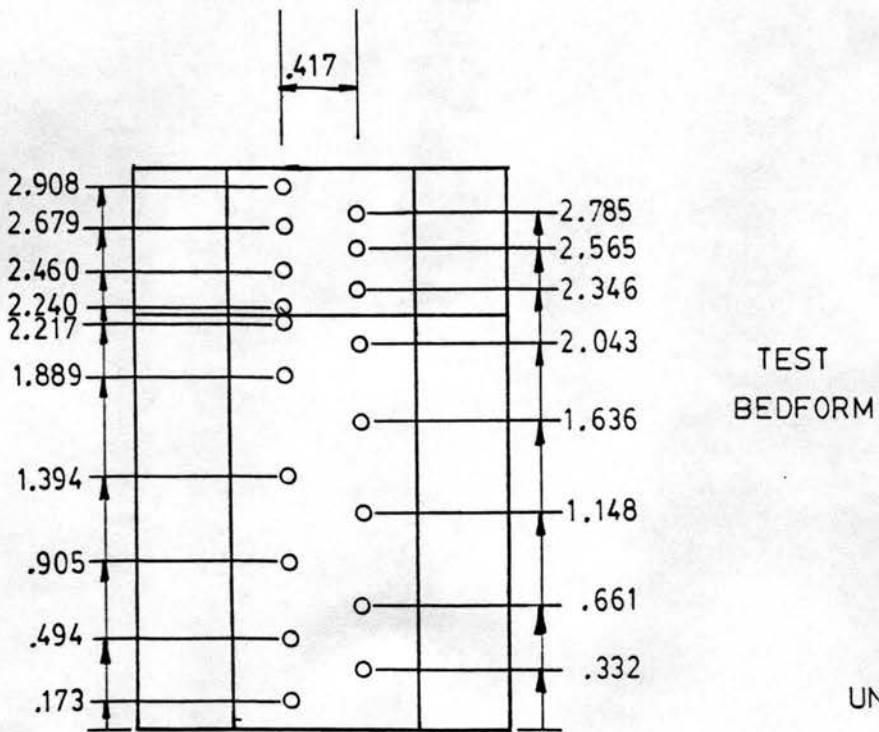
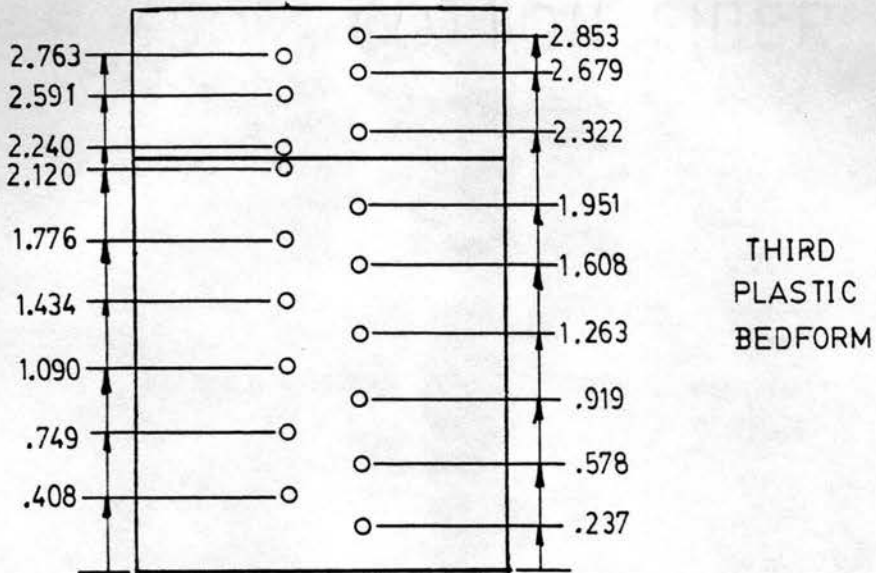


Figure 3.3. Locations of Bedform Surface Pressure Taps

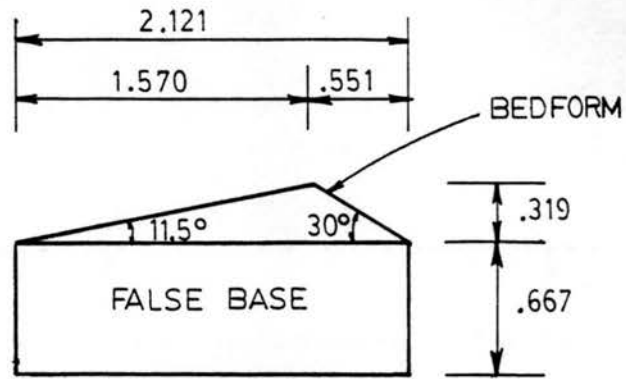
bedform was studied. Figure 3.4 illustrates the two different geometries used for the first plastic bedform in the nonuniform experiment. The upstream and downstream angles were equal to those used in the uniform experiments, but the bedform height and length was adjusted. A smaller dune was constructed using the height and length of the test dune divided by $\sqrt{2}$, and a larger dune was constructed using the dimensions of the test dune multiplied by $\sqrt{2}$.

For the roughened element study, sand with a median grain size of 1.75 mm was glued to thin sheets of plastic which were then affixed to six of the bedforms: two of the aluminum bedforms immediately upstream of the plastic bedforms; the plastic bedforms; and one aluminum bedform immediately downstream of the plastic bedforms. A spray adhesive was used to affix the roughness to the plastic sheets and to affix these sheets to the bedform elements. The grain size distribution of the sand used in this study is shown in Figure 3.5.

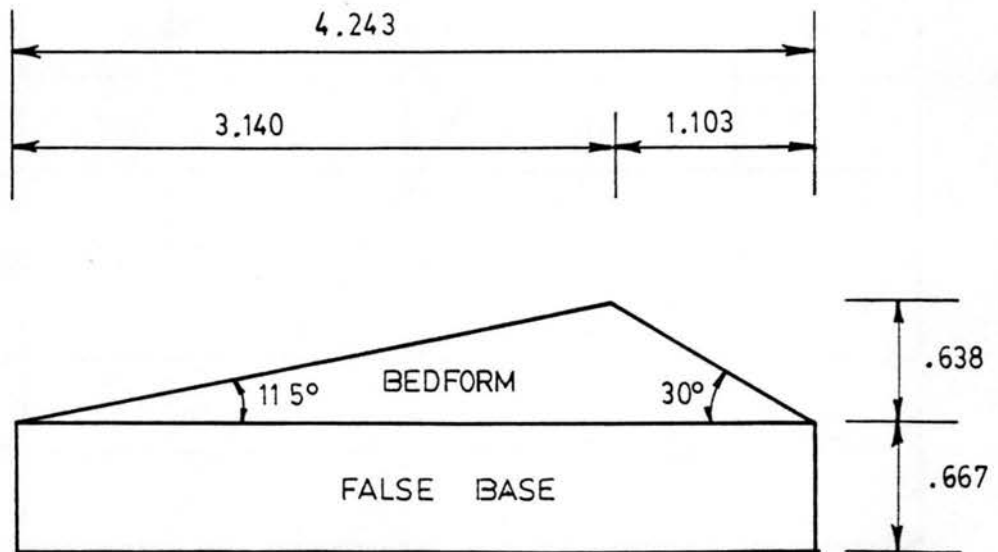
3.4 Experimental Procedures

In this section, a brief outline of the order and method of each measurement is presented, with a description of the employed equipment. A more detailed presentation of the measurement procedures follows this discussion.

For each uniform element experimental run, a specific discharge and depth at the crest of the test bedform was required. Uniform flow meeting the required restrictions was established for each run, using the water surface profile as criteria. The water surface profile was measured over the length of the test and third plastic bedform through the use of pressure taps installed in the side wall of the flume. These wall taps were positioned 4 in. apart in a line parallel to the



a) Small bedform model



b) Large bedform model

UNIT = FT

Figure 3.4. First Plastic Bedform Geometries Used in Nonuniform, Smooth Bedform Experiment

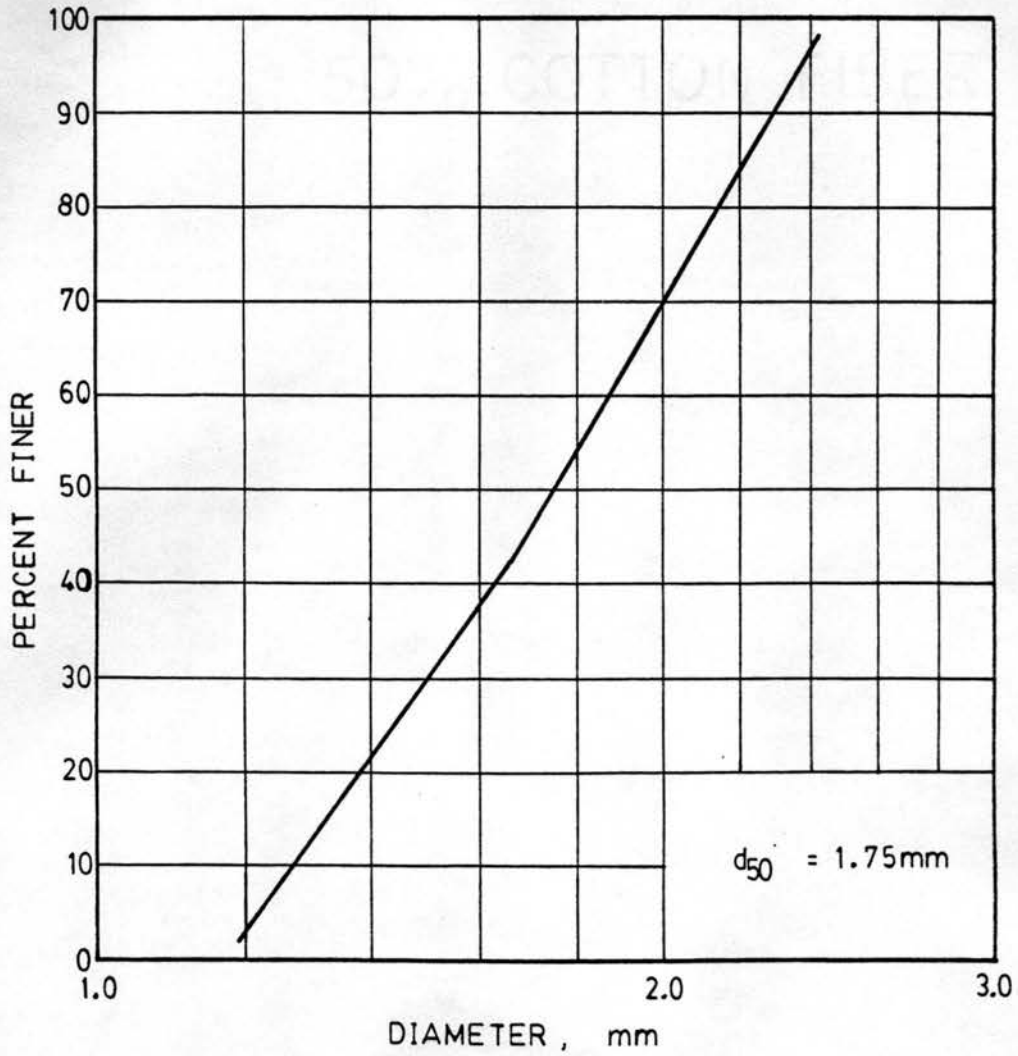


Figure 3.5. Size Distribution of Sand Used in Uniform, Rough Bedform Experiment

flume bed, approximately 4 in. above the bedform crests. The wall taps were connected to a pressure transducer through the same diaphragm arrangement used for pressure measurement along the bedform surface.

After uniform flow was established for a given run, the water surface profile was recorded and the pressure along the bedform surface was measured. Next, a shear probe 0.25 in. in diameter was mounted on the point gage used for depth measurement and shear measurements were made along the upstream face of the test bedform. Then the shear probe was replaced with a pitot-static probe 0.065 in. in diameter, and velocity profiles were measured at a number of locations over the test bedform. Finally, the total longitudinal force on the middle section of the test bedform was measured with the force balance.

The signal from each wall and bedform pressure tap was connected to the positive jack of a Validyne DP7 pressure transducer. The negative jack of the transducer was connected to a reference head source, a water column of constant height. The output voltage from the pressure transducer was transmitted to a calibrated analog voltmeter and an integrating voltmeter where digital output voltage was displayed. Using a calibration curve, the output voltage was converted to the piezometric head at the measuring station referring to a common datum. After reduction of the converted output, the flow depth above each wall tap and pressure distribution on the bedform surface was determined. This reduction technique will be described in Chapter 4.

The signal from the dynamic and static side of the shear and velocity probes was connected to the same transducer and voltmeter arrangement as was the signal from each pressure tap. The output

voltage was converted into velocity head in the velocity probe case, and was related to local shear stress for the case of the shear probe.

The output voltage from the strain gage force balance was also connected to the analog voltmeter and integrating voltmeter. Using a calibration curve, the output was converted into total longitudinal force acting on the midsection of the test bedform.

The integrating voltmeter was equipped with a number of time constants which may be used to vary the time over which an average output voltage is determined and displayed. For the total force measurements the time constant of 100 was used, which corresponds to a 400 second averaging time interval. For velocity, shear and pressure measurements, the time constant of 10 was used, which corresponds to a 40 second averaging time interval. For boundary layer velocity measurements and shear measurements, three readings of output voltage were recorded, 40 seconds apart. These readings were then averaged corresponding to a 2 min sample average. Free stream velocity and pressure measurements were taken using a single reading of the integrating voltmeter, after a sufficient amount of time had elapsed to insure a valid 40 sec sample. Sample time and method for each type of measurement is summarized in Table 3.1.

In order for the force balance to function, the middle section of the test bedform had to be allowed free movement within the limits imposed by its support structure. In preliminary studies, it was found that this free movement affected the pressure readings for the taps positioned on the test dune. Only after stabilizing the test bedform, and thus eliminating the use of the force balance, were the pressure readings over the surface of the test bedform comparable to those over

Chapter 3

EXPERIMENTAL SET-UP AND PROCEDURE

3.1 Introduction

In this chapter, the experimental set-up and procedure of the study is described. Three separate experiments using idealized bedforms were conducted: one with uniform, smooth elements; one with uniform, roughened elements; and one with nonuniform, smooth elements. These studies were performed in order to investigate the characteristics of open channel flow over idealized bedforms of fixed geometry and they concentrated on the topics of flow resistance and velocity distribution. All experimentation was conducted in the same flume in the hydraulics laboratory of the Engineering Research Center at Colorado State University.

3.2 Flume and Accessories

Each experiment was conducted in a recirculating flume which was 60 ft long, 2.0 ft wide, and 2.5 ft deep. The flume had clear plastic sidewalls. A constant speed 20-HP centrifugal pump circulated water from the tail sump to the head box through a cast-iron return pipe, 1.0 ft in diameter, located under the flume support structure. The flume was supported by hinges at the midsection and screw jacks at the upstream and downstream ends. The screw jacks were operated by a motor and allowed adjustment of the flume slope. A calibrated digital counter attached to the flume tilting device was used to determine the flume slope.

Table 3.1. Summary of Measurement Procedures

Measured Quantity	Measurement Instrument	Integrating Voltmeter Time Constant	Averaging Interval Per Reading (sec)	No. of Readings Per Measurement	Total Sample Time (sec)
Total Longitudinal Force	Force Balance	100	400	1	400
Local Shear Stress	Shear Probe	10	40	3	120
Boundary Layer Velocity	Pitot-Static Tube	10	40	3	120
Free Stream Velocity	Pitot-Static Tube	10	40	1	40
Local Pressure	Surface Pressure Tap	10	40	1	40
Water Surface Profile	Wall Pressure Tap	10	40	1	40

the surface of the third plastic bedform. Therefore, for the uniform smooth bedform experiment, each run was divided into two stages. For the first stage, the test bedform was stabilized by taping the middle section to its side sections and to the bedforms immediately upstream and downstream. Uniform flow was then established at the required discharge and depth. Uniform flow was defined as the condition when the depths of flow at three consecutive bedform toes were all equal. The flow depth above the downstream toe of each plastic bedform was measured using the wall taps. When these depths were equal, the energy slope was equal to the flume slope, and uniform flow was achieved. Reaching this condition required trial-and-error adjustment of the downstream tilt-gate and flume slope. After achieving uniform flow, the tilt-gate setting and flume slope was recorded, the water surface profile and bedform surface pressures were measured, and the flow was stopped. The first stage of the experimental run was complete. For the second stage, the tape used to stabilize the test dune was removed, and the uniform flow conditions were reproduced. Shear, velocity and total force measurements were then taken to complete the second stage.

For the roughened element experiment, the test bedform stabilization procedure used during the smooth element study was not applicable and each experimental run was accomplished in one stage: the test bedform was allowed free movement and bedform surface pressures were measured on the third plastic bedform. For the nonuniform bedform study, the test bedform was stabilized at all times and the force balance was not used. Flow conditions for six of the 12 smooth, uniform bedform experimental runs were repeated during the nonuniform study using bedforms of variable size immediately upstream of the test

bedform. Hence, uniform flow was no longer the case. Because the underside of the midsection of the test bedform was hollow, pressure gradients caused by nonuniform flow existed both above and below the surface of the test bedform causing erroneous force balance readings. The nonuniform experiment was performed primarily to investigate the effect of upstream form on shear and pressure profiles, and the lack of total force measurement did not detract from this study.

The following chapter contains a presentation of the data obtained in the course of the present laboratory experiments as well as analysis and comparison with data from other published studies.

Chapter 4

CHARACTERISTICS OF OPEN CHANNEL FLOW OVER BEDFORMS

4.1 Introduction

This chapter contains the presentation and analysis of data measured in the present study. A total of 30 experimental runs were conducted: 12 runs with smooth, uniform bedforms; 6 runs with rough, uniform bedforms; and 12 runs with smooth, nonuniform bedforms. The flow conditions for each experimental run are summarized in Table 4.1. For the uniform bedform studies, the average depth, D , is defined as

$$D = D_c + A/2 \quad (4.1)$$

where D_c is the flow depth above the test bedform crest, and A is the bedform height. The average velocity, V , is defined as

$$V = Q/(WD) \quad (4.2)$$

where Q is the pump discharge and W is the flume width. The Froude number, F , was computed from

$$F = V/\sqrt{gD} \quad (4.3)$$

where g is the acceleration of gravity. A value of 32.2 ft/s^2 was used for g .

For the smooth, uniform bedform experiment, the flow conditions were arranged in such a way as to allow the study of the variation of resistance and velocity characteristics due to both the flow depth and

Table 4.1. Summary of Flow Conditions

Run Number	Discharge Q ft ³ /s	Flow Depth at Crest D _c ft	Average Flow Depth D ft	Average Velocity V ft/s	Flume Slope S _b	Froude Number F	Temperature T °F
UNIFORM, SMOOTH BEDFORM EXPERIMENT							
1	0.700	0.500	0.726	0.482	0.000609	0.10	67
2	0.956	0.667	0.892	0.536	0.000551	0.10	68
3	1.236	0.833	1.059	0.584	0.000377	0.10	72
4	1.401	0.500	0.726	0.966	0.00235	0.20	66
5	1.911	0.667	0.892	1.071	0.00194	0.20	73
6	2.471	0.833	1.059	1.167	0.00188	0.20	72
7	2.102	0.500	0.726	1.449	0.00559	0.30	66
8	2.867	0.667	0.892	1.607	0.00362	0.30	61
9	3.707	0.833	1.059	1.751	0.00385	0.30	65
10	2.802	0.500	0.726	1.931	0.00999	0.40	72
11	3.822	0.667	0.892	2.142	0.00629	0.40	73
12	4.943	0.833	1.059	2.334	0.00640	0.40	74
UNIFORM, ROUGH BEDFORM EXPERIMENT							
1R	0.700	0.500	0.726	0.482	0.000782	0.10	64
2R	0.956	0.667	0.892	0.536	0.000667	0.10	64
3R	1.236	0.833	1.059	0.584	0.000435	0.10	64
7R	2.102	0.500	0.726	1.449	0.00640	0.30	64
8R	2.867	0.667	0.892	1.607	0.00466	0.30	64
9R	3.707	0.833	1.059	1.751	0.00466	0.30	63

Table 4.1. continued

Run Number	Discharge Q ft ³ /s	Flow Depth at Crest D ft	Average Flow Depth D ft	Average Velocity V ft/s	Flume Slope S _b	Froude Number F	Temperature T °F
NONUNIFORM, SMOOTH BEDFORM EXPERIMENT							
SMALL UPSTREAM BEDFORM							
1S	0.700	---	---	---	0.000609	---	62
2S	0.956	---	---	---	0.000551	---	62
3S	1.236	---	---	---	0.000377	---	70
7S	2.102	---	---	---	0.00559	---	73
8S	2.867	---	---	---	0.00362	---	70
9S	3.707	---	---	---	0.00385	---	71
LARGE UPSTREAM BEDFORM							
1B	0.700	---	---	---	0.000609	---	70
2B	0.956	---	---	---	0.000551	---	75
3B	1.236	---	---	---	0.000377	---	73
7B	2.102	---	---	---	0.00559	---	72
8B	2.867	---	---	---	0.00362	---	70
9B	3.707	---	---	---	0.00385	---	73

Froude number. For the smooth, nonuniform bedform experiment, six of these experimental runs were repeated twice: the first time with a smaller plastic bedform positioned immediately upstream of the test bedform; the second time with a larger plastic bedform positioned immediately upstream of the test bedform. The geometry of the smaller and larger bedforms is described in Chapter 3. For the rough, uniform bedform experiment, the Froude number and depth conditions of six of the smooth, uniform bedform experimental runs were repeated. However, the flume slope and downstream tilt-gate were adjusted to meet the requirements of uniform flow, as defined in Chapter 3. Energy slopes were different for comparable experimental runs of the smooth and rough studies due to the added skin resistance of the sand grains applied to the bedform surface in the rough bedform experiment.

The following sections describe the effect of different flow conditions on each quantity measured in the course of the present study.

4.2 Total Longitudinal Force

A strain gage arrangement, or force balance, was used to measure the total longitudinal force acting on the midsection of the test bedform during the uniform bedform studies. Details of the test bedform and force balance design may be found in Chapter 3 and in Meyer (1985).

The total longitudinal force per unit width acting on the test bedform for each experimental run is listed in Table 4.2. The total bed shear stress, τ_b , is computed from

$$\tau_b = \frac{F_b}{L} \quad (4.4)$$

Table 4.2. Total Resistance Parameters for Uniform Bedform Experimental Runs

Run No.	F_b lb/ft	τ_b lb/ft ²	f_b Measured	f_b^* Computed	R_b^* Computed
1	0.0825	0.0275	0.488	0.465	0.690
2	0.0719	0.0240	0.344	0.414	0.837
3	0.0586	0.0195	0.236	0.273	0.961
4	0.307	0.102	0.451	0.449	0.693
5	0.289	0.0964	0.347	0.364	0.840
6	0.276	0.920	0.279	0.350	0.988
7	0.665	0.222	0.436	0.478	0.697
8	0.652	0.217	0.347	0.301	0.834
9	0.624	0.208	0.280	0.319	0.988
10	1.417	0.472	0.522	0.483	0.700
11	1.178	0.393	0.353	0.296	0.840
12	1.172	0.391	0.296	0.292	0.987
1R	0.0932	0.0311	0.552	0.603	0.696
2R	0.0799	0.0266	0.382	0.509	0.844
3R	0.0745	0.0248	0.300	0.319	0.970
7R	0.791	0.264	0.519	0.548	0.700
8R	0.745	0.248	0.396	0.393	0.845
9R	0.665	0.222	0.299	0.390	0.997

f_b^* and R_b^* were calculated based on the flow conditions using a procedure suggested by Vanoni and Brooks (1957). R_b is the hydraulic radius of the bed.

where F_b is the total longitudinal force per unit width measured using the force balance, and L is the length of the bedform. The Darcy-Wiesbach friction factor, f_b , is computed from

$$f_b = \frac{8\tau_b}{\rho V^2} \quad (4.5)$$

where ρ is the density of the fluid. Values of τ_b and f_b were computed for each experimental run and are listed in Table 4.2.

Comparing Tables 4.1 and 4.2, it is observed that for the present experiment, τ_b increases with Froude number for a constant depth, but decreases as the depth increases with constant Froude number. For similar flow conditions, the bed shear stress and friction factor is noticeably larger for the roughened bedform experiment. The friction factor is observed to consistently decrease as flow depth is increased at a constant Froude number.

Using a side-wall correction procedure as outlined by Vanoni and Brooks (1957), the bed friction factor was computed based on the generated flow conditions for each experimental run of the uniform bedform studies. These computed bed friction factors are listed for comparison alongside the measured bed friction factors in Table 4.2. The computed bed friction factors exhibit the same trends as those measured in the present study. A plotted comparison of the independently determined friction factors is contained in Figure 4.1. Although there is deviation, the majority of the measured friction factors are within ten percent of those calculated using Vanoni and Brooks' procedure. It may be noted that the calculated friction factors tend to be greater than those directly measured, and this observation may be explained as follows: In Vanoni and Brooks' procedure, the average depth of flow

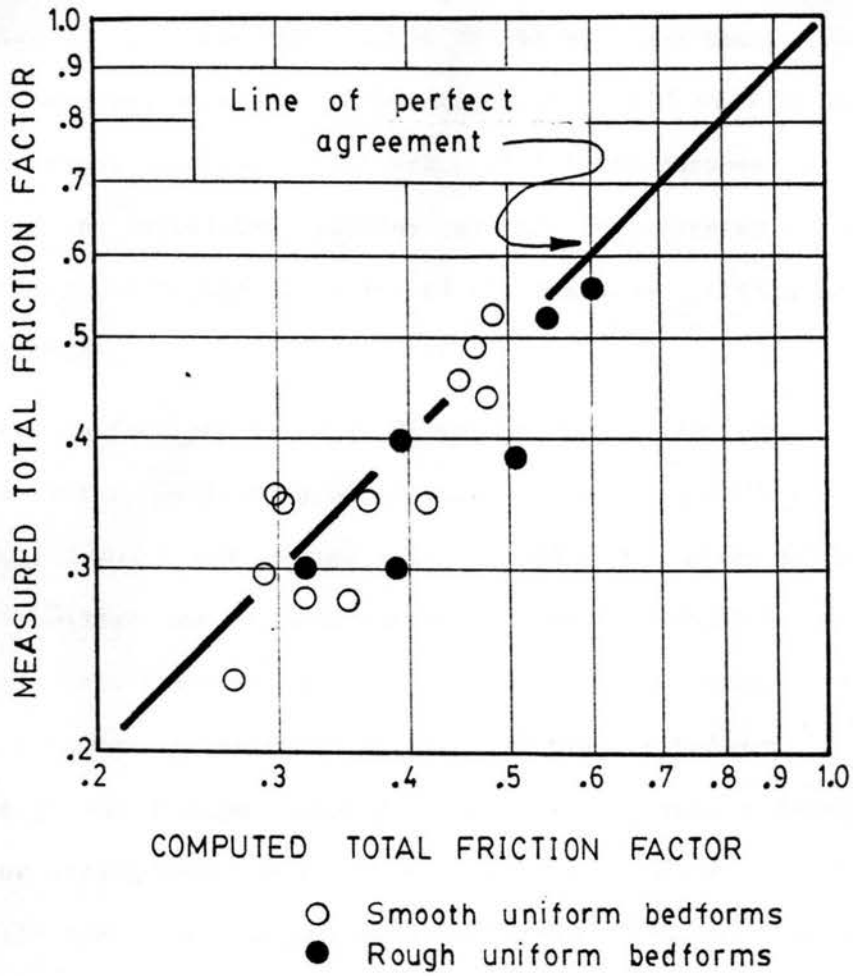


Figure 4.1. Comparison of the Measured Total Friction Factor with the Friction Factor Computed Using Vanoni and Brooks' (1957) Procedure

used was as defined in Table 4.1 which includes the separation region as part of the effective flow depth. Wang (1984) noted that including the separation region in the effective region of flow causes an over-estimation of the hydraulic radius of the bed, and hence, the friction factor. However, analysis of the effective field of flow and corrections in Vanoni and Brooks' procedure is not the purpose of the present study, and the calculated friction factors are presented for comparison and verification of the variation of the measured friction factors with flow parameters.

4.3 Water Surface and Pressure Distribution over Bedform

The water surface profile and pressure distribution over an individual bedform was measured using wall and surface pressure taps. For the uniform and nonuniform smooth bedform studies, measurements were made over the test bedform, whereas for the rough bedform study the profiles were measured over the third plastic bedform.

The pressure taps, when connected to a pressure transducer and voltmeter arrangement, measured the piezometric head at each tap location, relative to a constant reference head. The difference in relative piezometric head at wall taps located above consecutive bedform toes, divided by the bedform length, is equal to the average slope of the water surface. When the water surface slope was equal to the flume slope, uniform flow was achieved.

The water surface profiles for all experimental runs, after correction due to the channel slope effect, are summarized in Tables 4.3-4.5. Since the depth at the crest for each experimental run was controlled, the water surface elevation measured at each wall tap location minus that at the bedform crest (equivalent to the measured

Table 4.3. Summary of Water Surface Profiles for the Uniform, Smooth Bedform Experiment

x ^{1/} ft	Deviation from Water Surface Elevation ^{2/} at Bedform Crest, Ft.					
	Run 1	Run 2	Run 3	Run 4	Run 5	Run 6
0.088	-0.00138	-0.00143	-0.00072	-0.00193	-0.00264	-0.00425
0.421	0.00032	0.00001	-0.00026	0.00085	0.00058	-0.00389
0.754	0.00153	0.00102	0.00070	0.00605	0.00615	0.00374
1.088	0.00256	0.00080	0.00149	0.00734	0.00488	0.00604
1.421	0.00234	0.00081	0.00170	0.00720	0.00395	0.00674
1.754	0.00155	0.00074	0.00090	0.00582	0.00484	0.00745
2.088	0.00251	0.00026	0.00028	0.00111	0.00157	0.00125
2.421	-0.00046	-0.00047	-0.00051	-0.00161	-0.00228	-0.00180
2.754	-0.00068	-0.00046	-0.00063	-0.00217	-0.00255	-0.00475
3.088	-0.00097	-0.00127	-0.00075	-0.00205	-0.00257	-0.00587

^{1/} x is the longitudinal distance from the test bedform upstream toe.

^{2/}Water surface elevations were corrected for channel slope effect.

Table 4.3. Summary of Water Surface Profiles for the Uniform, Smooth Bedform Experiment (continued)

$x^{1/}$ ft	Deviation from Water Surface Elevation ^{2/} at Bedform Crest, Ft.					
	Run 7	Run 8	Run 9	Run 10	Run 11	Run 12
0.088	-0.00710	-0.00573	-0.00239	-0.0241	-0.0127	-0.00749
0.421	-0.00157	0.00488	-0.00126	0.00161	0.00368	0.00497
0.754	0.0154	0.0117	0.00410	0.0285	0.0230	0.0214
1.088	0.0191	0.0161	0.0184	0.0322	0.0324	0.0256
1.421	0.0161	0.0143	0.0137	0.0309	0.0272	0.0263
1.754	0.0127	0.0104	0.0103	0.0259	0.0193	0.0155
2.088	0.00375	0.00309	0.00281	0.00774	0.00691	0.00589
2.421	-0.00556	-0.00461	-0.00423	-0.0114	-0.0102	-0.00883
2.754	-0.00611	-0.00765	-0.0395	-0.0291	-0.0135	-0.00939
3.088	-0.00646	-0.00561	-0.00500	-0.0240	-0.0122	-0.00756

^{1/}x is the longitudinal distance from the test bedform upstream toe.

^{2/}Water surface elevations were corrected for channel slope effect.

Table 4.4. Summary of Water Surface Profiles for the Uniform, Rough Bedform Experiment

$x^{1/}$ ft	Deviation from Water Surface Elevation ^{2/} at Bedform Crest, Ft.					
	Run 1R	Run 2R	Run 3R	Run 7R	Run 8R	Run 9R
0.052	-0.00241	-0.00075	-0.00001	-0.00696	-0.00400	-0.00450
0.385	-0.00040	0.00030	0.00064	-0.00069	0.00021	0.00373
0.719	0.00061	0.00070	0.00144	0.0125	0.0128	0.00959
1.052	0.00112	0.00142	0.00126	0.0153	0.0162	0.0155
1.385	0.00163	0.00097	0.00207	0.0181	0.0166	0.0151
1.719	0.00114	0.00077	0.00188	0.0123	0.0100	0.00915
2.052	0.00040	0.00016	0.00003	0.00309	0.00157	0.00207
2.385	-0.00059	-0.00036	-0.00008	-0.00494	-0.00238	-0.00322
2.719	-0.00100	-0.00081	-0.00002	-0.00866	-0.00407	-0.00299
3.052	-0.00207	-0.00067	-0.00005	-0.00523	-0.00419	-0.00469

^{1/}x is the longitudinal distance from the third plastic bedform upstream toe.

^{2/}Water surface elevations were corrected for channel slope effect.

Table 4.5. Summary of Water Surface Profiles for the Nonuniform, Smooth Bedform Experiment

x ^{1/} ft	Deviation from Water Surface Elevation ^{2/} at Bedform Crest, Ft.					
	Run 1S	Run 2S	Run 3S	Run 7S	Run 8S	Run 9S
0.088	0.00153	0.00257	0.00062	0.0194	0.0221	0.0147
0.421	0.00282	0.00293	0.00207	0.0223	0.0248	0.0194
0.754	0.00311	0.00252	0.00212	0.0279	0.0260	0.0228
1.088	0.00314	0.00255	0.00224	0.0255	0.0256	0.0228
1.421	0.00276	0.00206	0.00195	0.0237	0.0209	0.0177
1.754	0.00179	0.00124	0.00132	0.0162	0.0137	0.0104
2.088	0.00059	0.00034	0.00037	0.00425	0.00402	0.00298
2.421	-0.00080	-0.00047	-0.00051	-0.00631	-0.00603	-0.00440
2.754	-0.00101	-0.00012	-0.00038	-0.00803	-0.00917	-0.00428
3.088	-0.00097	-0.00027	-0.00051	-0.0118	-0.00807	-0.00417

^{1/} x is the longitudinal distance from the test bedform upstream toe.

^{2/}Water surface elevations were corrected for channel slope effect.

Table 4.5. Summary of Water Surface Profiles for the Nonuniform, Smooth Bedform Experiment (continued)

$x^{1/}$ ft	Deviation from Water Surface Elevation ^{2/} at Bedform Crest, Ft.					
	Run 1B	Run 2B	Run 3B	Run 7B	Run 8B	Run 9B
0.088	-0.00405	-0.00476	-0.00355	-0.0332	-0.0210	-0.0293
0.421	-0.00368	-0.00399	-0.00293	-0.0116	-0.0198	-0.0259
0.754	-0.00189	-0.00223	-0.00247	-0.00646	-0.0138	-0.0197
1.088	-0.00036	-0.00121	-0.00134	0.00099	-0.0104	-0.0155
1.421	0.00051	-0.00077	0.00003	0.00680	-0.00440	-0.00833
1.754	-0.00035	-0.00043	0.00016	0.00405	0.00231	-0.00138
2.088	-0.00008	0.00001	0.00003	0.00167	0.00027	0.00081
2.421	0.00012	-0.00006	-0.00001	-0.00247	-0.00036	-0.00123
2.754	0.00032	0.00088	0.00028	-0.00011	0.00626	0.00080
3.088	0.00111	0.00107	0.00083	0.00642	0.00855	0.0102

^{1/} x is the longitudinal distance from the test bedform upstream toe.

^{2/}Water surface elevations were corrected for channel slope effect.

piezometric head at each wall tap corrected for slope effect minus the interpolated piezometric head at the crest using nearby wall taps) is the form of the data listed in these tables. Thus, the data in Tables 4.3-4.5 indicate the variation in the water surface profile over the length of the bedform, relative to its position above the bedform crest.

The bedform surface pressure profiles for all experimental runs, as indicated by the pressure taps located on the bedform surface, are summarized in Tables 4.6-4.8. The present data are of the form of relative piezometric head, corrected for channel slope effect. Relative piezometric head is the measured piezometric head at each location minus the interpolated piezometric head at the crest of the bedform.

The water surface profiles and piezometric head distributions over the bedform surface are illustrated in Figures 4.2-4.10. In examining these figures a number of characteristics may be noted. The location of peak piezometric head measured for the uniform bedform studies is between 1.0 and 1.3 ft downstream of the toe for the majority of these experimental runs. These locations correspond to distances of 3.9 and 4.6 bedform heights downstream from the crest of the immediately upstream bedform, respectively. The location of peak piezometric head measured for the nonuniform bedform studies was between 0.6 and 0.9 ft downstream of the toe for the runs with the smaller-scaled bedform upstream of the test bedform, and between 1.3 and 1.6 ft downstream of the toe for the runs with the larger-scaled bedform upstream of the test bedform. These locations correspond to distances 3.6-4.6 and 3.8-4.2 times the appropriate upstream bedform height from the point of separation at the immediately upstream crest. Assuming that the

Table 4.6. Summary of Piezometric Head Distributions on Bedform Surface for the Uniform, Smooth Bedform Experiment

$x^{1/}$ ft	$\Delta h_z =$ Deviation from Piezometric Head ^{2/} at Bedform Crest, Ft.					
	Run 1	Run 2	Run 3	Run 4	Run 5	Run 6
0.173	-0.00100	0.00020	-0.00044	-0.00190	-0.00140	-0.00453
0.332	-0.00023	0.00038	-0.00071	-0.00019	0.00	-0.00231
0.494	0.00037	0.00105	-0.00049	0.00386	0.00140	0.000826
0.661	0.00172	0.00247	0.00141	0.00743	0.00619	0.00706
0.905	0.00270	0.00327	0.00300	0.0117	0.00944	0.0107
1.148	0.00410	0.00424	0.00310	0.0157	0.0132	0.0157
1.394	0.00333	0.00379	0.00319	0.0143	0.0136	0.0144
1.636	0.00331	0.00335	0.00270	0.0132	0.0139	0.0141
1.889	0.00213	0.00224	0.00195	0.0105	0.00945	0.00997
2.043	0.00197	0.00182	0.00160	0.00733	0.00690	0.00591
2.217	0.00025	0.00008	0.00008	0.00057	0.000657	0.00016
2.240	-0.00100	-0.00032	-0.00024	-0.00221	-0.00230	-0.00063
2.346	-0.00043	-0.00010	-0.00037	-0.00088	-0.00243	-0.00010
2.460	-0.00061	-0.00012	-0.00016	-0.00244	-0.00179	-0.00305
2.565	-0.00096	-0.00006	-0.00070	-0.00077	-0.00158	-0.00185
2.679	-0.00056	0.00034	-0.00075	-0.00126	-0.00269	-0.00406
2.785	-0.00049	0.00006	-0.00012	-0.00193	-0.00216	-0.00161
2.908	-0.00050	0.00055	-0.00049	-0.00164	-0.00167	-0.00146

^{1/} x is the longitudinal distance from the test bedform upstream toe.

^{2/} Piezometric heads were corrected for channel slope effect.

Table 4.6. Summary of Piezometric Head Distributions on Bedform Surface for the Uniform, Smooth Bedform Experiment (continued)

x ^{1/} ft	Δh_z = Deviation from Piezometric Head ^{2/} at Bedform Crest, Ft.					
	Run 7	Run 8	Run 9	Run 10	Run 11	Run 12
0.173	-0.00270	-0.00475	-0.00239	0.00033	-0.00430	-0.00737
0.332	-0.00215	-0.00151	-0.00020	0.0160	0.00692	-0.00120
0.494	0.00764	0.00804	0.00768	0.0244	0.0153	0.0132
0.661	0.0112	0.0134	0.0163	0.0433	0.0263	0.0268
0.905	0.0265	0.0248	0.0214	0.0559	0.0446	0.0462
1.148	0.0339	0.0344	0.0325	0.0680	0.0558	0.0570
1.394	0.0327	0.0323	0.0317	0.0734	0.0561	0.0553
1.636	0.0309	0.0336	0.0290	0.0676	0.0580	0.0517
1.889	0.0232	0.0257	0.0227	0.0538	0.0438	0.0381
2.043	0.0195	0.0192	0.0194	0.0454	0.0344	0.0294
2.217	0.00172	0.00098	0.00048	0.00412	0.00172	0.00230
2.240	-0.00607	-0.00336	-0.00143	-0.0149	-0.00614	-0.00830
2.346	-0.00164	-0.00480	-0.00452	-0.0139	-0.00897	-0.00871
2.460	-0.00125	-0.00314	-0.00258	-0.00852	-0.00675	-0.00998
2.565	-0.00533	-0.00359	-0.00068	-0.00415	-0.00726	-0.00960
2.679	-0.00395	-0.00535	-0.00316	-0.00302	-0.00638	-0.0105
2.785	-0.00177	-0.00363	-0.00402	-0.00113	-0.00638	-0.00980
2.908	-0.00442	-0.00360	-0.00186	-0.00157	-0.00561	-0.00819

^{1/} x is the longitudinal distance from the test bedform upstream toe.

^{2/}Piezometric heads were corrected for channel slope effect.

Table 4.7. Summary of Piezometric Head Distributions on Bedform Surface for the Uniform, Rough Bedform Experiment

$x^{1/}$ ft	$\Delta h_z =$ Deviation from Piezometric Head ^{2/} at Bedform Crest, Ft.					
	Run 1R	Run 2R	Run 3R	Run 7R	Run 8R	Run 9R
0.237	-0.00052	0.00028	-0.00035	-0.00261	-0.00214	-0.00539
0.408	0.00003	0.00040	0.00015	0.00045	0.00604	-0.00251
0.578	0.00108	0.00126	0.00097	0.00824	0.0132	0.00933
0.749	0.00255	0.00172	0.00214	0.0171	0.0163	0.0152
0.919	0.00284	0.00258	0.00312	0.0216	0.0205	0.0203
1.090	0.00332	0.00269	0.00353	0.0264	0.0265	0.0271
1.263	0.00386	0.00347	0.00260	0.0268	0.0269	0.0215
1.434	0.00434	0.00375	0.00301	0.0312	0.0275	0.0248
1.608	0.00272	0.00320	0.00300	0.0270	0.0237	0.0241
1.776	0.00251	0.00265	0.00224	0.0221	0.0218	0.0203
1.951	0.00215	0.00210	0.00148	0.0178	0.0135	0.0158
2.120	0.00062	0.00063	0.00056	0.00511	0.00564	0.00497
2.240	-0.00062	-0.00063	-0.00047	-0.00495	-0.00548	-0.00481
2.322	-0.00056	0.00018	-0.00019	-0.00693	-0.00767	-0.00442
2.591	-0.00068	0.00027	-0.00032	-0.00646	-0.00949	-0.00417
2.679	-0.00053	-0.00009	-0.00037	-0.00506	-0.00451	-0.00601
2.763	-0.00088	0.00022	-0.00033	-0.00578	-0.00712	-0.00637
2.853	-0.00055	0.00012	-0.00029	-0.00270	-0.00395	-0.00445

^{1/} x is the longitudinal distance from the third plastic bedform upstream toe.

^{2/}Piezometric heads were corrected for channel slope effect.

Table 4.8. Summary of Piezometric Head Distributions on Bedform Surface for the Nonuniform, Smooth Bedform Experiment

$x^{1/}$ ft	$\Delta h_z =$ Deviation from Piezometric Head ^{2/} at Bedform Crest, Ft.					
	Run 1S	Run 2S	Run 3S	Run 7S	Run 8S	Run 9S
0.173	0.00283	0.00304	-0.00011	0.0232	0.0297	0.0175
0.332	0.00385	0.00388	0.00221	0.0325	0.0363	0.0294
0.494	0.00462	0.00363	0.00293	0.0349	0.0383	0.0318
0.661	0.00605	0.00514	0.00391	0.0476	0.0442	0.0429
0.905	0.00603	0.00519	0.00350	0.0439	0.0485	0.0405
1.148	0.00602	0.00491	0.00343	0.0466	0.0475	0.0410
1.394	0.00475	0.00412	0.00336	0.0395	0.0415	0.0356
1.636	0.00414	0.00360	0.00261	0.0355	0.0333	0.0320
1.889	0.00322	0.00290	0.00154	0.0273	0.0246	0.0230
2.043	0.00096	0.00215	0.00093	0.0214	0.0175	0.0163
2.217	0.00008	0.00008	0.00008	0.00122	0.00098	0.00048
2.240	-0.00016	-0.00032	-0.00033	-0.00448	-0.00352	-0.00160
2.346	-0.00001	-0.00035	-0.00079	-0.00481	-0.00313	-0.00127
2.460	-0.00036	-0.00012	-0.00124	-0.00484	-0.00314	-0.00650
2.565	-0.00104	-0.00039	-0.00104	-0.00283	-0.00193	0.00007
2.679	-0.00056	-0.00083	-0.00125	-0.00620	-0.00210	-0.00407
2.785	-0.00257	-0.00077	-0.00221	-0.00460	-0.00229	-0.00953
2.908	-0.00075	-0.00029	-0.00157	-0.00600	-0.00244	0.00039

^{1/} x is the longitudinal distance from the test bedform upstream toe.

^{2/}Piezometric heads were corrected for channel slope effect.

Table 4.8. Summary of Piezometric Head Distributions on Bedform Surface for the Nonuniform, Smooth Bedform Experiment (continued)

$x^{1/}$ ft	$\Delta h_z = \text{Deviation from Piezometric Head}^{2/}$ at Bedform Crest, Ft.					
	Run 1B	Run 2B	Run 3B	Run 7B	Run 8B	Run 9B
0.173	-0.00483	-0.00338	-0.00294	-0.0147	-0.0293	-0.0413
0.332	-0.00457	-0.00471	-0.00304	-0.0214	-0.0251	-0.0394
0.494	-0.00272	-0.00362	-0.00173	0.00744	-0.00564	-0.0225
0.661	-0.00153	-0.00261	-0.00192	0.0109	-0.00365	-0.0192
0.905	0.00195	0.00002	0.00192	0.0281	0.0195	0.00813
1.148	0.00210	0.00074	0.00110	0.0277	0.0221	0.0115
1.394	0.00375	0.00371	0.00236	0.0372	0.0333	0.0260
1.636	0.00297	0.00376	0.00178	0.0292	0.0260	0.0210
1.889	0.00280	0.00307	0.00187	0.0264	0.0281	0.0191
2.043	0.00114	0.00157	0.00126	0.0146	0.0159	0.0123
2.217	0.00025	0.00008	0.00017	0.00006	0.00098	0.00198
2.240	-0.00091	-0.00041	-0.00074	-0.00023	-0.00343	-0.00726
2.346	-0.00217	-0.00151	-0.00135	-0.0101	-0.0134	-0.0195
2.460	-0.00094	-0.00095	-0.00066	-0.00609	-0.00289	-0.00891
2.565	-0.00171	-0.00131	-0.00104	-0.00633	-0.0124	-0.00948
2.679	-0.00105	-0.00025	-0.00116	-0.00153	-0.00252	-0.00824
2.785	-0.00133	-0.00052	-0.00154	-0.00093	-0.00613	-0.00475
2.908	-0.00017	-0.00029	-0.00132	0.00508	-0.00152	-0.00419

$^{1/}x$ is the longitudinal distance from the test bedform upstream toe.

$^{2/}$ Piezometric heads were corrected for channel slope effect.

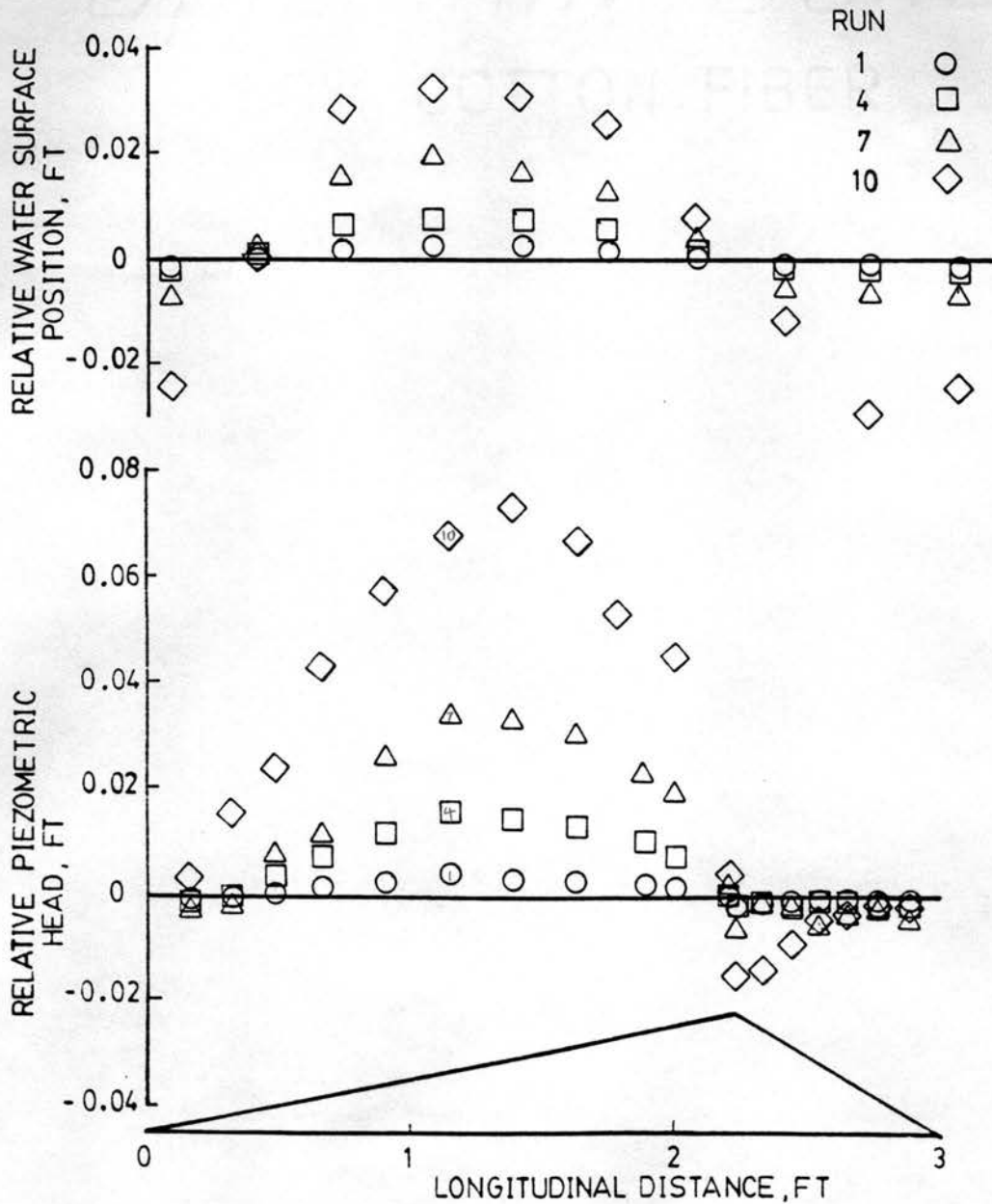


Figure 4.2. Relative Piezometric Head Distribution and Relative Water Surface Profile for Uniform, Smooth Bedform Experiment: Depth at Crest = 6 in.

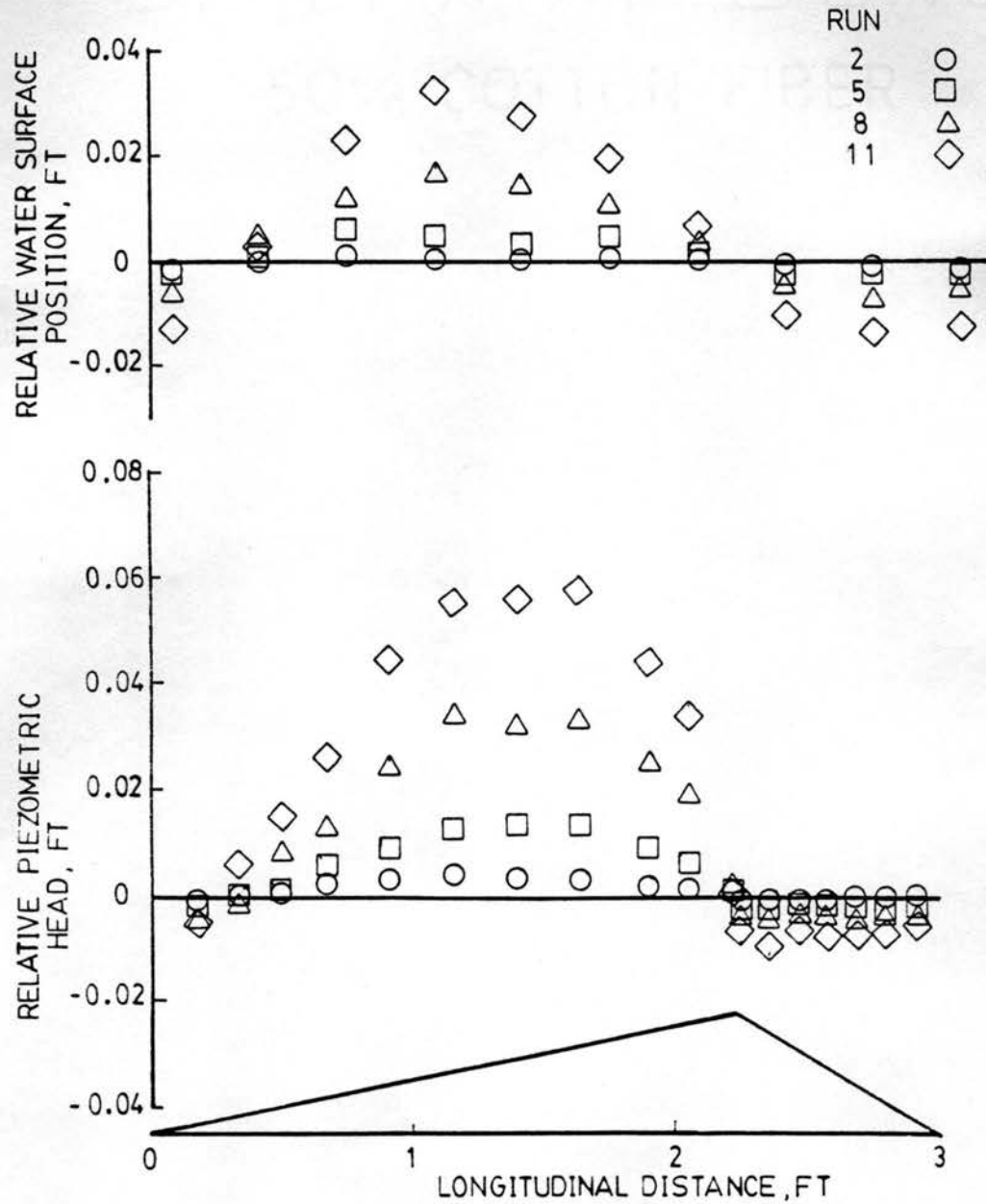


Figure 4.3. Relative Piezometric Head Distribution and Relative Water Surface Profile for Uniform, Smooth Bedform Experiment: Depth at Crest = 8 in

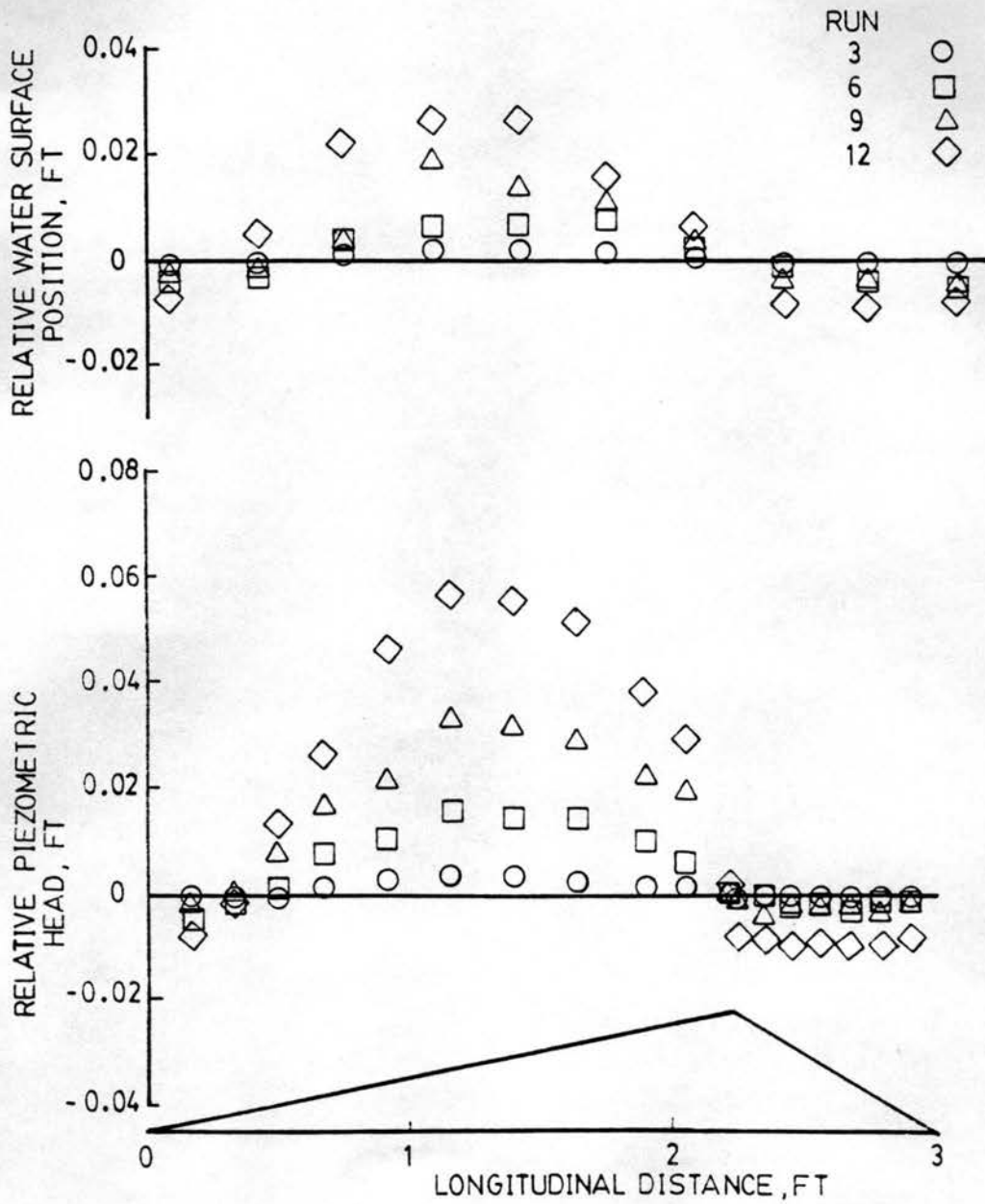


Figure 4.4. Relative Piezometric Head Distribution and Relative Water Surface Profile for Uniform, Smooth Bedform. Experiment: Depth at Crest = 10 in

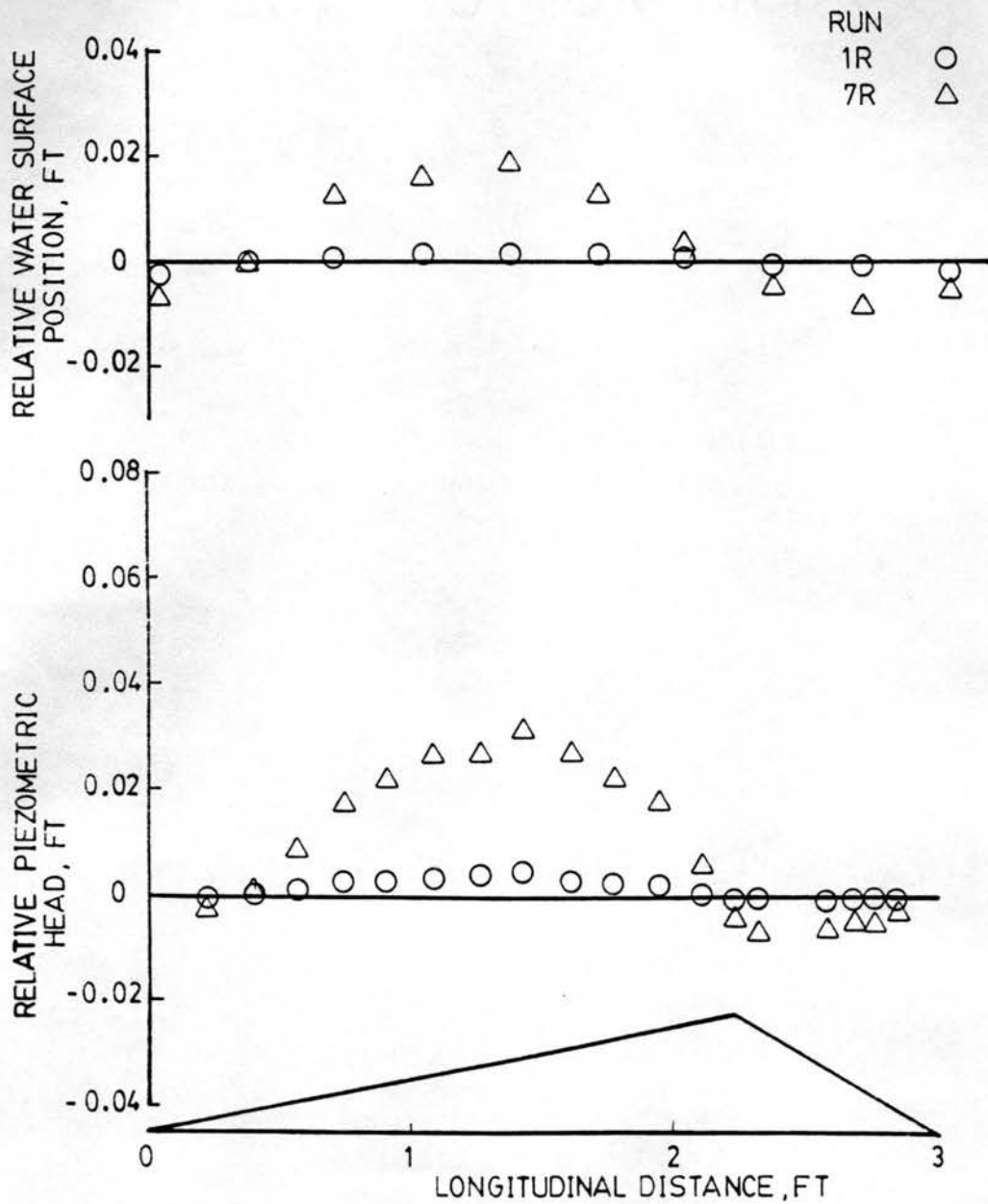


Figure 4.5. Relative Piezometric Head Distribution and Relative Water Surface Profile for Uniform, Rough Bedform Experiment: Depth at Crest = 6 in

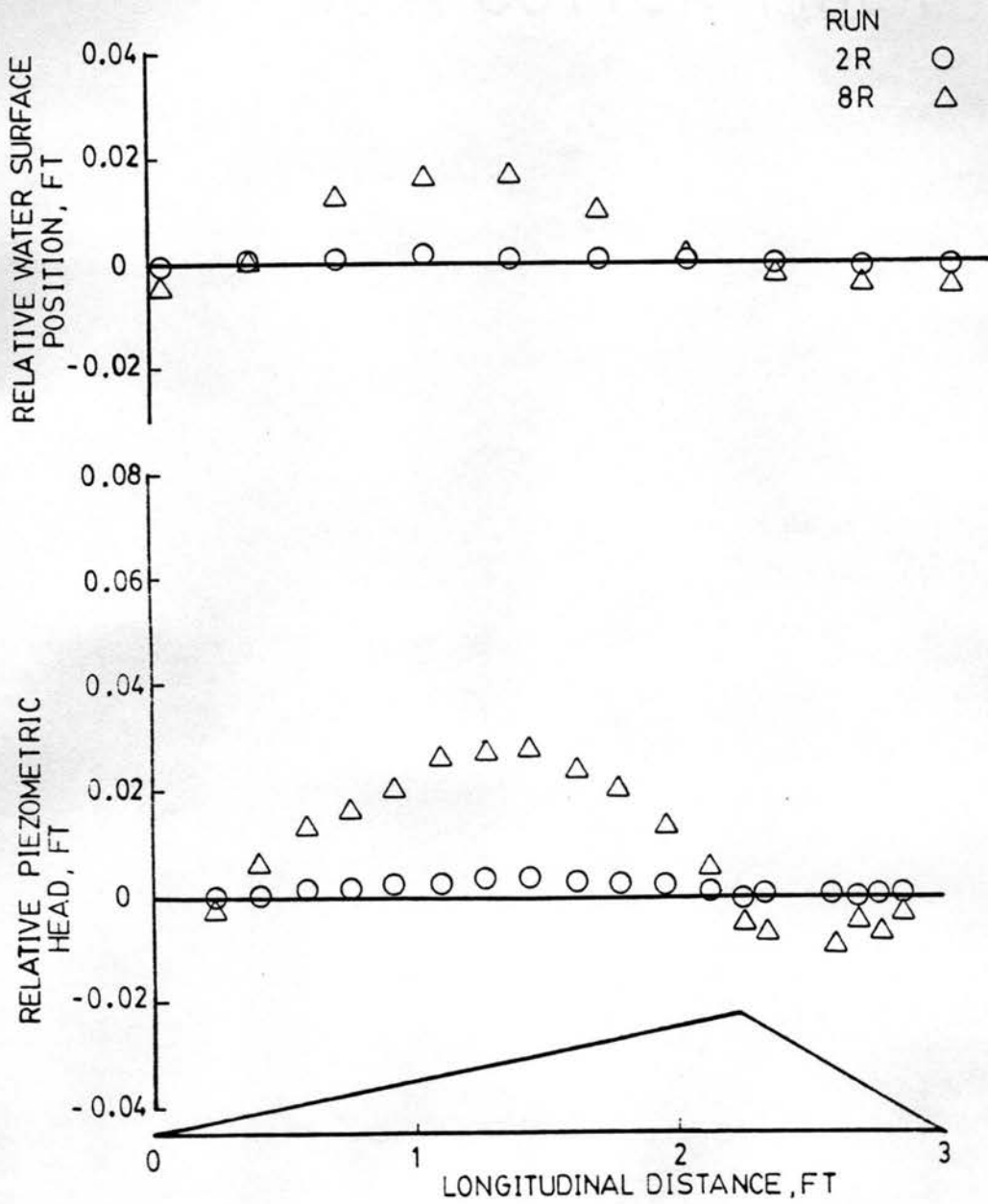


Figure 4.6. Relative Piezometric Head Distribution and Relative Water Surface Profile for Uniform, Rough Bedform Experiment: Depth at Crest = 8 in

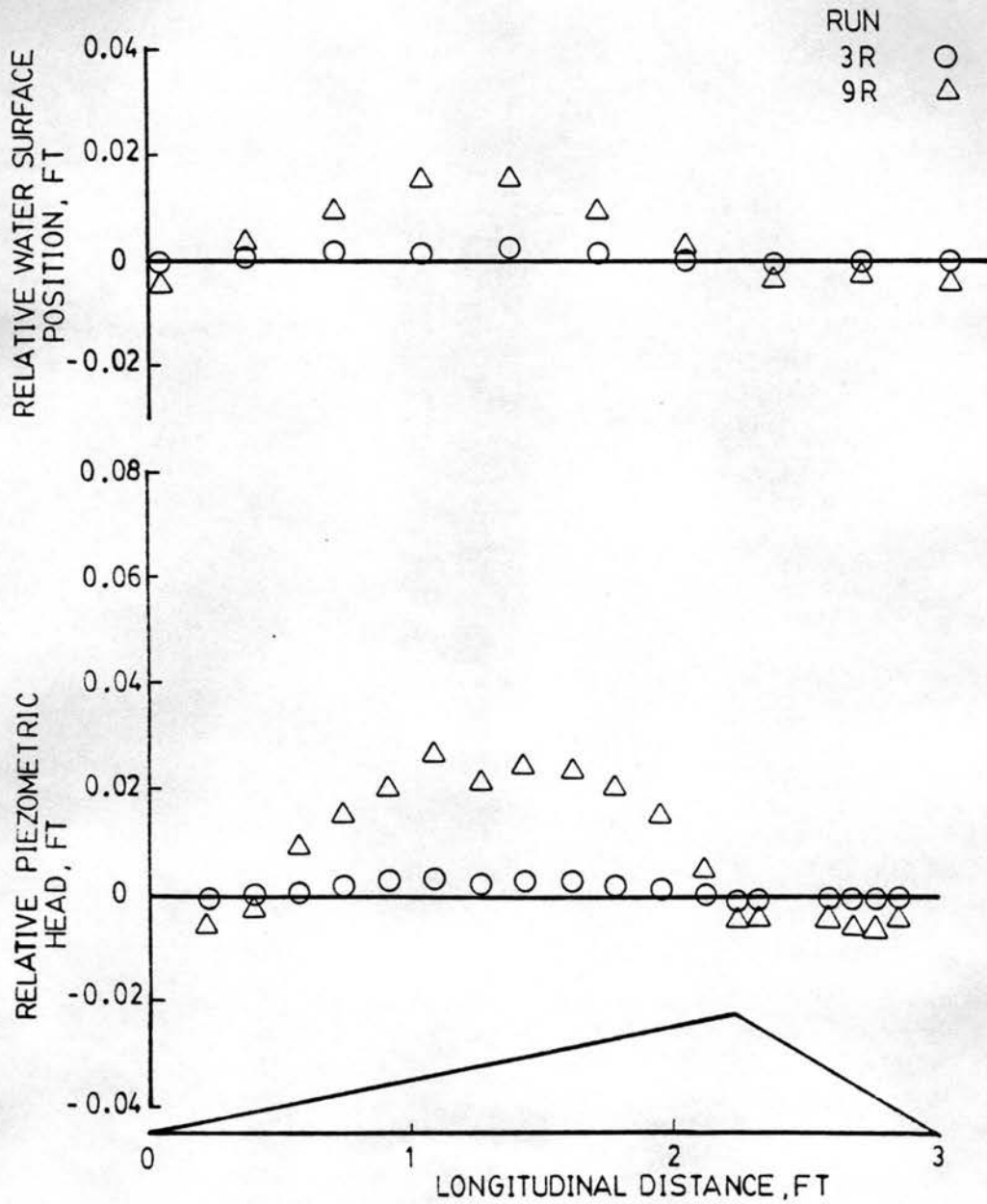


Figure 4.7. Relative Piezometric Head Distribution and Relative Water Surface Profile for Uniform, Rough Bedform Experiment: Depth at Crest = 10 in

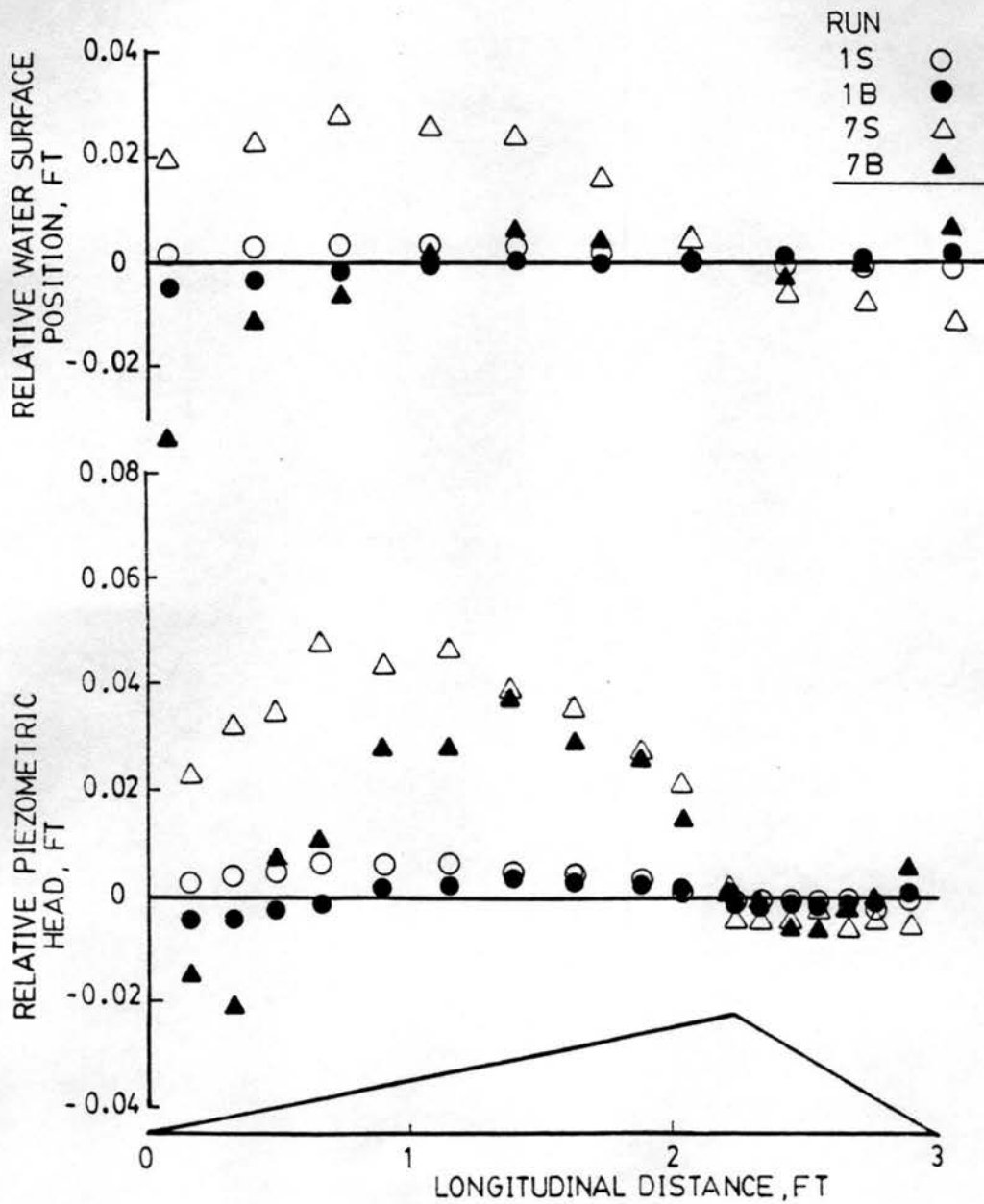


Figure 4.8. Relative Piezometric Head Distribution and Relative Water Surface Profile for Nonuniform, Smooth Bedform Experiment: Runs 1S, 1B, 7S, 7B

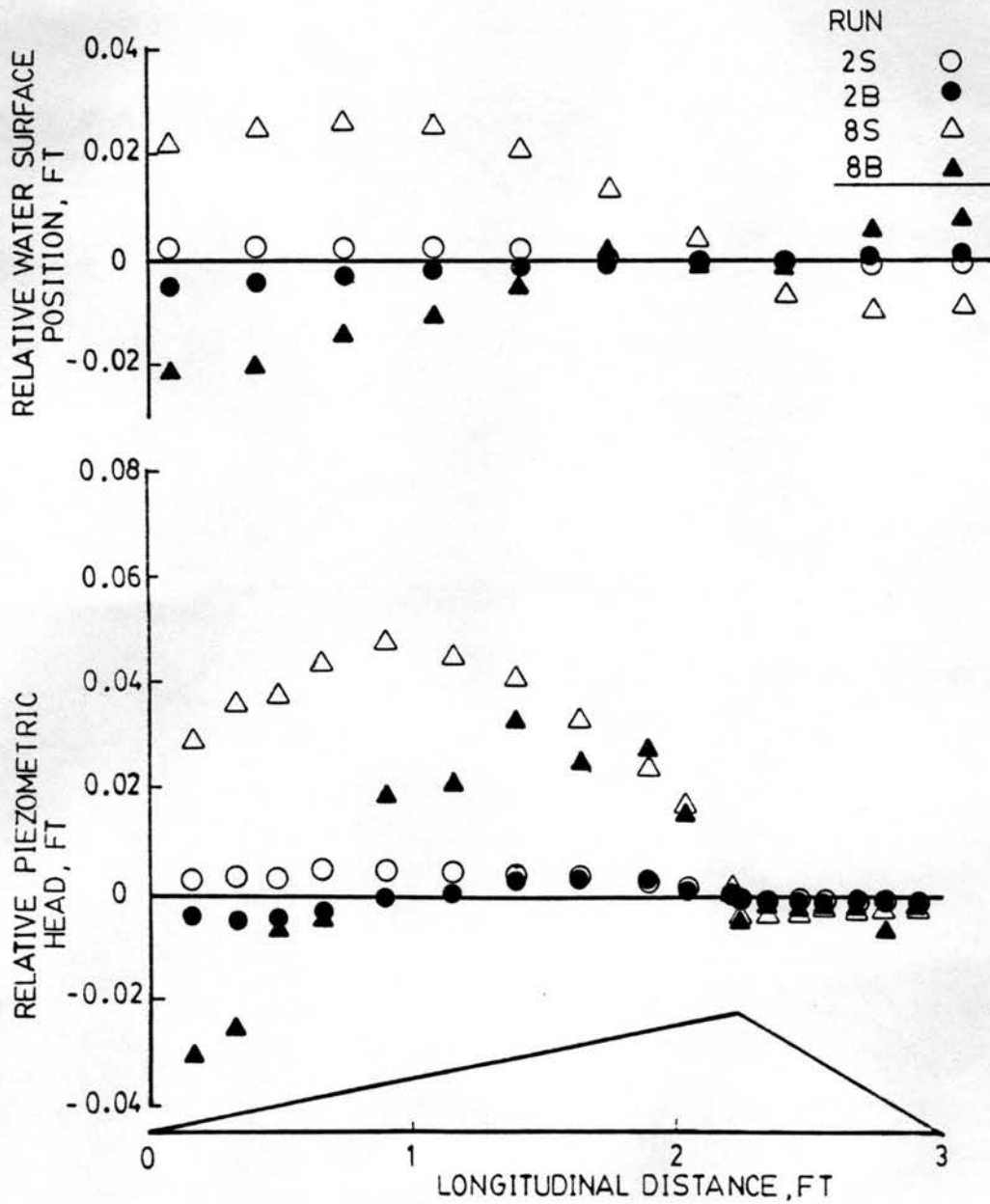


Figure 4.9. Relative Piezometric Head Distribution and Relative Water Surface Profile for Nonuniform, Smooth Bedform Experiment: Runs 2S, 2B, 8S, 8B

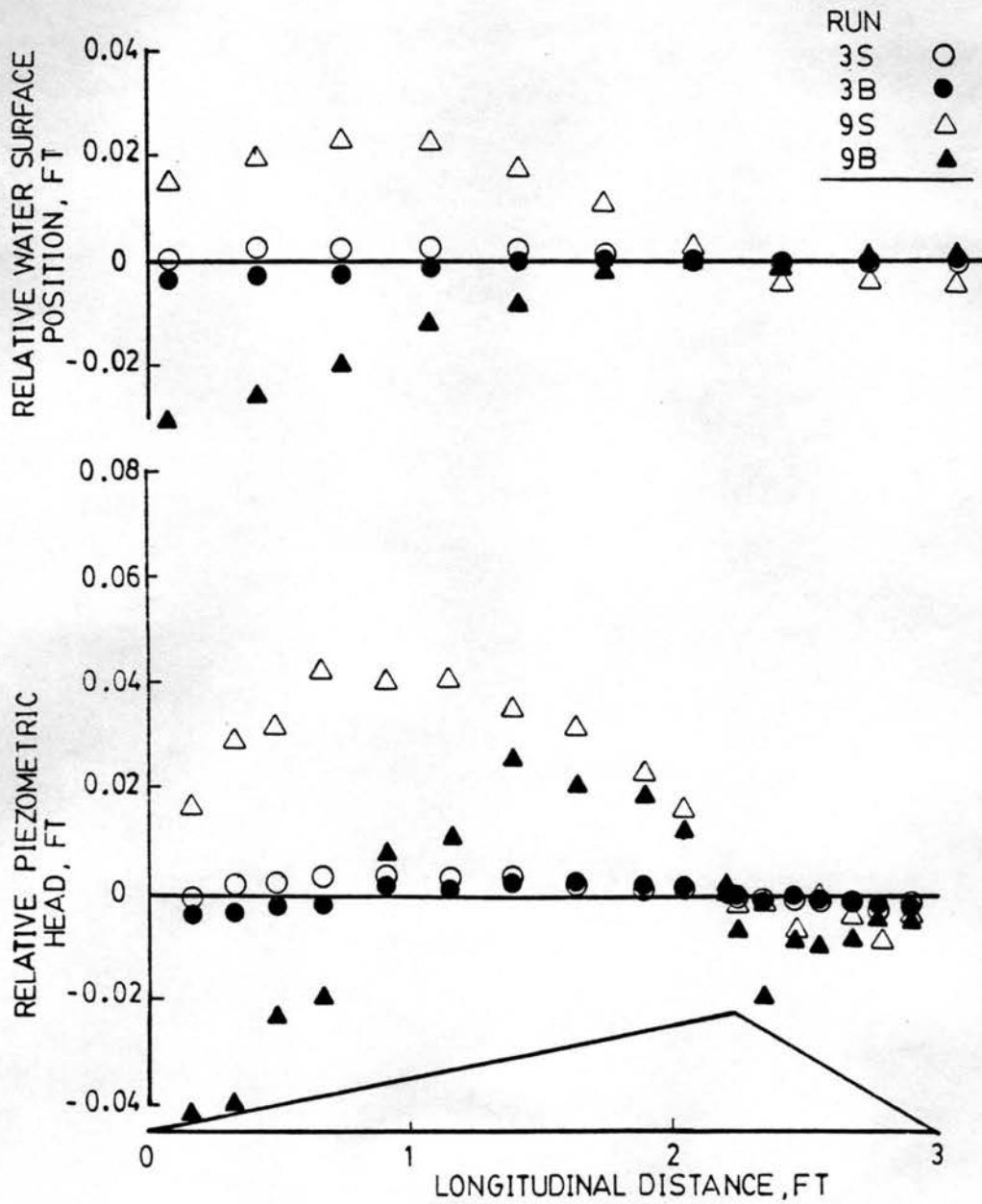


Figure 4.10. Relative Piezometric Head Distribution and Relative Water Surface Profile for Nonuniform, Smooth Bedform Experiment: Runs 3S, 3B, 9S, 9B

location of maximum piezometric head is also the location of reattachment, the results of the present study agree well with those obtained by Engel (1981), who found that for dunes with height-to-length ratios greater than 0.05, the separation length is approximately equal to four times the height of the upstream dune. Engel's study was performed using uniform bedforms, but the piezometric head results of the present study indicate that his observations may be applicable to nonuniform bedforms as well.

An additional observation of note may be made by comparing Figures 4.2-4.4 with Figures 4.5-4.7. These figures indicate that for the same Froude number and flow depth, the piezometric head distributions over smooth and rough bedforms are generally the same. Therefore, the idea of a resistance component based solely on form is supported.

The piezometric head differences listed in Table 4.6 may be adjusted by appropriate flow variables to create a nondimensional relative pressure, ΔP_r , defined as

$$\Delta P_r = \frac{\gamma \Delta h_z}{\frac{1}{2} \rho V^2} \quad (4.6)$$

where γ is the specific weight of the fluid and Δh_z is the relative piezometric head corrected for channel slope effect. Figures 4.11-4.13 illustrate the variation of ΔP_r with longitudinal distance along the bedform for each of the smooth, uniform bedform runs. It may be observed that the nondimensional pressure distribution is generally a single curve for various Froude numbers at constant flow depth. Also, the difference in ΔP_r across the bedform is the greatest for the shallowest flow, and decreases as the flow depth increases. These

NON-DIMENSIONAL RELATIVE PRESSURE

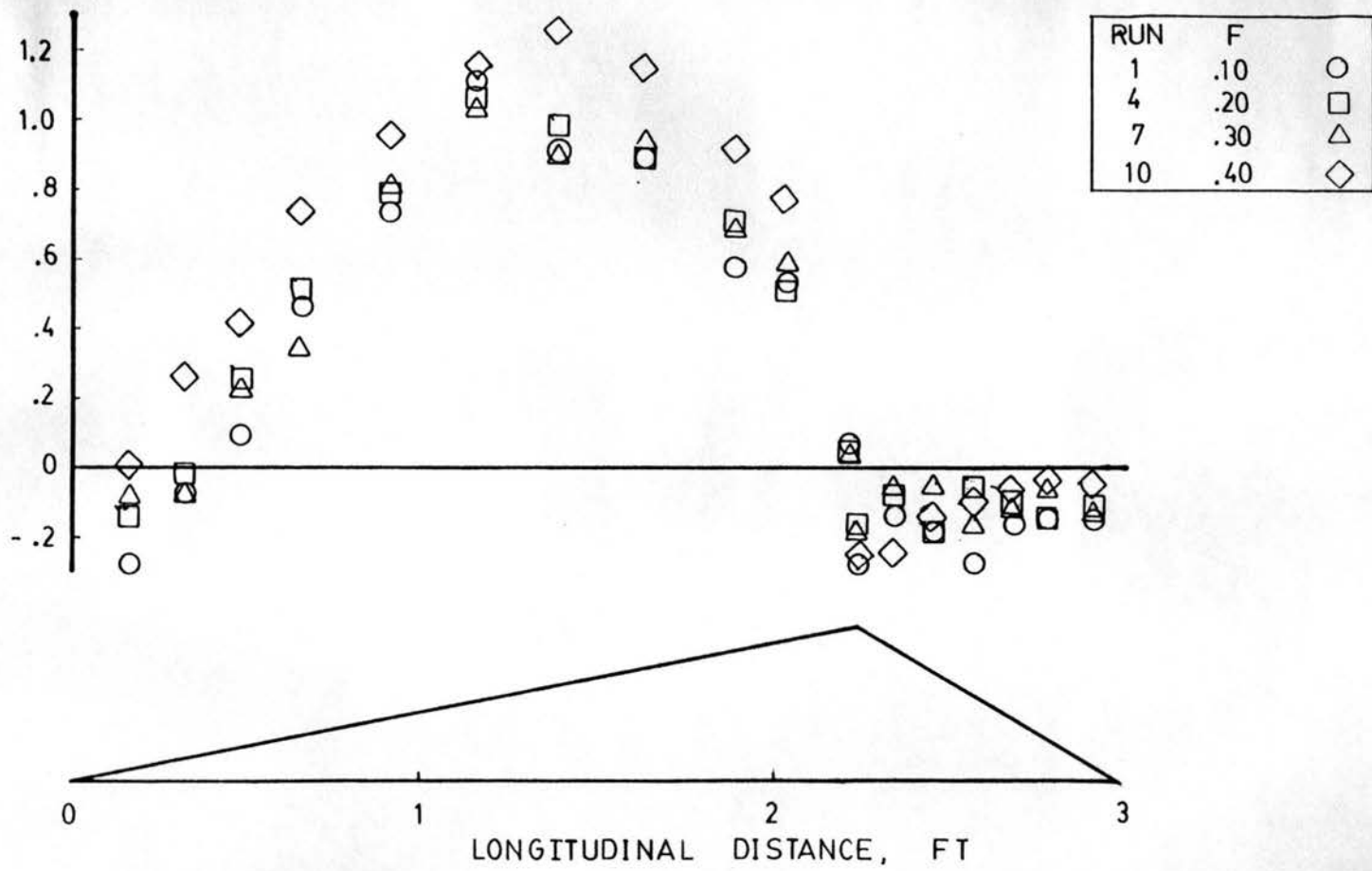


Figure 4.11. Nondimensional Pressure Distribution for Uniform, Smooth Bedform Experiment: Depth at Crest = 6 in

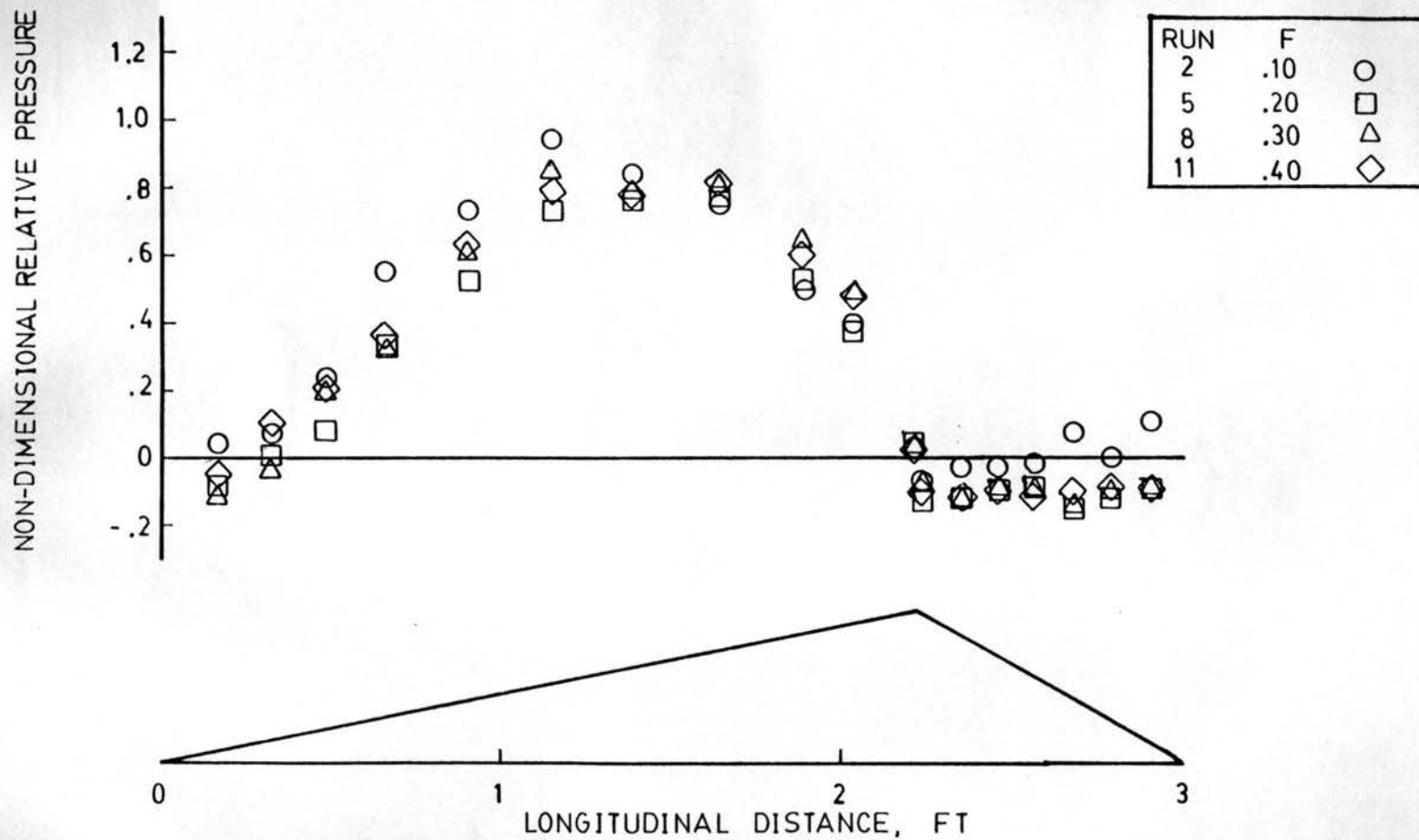


Figure 4.12. Nondimensional Pressure Distribution for Uniform, Smooth Bedform Experiment: Depth at Crest = 8 in

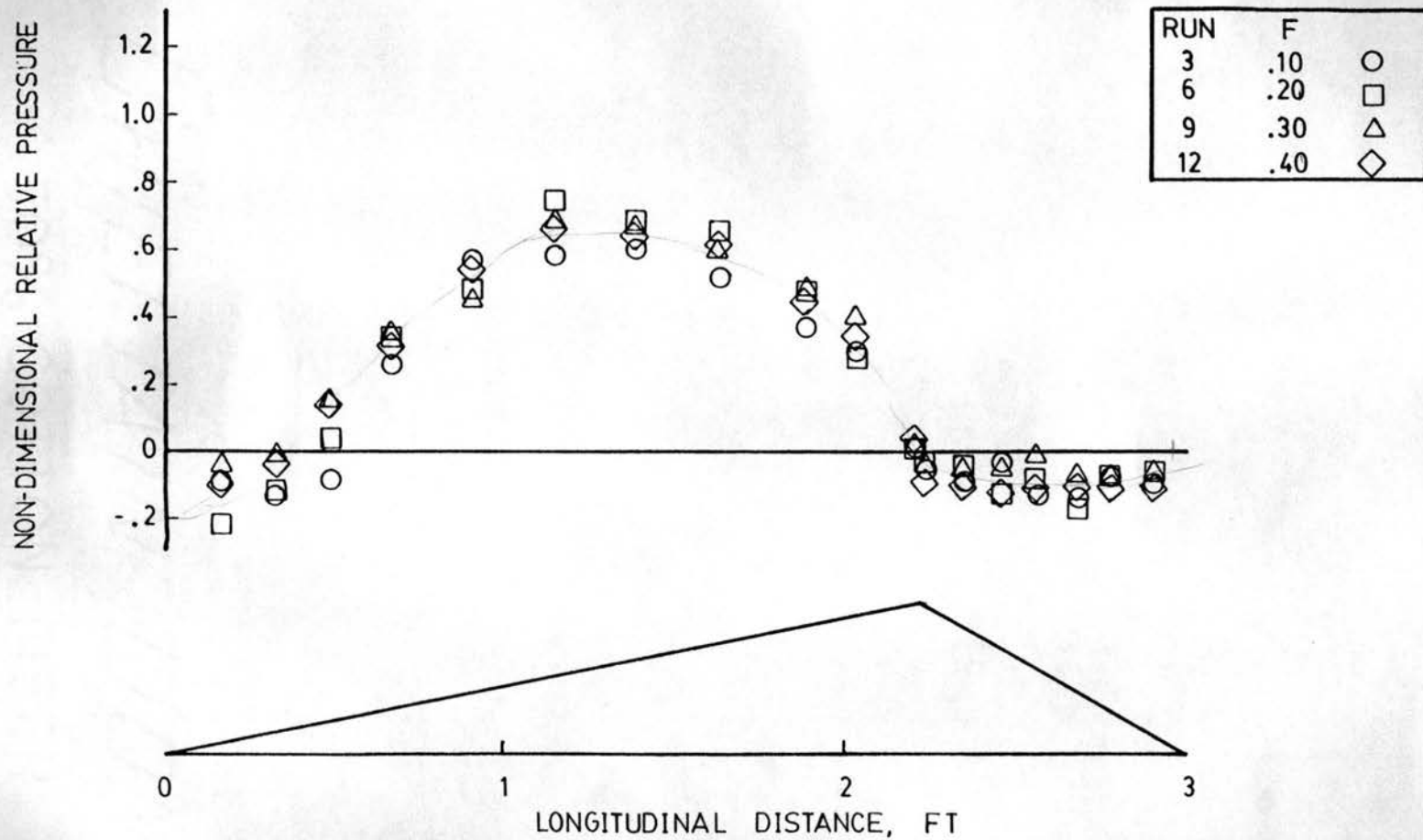


Figure 4.13. Nondimensional Pressure Distribution for Uniform, Smooth Bedform Experiment: Depth at Crest = 10 in

results are in complete agreement with those reported by Vanoni and Hwang (1967) from a study where measurements were made over a naturally formed, stabilized bedform.

4.4 Pressure Drag

A complete discussion of pressure drag and how it may be computed from piezometric head measurement along the surface of a bedform is presented in this section. The majority of this discussion was initially presented by Wang (1984).

The longitudinal variation of the surface pressure along the bedform surface results in an imbalance of pressure force in the longitudinal direction and becomes a resistance force to the flow. The pressure drag is defined as this unbalanced longitudinal pressure force over a unit width of a bedform. Since the resulting longitudinal pressure force is in the downstream direction on the upstream face and in the upstream direction on the downstream face, the pressure drag can be calculated as follows:

$$F_p = \int_0^{s_c} p \sin \theta_u ds - \int_{s_c}^{s_t} p \sin \theta_d ds \quad (4.7)$$

where p is the local surface pressure; s is the distance along the inclined bedform surface from the upstream toe to the local point considered; s_c and s_t are values of s at the crest and downstream heel, respectively; θ_u and θ_d are the upstream and downstream angles relative to the longitudinal direction, respectively; and F_p is the pressure drag taken as positive in the downstream direction. The local surface pressure p can be calculated from the observed piezometric head as follows: referring to Figure 4.14, the piezometric head h'_z

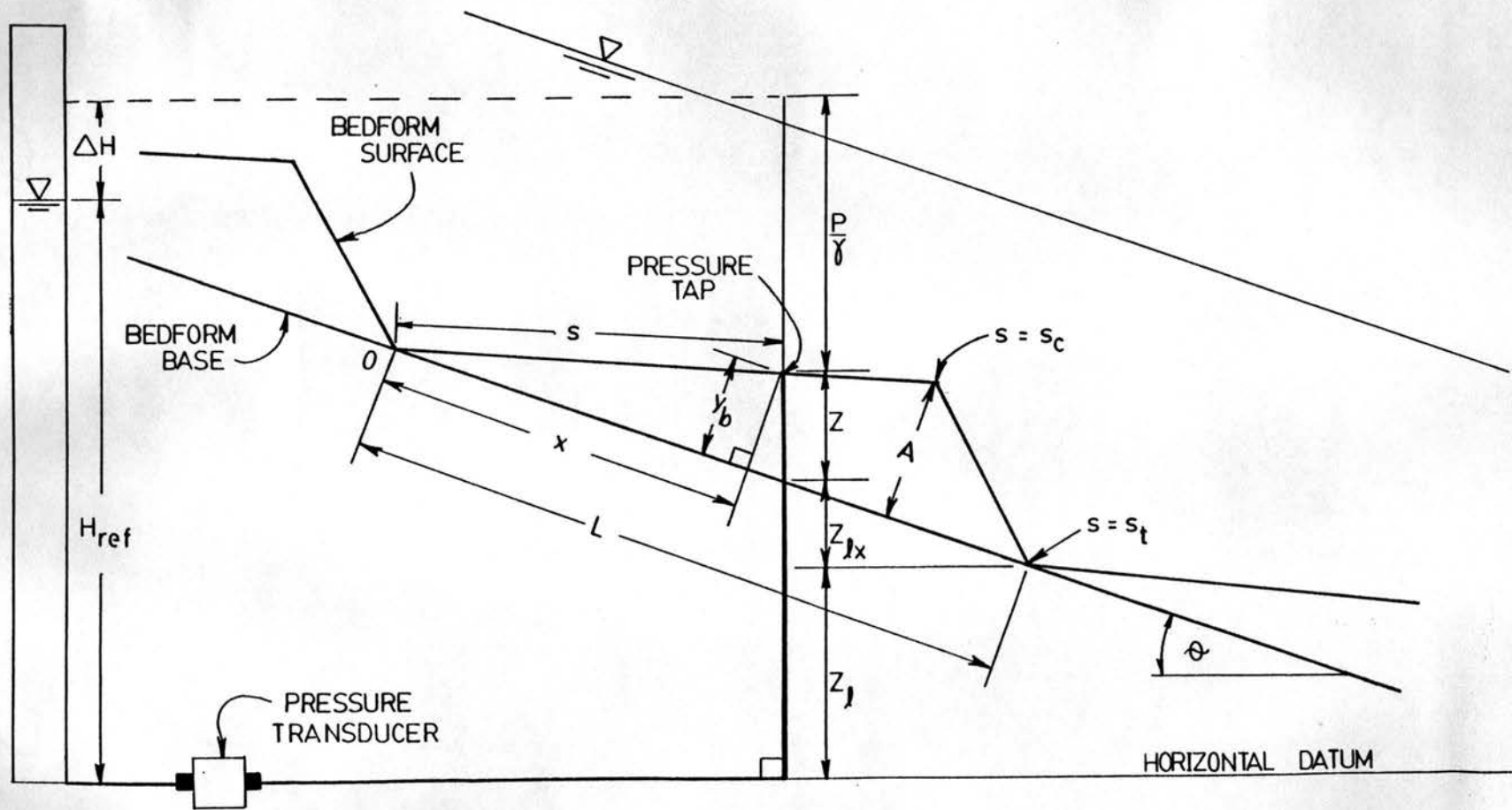


Figure 4.14. Definition Sketch Showing the Variables Used in the Calculation of Pressure Drag

from a horizontal datum and without channel slope correction can be expressed as

$$h'_z = \frac{p}{\gamma} + z + z_{lx} + z_l \quad (4.8)$$

where p is the local surface pressure at the measuring station on the bedform surface with a longitudinal distance (x) parallel to the flume floor from the upstream toe, (z) is the elevation difference in the vertical direction between the measuring station on the bedform surface and the point on the bedform base corresponding to the same longitudinal distance (x) , (z_{lx}) is the elevation difference in the vertical direction between the point on the bedform base at a longitudinal distance x and the downstream heel, and z_l is the elevation difference in the vertical direction at the downstream heel from the horizontal datum. The relation between the pressures transmitted to the two input jacks of the pressure transducer from the reference head source (using water) and the pressure tap on the bedform surface can be expressed as follows

$$h'_z = H_{REF} + \Delta H \quad (4.9)$$

where H_{REF} is the reference constant water head based on the horizontal datum, and ΔH is the head difference between the reference head source and the piezometric head h'_z from the pressure tap on the bedform surface. ΔH was measured by the pressure transducer in the present experiment. The piezometric head h'_{zc} at the crest without channel slope correction can also be expressed as

$$h'_{zc} = \frac{p_c}{\gamma} + z_c + z_{lc} + z_l \quad (4.10)$$

$$\text{and } h'_{z_c} = H_{\text{REF}} + \Delta H_c \quad (4.11)$$

where p_c is the local surface pressure at the crest, z_c and $z_{\ell c}$ are the values of z_x and $z_{\ell x}$ respectively at the crest, and ΔH_c is the value of ΔH at the crest. In the present experiment, ΔH_c was interpolated from nearby measuring stations. The variation of piezometric head along the bedform surface without channel slope correction can be expressed in terms of the local piezometric head h'_z minus the interpolated piezometric head h'_{z_c} at the crest as follows

$$\Delta h'_z = h'_z - h'_{z_c} \quad (4.12)$$

Substituting h'_z from Eq. 4.8 and h'_{z_c} from Eq. 4.10 into Eq. 4.12 yields

$$\Delta h'_z = \frac{p}{\gamma} + z - \left(\frac{p_c}{\gamma} + z_c \right) + (z_{\ell x} - z_{\ell c}) \quad (4.13)$$

In the above equation, the term $(z_{\ell x} - z_{\ell c})$ is the channel slope effect on $\Delta h'_z$ and can be expressed as

$$z_{\ell x} - z_{\ell c} = (x_c - x)S_b \quad (4.14)$$

where S_b is the channel slope. The variation of piezometric head Δh_z along the bedform surface after channel slope correction can be calculated as

$$\Delta h_z = \Delta h'_z - (z_{\ell x} - z_{\ell c}) \quad (4.15)$$

Substituting $(z_{\ell x} - z_{\ell c})$ from Eq. 4.14, and $\Delta h'_z$ from Eq. 4.12 into Eq. 4.15 yields

$$\Delta h_z = h'_z - h'_{z_c} - (x_c - x)S_b \quad (4.16)$$

Substituting h'_z from Eq. 4.9 and h'_{z_c} from Eq. 4.11 into Eq. 4.16 yields

$$\Delta h_z = \Delta H - \Delta H_c - (x_c - x)S_b \quad (4.17)$$

The variation of piezometric head Δh_z on the bedform surface after channel slope correction calculated using Eq. 4.13 are previously summarized in Tables 4.6-4.8. Notice that the same analysis applies to the measurement of water surface profiles using the wall pressure taps. The variation of water surface elevation over the bedform surface after channel slope correction are previously summarized in Tables 4.3-4.5.

Further substituting $\Delta h'_z$ from Eq. 4.13 into Eq. 4.15 yields

$$\Delta h_z = \frac{p}{\gamma} + z - \left(\frac{p_c}{\gamma} + z_c \right) \quad (4.18)$$

The term $(p_c/\gamma + z_c)$ is constant for each experimental run and may be denoted as h_{zc} , i.e.,

$$h_{zc} = \frac{p_c}{\gamma} + z_c \quad (4.19)$$

Substituting h_{zc} from Eq. 4.19 into Eq. 4.18 and rearranging the terms yields

$$p = \gamma(\Delta h_z + h_{zc} - z) \quad (4.20)$$

Referring to Figure 4.14, the variable z can be expressed as

$$z = y_b \cos \theta \quad (4.21)$$

where θ is the inclined angle between the flume floor and a horizontal plane and y_b is the distance perpendicular to the flume floor from the bedform base to the bedform surface. The term y_b may be expressed as

$$y_b = s \sin \theta_u \quad \text{for } 0 \leq s \leq s_c \quad (4.22)$$

$$\text{and } y_b = (s_t - s) \sin \theta_d \quad \text{for } s_c \leq s \leq s_t \quad (4.23)$$

Substituting y_b from Eqs. 4.22 and 4.23, respectively, into Eq. 4.21 yields

$$z = s \sin \theta_u \cos \theta \quad \text{for } 0 \leq s < s_c \quad (4.24)$$

and
$$z = (s_t - s) \sin \theta_d \cos \theta \quad \text{for } s_c \leq s \leq s_t \quad (4.25)$$

In order to calculate the pressure data, local surface pressure p from Eq. 4.20 can be substituted into Eq. 4.7 to yield

$$\begin{aligned} F_p &= \int_0^{s_c} \gamma \Delta h_z \sin \theta_u ds - \int_{s_c}^{s_t} \gamma \Delta h_z \sin \theta_d ds \\ &+ \int_0^{s_c} \gamma h_{zc} \sin \theta_u ds - \int_{s_c}^{s_t} \gamma h_{zc} \sin \theta_d ds \\ &- \int_0^{s_c} \gamma z \sin \theta_u ds + \int_{s_c}^{s_t} \gamma z \sin \theta_d ds \end{aligned} \quad (4.26)$$

The sum of the third and fourth terms on the right hand side of Eq. 4.26 can be shown to go to zero as follows

$$\begin{aligned} \int_0^{s_c} \gamma h_{zc} \sin \theta_u ds - \int_{s_c}^{s_t} \gamma h_{zc} \sin \theta_d ds &= \gamma h_{zc} \sin \theta_u \int_0^{s_c} ds - \gamma h_{zc} \sin \theta_d \int_{s_c}^{s_t} ds \\ &= \gamma h_{zc} \sin \theta_u s_c - \gamma h_{zc} \sin \theta_d (s_t - s_c) \end{aligned} \quad (4.27)$$

Since the bedform height A is related to s_c and $(s_t - s_c)$ as follows

$$A = \sin \theta_u s_c = \sin \theta_d (s_t - s_c) \quad (4.28)$$

Eq. 4.27 can be rewritten as

$$\int_0^{s_c} \gamma h_{zc} \sin \theta_u ds - \int_{s_c}^{s_t} \gamma h_{zc} \sin \theta_d ds = \gamma h_{zc} A - \gamma h_{zc} A = 0 \quad (4.29)$$

The sum of the fifth and sixth terms on the right hand side of Eq. 4.26 can also be shown to go to zero as follows:

$$-\int_0^{s_c} \gamma z \sin \theta_u ds + \int_{s_c}^{s_t} \gamma z \sin \theta_d ds = -\gamma \sin \theta_u \int_0^{s_c} z ds + \gamma \sin \theta_d \int_{s_c}^{s_t} z ds \quad (4.30)$$

Substituting for the appropriate z in Eqs. 4.24 and 4.25 into Eq. 4.30 yields

$$\begin{aligned} & -\int_0^{s_c} \gamma z \sin \theta_u ds + \int_{s_c}^{s_t} \gamma z \sin \theta_d ds \\ &= -\gamma \sin \theta_u \int_0^{s_c} s \sin \theta_u \cos \theta ds + \gamma \sin \theta_d \int_{s_c}^{s_t} (s_t - s) \sin \theta_d \cos \theta ds \\ &= \gamma \cos \theta \left[-\sin^2 \theta_u \frac{s_c^2}{2} + \sin^2 \theta_d \left(s_t^2 - \frac{s_t^2}{2} - s_t s_c + \frac{s_c^2}{2} \right) \right] \\ &= \gamma \cos \theta \left[-\frac{1}{2} s_c^2 \sin^2 \theta_u + \frac{1}{2} (s_t - s_c)^2 \sin^2 \theta_d \right] \end{aligned} \quad (4.31)$$

Rearranging Eq. 4.28 yields

$$\sin \theta_u = \frac{A}{s_c} \quad (4.32)$$

$$\text{and } \sin \theta_d = \frac{A}{s_t - s_c} \quad (4.33)$$

Substituting $\sin \theta_u$ and $\sin \theta_d$ from Eqs. 4.32 and 4.33, respectively, into Eq. 4.31 yields

$$\begin{aligned}
& - \int_0^{s_c} \gamma_z \sin \theta_u ds + \int_{s_c}^{s_t} \gamma_z \sin \theta_d ds \\
& = \gamma \cos \theta \left[-\frac{1}{2} s^2 \left(\frac{A}{s_c}\right)^2 + \frac{1}{2} (s_T - s_c)^2 \left(\frac{A}{s_T - s_c}\right)^2 \right] \\
& = \gamma \cos \theta \left[-\frac{1}{2} A^2 + \frac{1}{2} A^2 \right] = 0
\end{aligned} \tag{4.34}$$

Equation 4.26 therefore can be simplified as follows

$$F_p = \int_0^{s_c} \gamma \Delta h_z \sin \theta_u ds - \int_{s_c}^{s_t} \gamma \Delta h_z \sin \theta_d ds \tag{4.35}$$

Using the values of Δh_z summarized in Tables 4.6-4.8 and using Eq. 4.35, F_p was calculated for each experimental run. These pressure drags are summarized in Table 4.9.

The bed shear stress due to form drag, τ'' , is defined as

$$\tau'' = \frac{F_p}{L} \tag{4.36}$$

and the form friction factor is computed from

$$f'' = \frac{8\tau''}{\rho V^2} \tag{4.37}$$

Computed values of τ'' and f'' for each experimental run of the uniform bedform studies are also presented in Table 4.9. It may be noted that the form shear stress increases with Froude number, while the form friction factor seems to depend only on the depth of flow. This is in agreement with the findings that, for a given flow depth, the curves of nondimensionalized pressure distribution over the bedform are similar for all velocities (see Figures 4.11-4.13). It may also be

Table 4.9. Form Resistance Parameters for the Present Study

Run No.	F_p lb/ft	τ'' lb/ft ²	f''	C_D
1	0.0736	0.0245	0.433	0.722
2	0.0645	0.0215	0.309	0.515
3	0.0586	0.0195	0.236	0.393
4	0.285	0.0950	0.420	0.700
5	0.271	0.0903	0.325	0.542
6	0.275	0.0917	0.277	0.462
7	0.625	0.208	0.408	0.680
8	0.651	0.217	0.347	0.578
9	0.588	0.196	0.263	0.438
10	1.451	0.484	0.535	0.892
11	1.152	0.384	0.345	0.575
12	1.161	0.387	0.292	0.487
1R	0.0726	0.0242	0.428	0.713
2R	0.0532	0.0177	0.254	0.423
3R	0.0569	0.0190	0.230	0.383
7R	0.577	0.192	0.377	0.628
8R	0.613	0.204	0.326	0.543
9R	0.520	0.173	0.232	0.387
1S	0.138	0.0460	---	---
2S	0.118	0.0393	---	---
3S	0.0992	0.0331	---	---
7S	1.098	0.366	---	---
8S	1.060	0.353	---	---
9S	0.938	0.313	---	---
1B	0.0411	0.0137	---	---
2B	0.0257	0.0086	---	---
3B	0.0366	0.0122	---	---
7B	0.500	0.167	---	---
8B	0.420	0.140	---	---
9B	0.221	0.737	---	---

observed that the form shear stress does not depend on the roughness of the bedform model. For experimental runs of equal Froude number and flow depth, the majority of form drags calculated for the rough bedform experiment are within ten percent of those calculated for the smooth bedform experiment. The rough bedform form drags were consistently smaller than calculated for the smooth bedform experimental runs of equal flow conditions. However, this trend was most likely due to systematic errors associated with measurement. As stated in Chapter 3, the pressure distribution was measured on the third plastic bedform during the rough bedform study, as compared to the test bedform used for all other experimental runs. Slight differences in alignment and geometry, as well as a possible effect due to sand grains sheltering the pressure taps of the rough bedform, may have all led to systematic errors of the magnitude noted. Thus, within the range of the present study, form drag is observed to depend only on the gross geometry of the bedform and the flow conditions. The surface roughness is observed to have no significant effect on form drag.

The size of the upstream bedform had a significant effect on the form drag of the test bedform, as can be seen by the results of the nonuniform study contained in Table 4.9. During this experiment the bedform immediately upstream of the test bedform was replaced with a bedform of different scale, and the discharge, slope, and tilt-gate setting characteristic to a given uniform bedform experimental run was repeated. For the runs using a smaller scale upstream bedform, the form drag of the test dune was observed to be approximately 1.8 times the form drag observed during the corresponding run of the uniform study, on average. When the larger scale upstream bedform was in

place, this multiplier was reduced to approximately 0.56, or 1/1.8, on average. As discussed in Chapter 3 of his thesis, the scale factor used in constructing the modified upstream bedforms was $\sqrt{2}$. The height and length of the test bedform were multiplied by $\sqrt{2}$ to construct the larger bedform, and multiplied by $1/\sqrt{2}$ to create the smaller bedform. Based on the measured form drags for the nonuniform studies, it appears that the change in form drag due to change in scale of the upstream bedform is related to the scale factor. Multiplying the dimensions of the uniform upstream bedform by $\sqrt{2}$ resulted in the uniform form drag of the test bedform being divided by 1.8. Dividing the dimensions of the uniform upstream bedform by $\sqrt{2}$ resulted in the uniform form drag of the test bedform being multiplied by 1.8. Only further experimentation will determine whether this trend is characteristic for all scale factors.

The characteristics of pressure drag may be studied through the use of the pressure drag coefficient, C_D , defined as

$$C_D = \frac{F_p}{\frac{1}{2} \rho V^2 A} \quad (4.38)$$

where A is the bedform height. The calculated pressure drag coefficients for the uniform bedform studies are included in Table 4.9. Combining Eqs. 4.37 and 4.38 yields

$$C_D = \frac{1}{4} f'' \frac{L}{A} \quad (4.39)$$

and thus, for bedforms of constant geometry, the pressure drag coefficient and form friction factor are proportional. As observed in Table 4.9, the pressure drag coefficient is seemingly independent of Froude number and is inversely related to flow depth. These findings

are in agreement with those reported by Vanoni and Hwang (1967), Rifai and Smith (1969) and Wang (1984). In order to determine the form of the relation between the pressure drag coefficient and flow depth, data from a number of published studies was collected and plotted as shown in Figure 4.15. The pressure drag coefficient is plotted against relative roughness, A/D , in which A is the bedform height and D is the average flow depth. Data from studies using natural and artificial bedforms, all stabilized, with bedform steepness ratios (A/L) ranging between 0.05 and 0.17 are presented. Pressure distributions reported by Raudkivi (1963), Vanoni and Hwang (1967), Rifai and Smith (1967) were integrated by Wang (1984), and Figure 4.15 contains the pressure drag coefficients based on these integrations. Figure 4.15 also illustrates the relations developed by Vittal et al. (1977), over the range of relative roughnesses used in their study. These investigators proposed the following relation:

$$C_D = m \left(\frac{A}{D} \right)^{3/8} \quad (4.40)$$

where m is a variable dependent only on the steepness ratio of the bedform. The reported m values ranged between 0.36 and 0.53, and seemed to vary randomly for different bedform geometries. The reported values of m fall within twenty percent of a mid-range value of $4/9$. This scatter about the mid-range is approximately equal to the scatter observed using data from Wang (1984), Vanoni and Hwang (1967) and the present study, for bedforms of constant geometry. This may be illustrated by drawing a best-fit line through the data points for which A/D is greater than 0.34 and two additional lines representing C_D values 20 percent greater and less than the best fit values, as shown

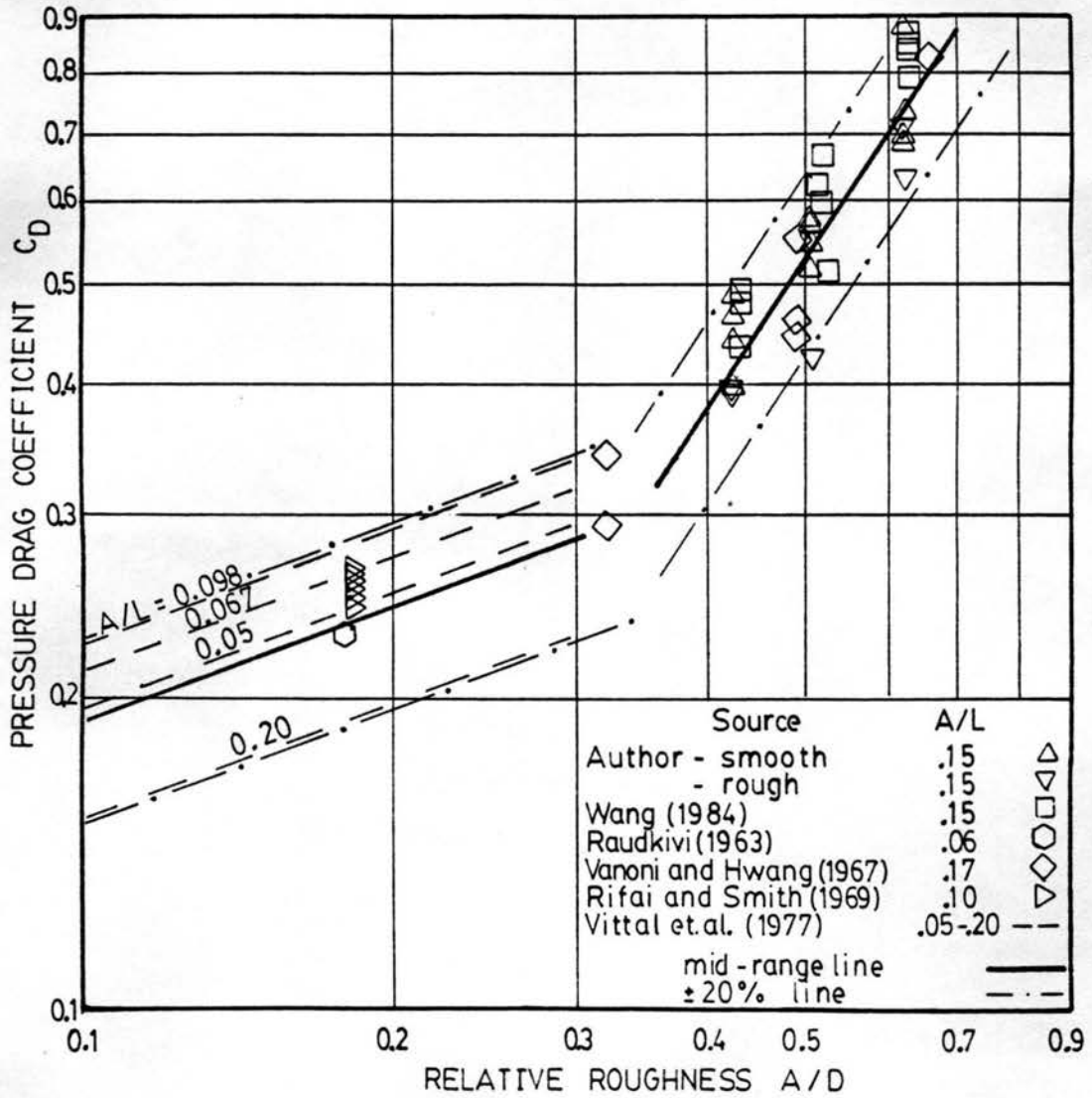


Figure 4.15. Variation of Pressure Drag Coefficient with Relative Roughness

in Figure 4.15. Equation 4.35, with a mid-range m value of $4/9$ is shown plotted for A/D less than 0.34, also with accompanying ± 20 percent lines. Because the variability of the pressure drag coefficient seems to be plus or minus 20 percent of the mean value for bedforms of constant geometry, the practice of varying m with the steepness ratio of the bedform may not be justified.

In order to more clearly illustrate the variation of pressure drag coefficient with relative roughness, Figure 4.16 was plotted using average C_D values. Where more than one pressure drag coefficient was reported for a given relative roughness value, the mean C_D value was determined and plotted. The data reported by Vittal et al. (1977) is represented by a single line using the proposed relation (Eq. 4.40) with a mid-range m value of $4/9$. As indicated in Figure 4.16, the pressure drag coefficient may be best related to the relative roughness using two different equations. The validity of Eq. 4.40 with m equal to $4/9$ is verified by data from Raudkivi (1963), Rifai and Smith (1969) and Vanoni and Hwang (1967), for relative roughness values less than about 0.35. For relative roughness greater than 0.35 a completely different relation is indicated. A power relation of the form of Eq. 4.40 with an exponent of $3/2$ and m value of $3/2$ seems to fit the data well. Note that these two curves intersect at a relative roughness value of 0.34.

In summary, two separate power relations may be used to estimate the pressure drag coefficient for given relative roughness values. The pressure drag coefficient may be calculated using the following relations:

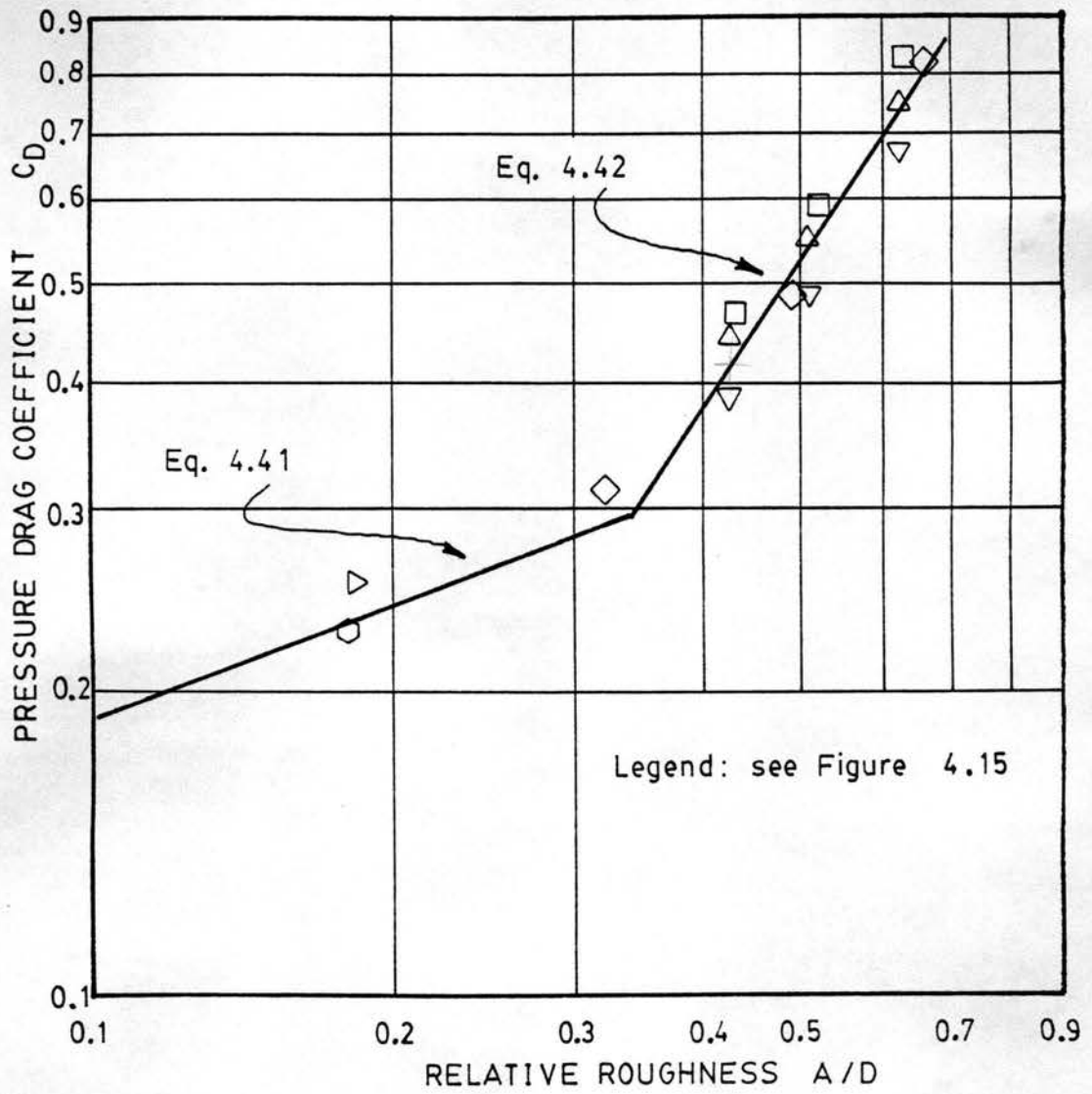


Figure 4.16. Variation of Average Pressure Drag Coefficient with Relative Roughness

$$C_D = 4/9 \left(\frac{A}{D}\right)^{3/8} \quad \text{for } \frac{A}{D} \leq 0.34 \quad (4.41)$$

and
$$C_D = 3/2 \left(\frac{A}{D}\right)^{3/2} \quad \text{for } \frac{A}{D} \geq 0.34 \quad (4.42)$$

The form friction factor can be computed from the pressure drag coefficient and bedform steepness ratio as follows:

$$f'' = 4 C_D \frac{A}{L} \quad (4.43)$$

which is a rearrangement of Eq. 4.39. Hence, the pressure drag coefficient may be determined from a given value of relative roughness, but for computation of the form friction factor, the bedform steepness ratio must also be known.

4.5 Skin Shear

Local shear stress on the test bedform surface was measured using a large diameter pitot tube. Measurements were made along the upstream face of the test bedform at a number of locations between the reattachment point and crest. Shear stress within the separation region was not considered in this study.

The use of pitot tubes for shear stress measurements is well known in hydraulic research. Preston (1954), Hsu (1955), Ippen et al. (1960), Raudkivi (1963), Patel (1965), and Vittal et al. (1977) have used modified pitot tubes for the measurement of shear stress on a variety of boundaries. The various techniques are all based on the principle that if the velocity distribution is known or can be estimated at the location of study, then the shear stress may be related to the differential head measured with a pitot tube at that location. A preliminary study involving flow over a long ramp with similar geometry to the bedforms used for the present experiments, indicated that the

calibration technique used by Ippen et al. (1960), could also be applied in the case of contracting flow. This technique was used for shear measurement in all runs of the present study, and was verified by measured velocity profiles which are presented later in this report.

4.5.1 Uniform, Smooth Bedform Experiment

For the smooth study, the assumed boundary layer velocity equation was

$$\frac{u}{u_x'} = 8.61 \left(\frac{u_x' y}{\nu} \right)^{1/7} \quad (4.44)$$

From Eq. 4.44, the shear stress may be related to the differential head measured by a 0.25 inch diameter pitot tube placed on the boundary by the following equation:

$$\tau_x' = 2.64 \rho \nu^{1/4} \Delta H_x^{1/8} \quad (4.45)$$

as derived by Ippen et al. (1960), where ΔH_x is the differential head in feet of water, and τ_x' is the local shear stress. The differential head was measured at an average of 12 locations along the upstream face for each experimental run of the smooth, uniform bedform study. The data was converted to shear stress using Eq. 4.45. A summary of this converted data is presented in Table 4.10.

The variation of shear stress along the upstream face of a bedform may be studied through the use of a local skin shear coefficient, C_f , defined as

$$C_f = \frac{\tau_x'}{\frac{1}{2} \rho V_x^2} \quad (4.46)$$

Table 4.10. Summary of Shear Stress Distributions for Uniform, Smooth Bedform Experiment

x ft	τ'_x , lb/ft ²					
	Run 1	Run 2	Run 3	Run 4	Run 5	Run 6
2.182	0.00409	0.00395	0.00433	0.0132	0.0142	0.0143
2.082	0.00328	0.00347	0.00339	0.0112	0.0106	0.0112
1.982	0.00287	0.00289	0.00274	0.00976	0.00910	0.00865
1.882	0.00244	0.00264	0.00249	0.00858	0.00762	0.00795
1.782	0.00188	0.00209	0.00211	0.00672	0.00655	0.00676
1.682	0.00170	0.00165	0.00158	0.00570	0.00500	0.00618
1.582	0.00143	0.00137	0.00149	0.00547	0.00500	0.00559
1.482	0.00110	0.00070	0.00108	0.00446	0.00408	0.00327
1.382	0.00085	0.00059	0.00069	0.00329	0.00337	0.00331
1.282	0.00070	0.00038	0.00026	0.00206	0.00227	0.00127
1.182	---	0.00015	---	0.00086	0.00201	0.000639
1.082	---	---	---	-.00060	0.00184	0.000484

Table 4.10. Summary of Shear Stress Distributions for Uniform, Smooth Bedform Experiment (continued)

x ft	τ'_x , lb/ft ²					
	Run 7	Run 8	Run 9	Run 10	Run 11	Run 12
2.182	0.0276	0.0302	0.0316	0.0452	0.0459	0.0470
2.082	0.0230	0.0228	0.0241	0.0323	0.0334	0.0354
1.982	0.0188	0.0204	0.0212	0.0276	0.0295	0.0303
1.882	0.0153	0.0180	0.0175	0.0253	0.0241	0.0268
1.782	0.0146	0.0144	0.0143	0.0191	0.0219	0.0224
1.682	0.0123	0.0143	0.0128	0.0166	0.0181	0.0182
1.582	0.00956	0.0118	0.00981	0.0136	0.0159	0.0166
1.482	0.00784	0.00858	0.00939	0.00949	0.0128	0.0150
1.382	0.00678	0.00759	0.00740	0.00952	0.00750	0.0100
1.282	0.00308	0.00545	0.00643	0.00830	0.00729	0.00950
1.182	0.00232	0.00183	0.00193	0.00426	0.00482	0.00666
1.082	0.00166	0.000233	0.00137	0.00232	0.00318	0.00523

where V_x is the average velocity at position x . The Blasius equation, empirically determined for flow in smooth pipes, relates the local skin friction factor, f'_x , to the Reynolds number, R_N , as follows:

$$f'_x = \frac{0.316}{R_N^{0.25}} \quad (4.47)$$

In Eq. 4.47, the local skin friction factor is defined as

$$f'_x = \frac{8 \tau'_x}{\rho V_x^2} \quad (4.48)$$

and the Reynolds number is given by

$$R_N = \frac{q}{\nu} \quad (4.49)$$

where q is the discharge per unit width. Combining Eqs. 4.46 and 4.48 yields

$$C_f = \frac{1}{4} f'_x \quad (4.50)$$

and the Blasius equation may be rewritten as

$$C_f = \frac{0.079}{R_N^{0.25}} \quad (4.51)$$

The local skin shear coefficients were computed for each shear stress value contain in Table 4.10 using Eq. 4.46, and are shown plotted against the Reynolds number in Figure 4.17. The local shear stress was measured at identical locations along the bedform surface for each of the 12 experimental runs. Each section of Figure 4.17 represents a different position along the surface of the bedform, and x is the longitudinal distance of this position from the upstream toe. The Blasius equation (Eq. 4.51) is plotted in each section for comparison.

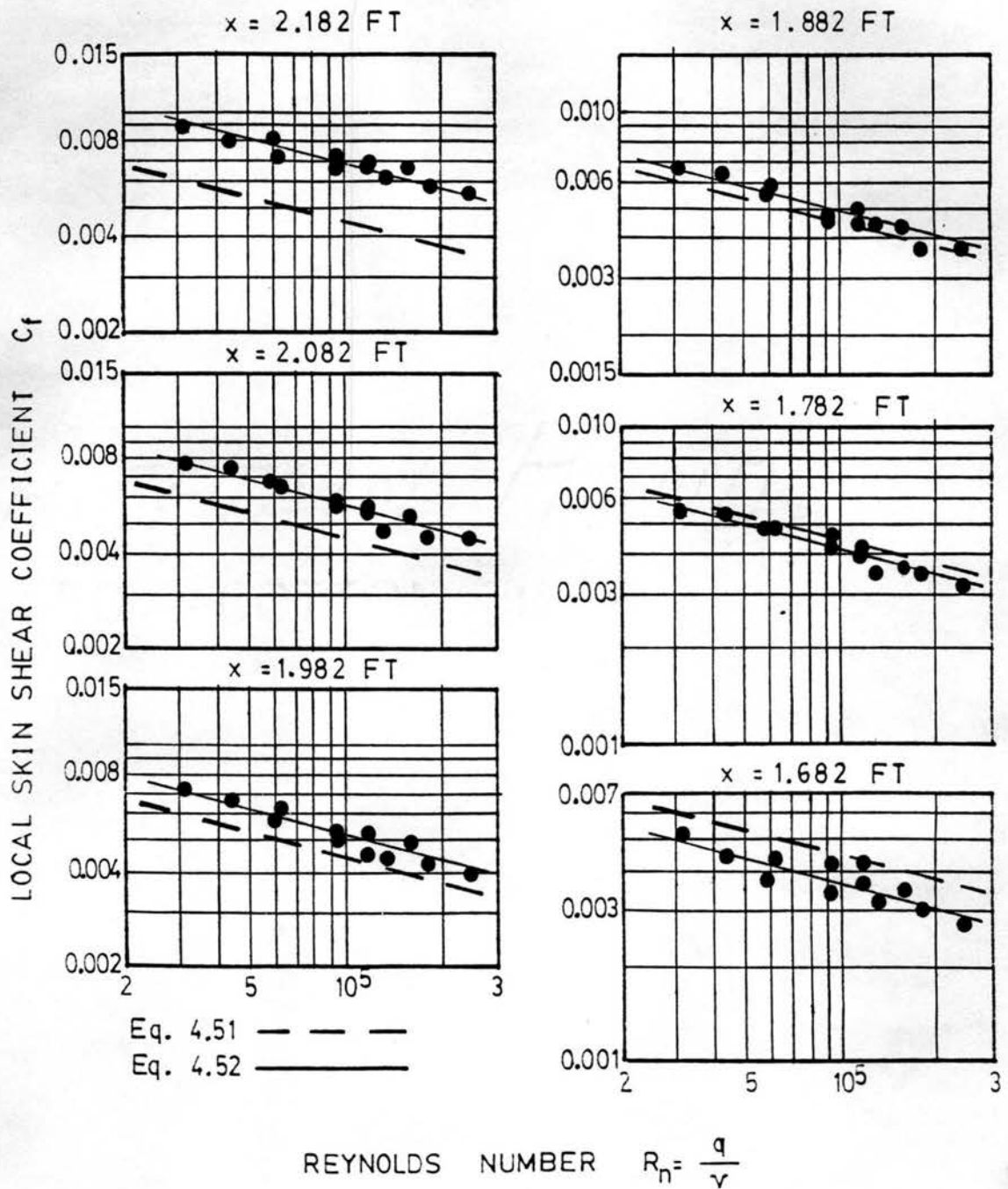


Figure 4.17. Variation of Local Skin Shear Coefficient with Reynolds Number and Position for Uniform, Smooth Bedform Experiment

Figure 4.17 illustrates that the skin shear coefficient is related to the same power of Reynolds number as reported by Blasius for the six positions shown. Although all the measured data is not presented in this figure, the same trend was observed at each measurement position along the bedform surface. The scatter of the data was observed to increase as x decreased. However, the scatter is to be expected due to the unsteady nature of flow near the reattachment point. In general, the measured data fit the following relation:

$$C_f = \frac{B}{R_N^{0.25}} \quad (4.52)$$

where B is a variable whose value depends on the position along the bedform surface. The variable B was determined from nine of the measurement positions, and these values are illustrated in Figure 4.18. A best fit line was determined for these data points, and it was found that the equation

$$B = 0.091x - 0.085 \quad (4.53)$$

where x is the longitudinal distance from the upstream toe in feet, fairly represents the data. Note that this equation yields a zero value for B , and therefore τ_x , at $x = 0.93$ ft, which corresponds to a distance 3.8 times the height of the bedform from the upstream crest. This zero shear location is comparable to the location of maximum piezometric head observed during the same study and agrees well with the position of reattachment predicted by Engel (1981).

Combining Eqs. 4.53, 4.52 and 4.46 yields after some manipulation

$$\tau_x = \frac{\frac{1}{2} \rho v^{1/4} q^{7/4} (0.091x - 0.085)}{(D_c + A - x \tan 11.5^\circ)^2} \quad (4.54)$$

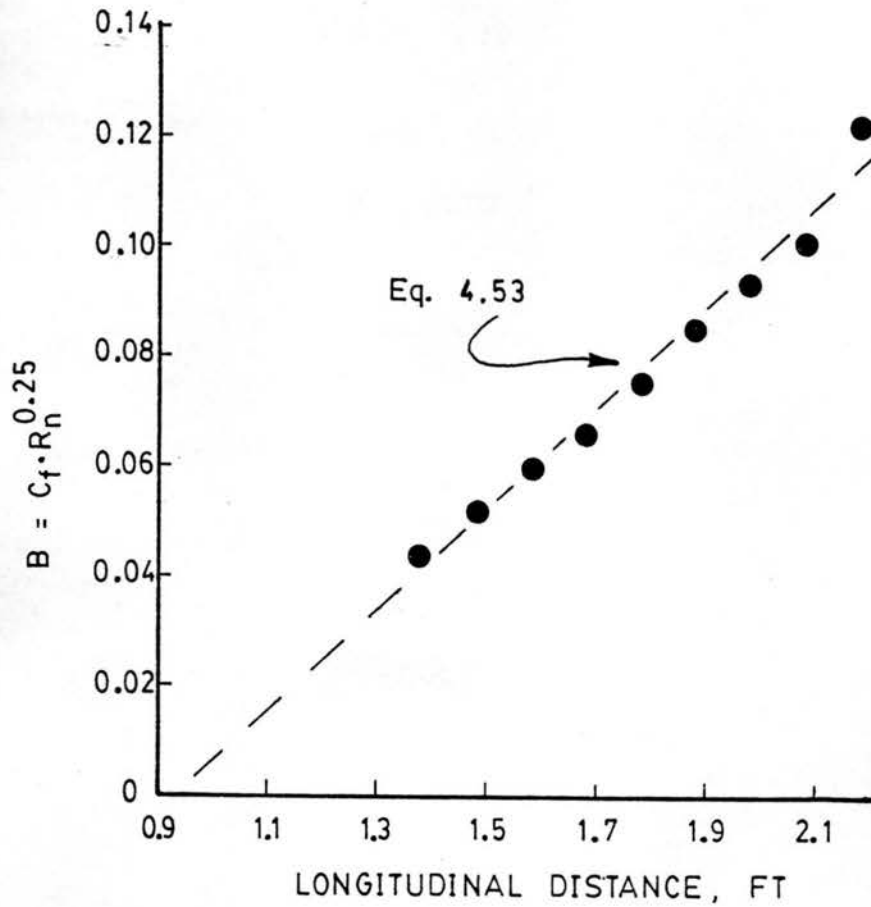


Figure 4.18. Variation of B with Position along the Bedform Surface for Uniform, Smooth Bedform Experiment

This equation may be used to estimate the local shear stress at any position along the surface of the bedform downstream of the reattachment point and upstream of the crest. Equation 4.54 and the data presented in Table 10 are plotted for comparison in Figures 4.19-4.21.

In order to determine the force due to skin shear acting on the bedform, the measured shear stress values were integrated over the bedform surface, and the component of this force in the longitudinal direction was determined. Neglecting small shear stresses present within the separation region, the longitudinal force per unit width due to skin shear, F_s , may be determined as

$$F_s = \int_{s_r}^{s_c} \tau_x \cos \theta_u ds \quad (4.55)$$

where s is the distance along the inclined bedform surface from the upstream toe to the local point considered, s_r and s_c are values of s at the reattachment point and crest, respectively, and θ_u is the upstream angle of the bedform relative to the longitudinal direction. Since s and x may be related by the equation

$$ds = \frac{dx}{\cos \theta} \quad (4.56)$$

Equation 4.50 may be rewritten as

$$F_s = \int_{x_r}^{x_c} \tau_x dx \quad (4.57)$$

where x_r and x_c are the values of x at the reattachment point and crest respectively. Equation 4.57 was used to determine the longitudinal force due to skin shear acting on the test bedform for each experimental run using the data presented in Table 4.10. The results are presented in Table 4.11.

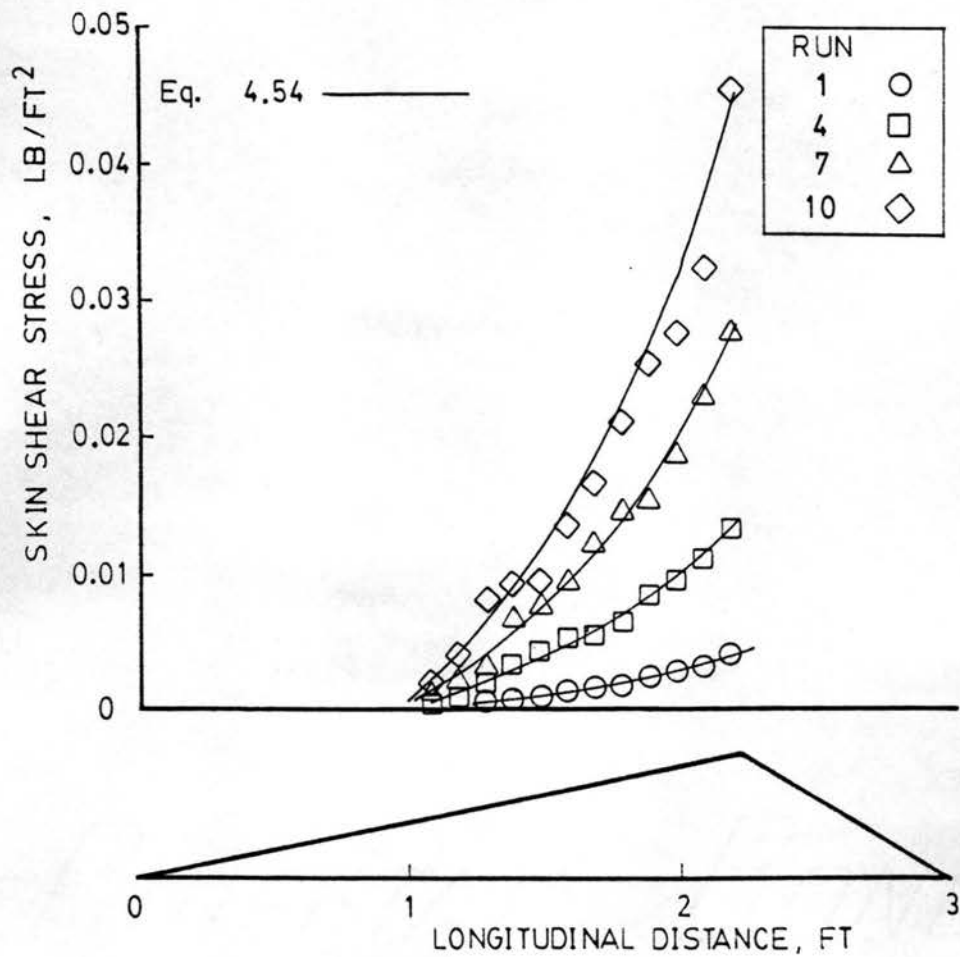


Figure 4.19. Shear Stress Distribution for Uniform, Smooth Bedform Experiment: Depth at Crest = 6 in

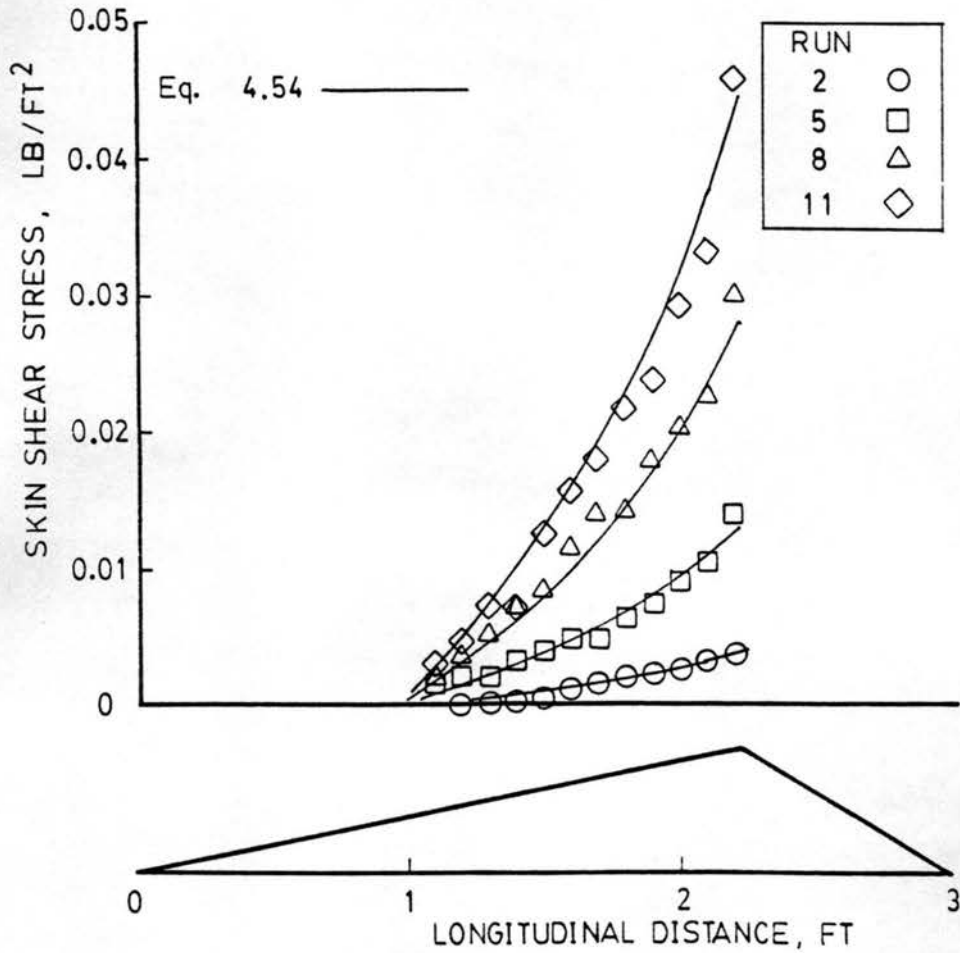


Figure 4.20. Shear Stress Distribution for Uniform, Smooth Bedform Experiment: Depth at Crest = 8 in

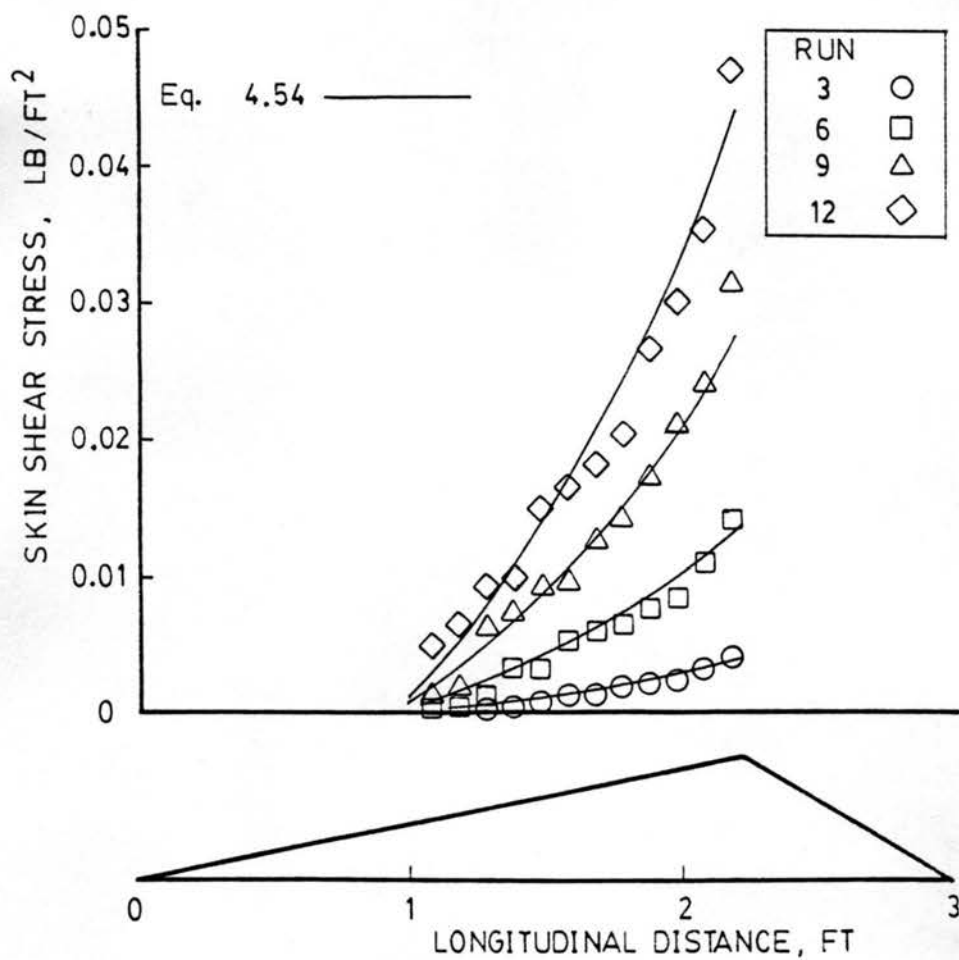


Figure 4.21. Shear Stress Distribution for Uniform, Smooth Bedform Experiment: Depth at Crest = 10 in

Table 4.11. Skin Resistance Parameters for the Uniform, Smooth Bedform Experiment

Run No.	F_s lb/ft	τ' lb/ft ²	f' Measured	f'^* Computed
1	0.00197	0.000657	0.0117	0.0115
2	0.00194	0.000647	0.00929	0.00980
3	0.00199	0.000663	0.00802	0.00863
4	0.00706	0.00235	0.0104	0.00975
5	0.00696	0.00232	0.00834	0.0811
6	0.00684	0.00228	0.00690	0.00725
7	0.0140	0.00467	0.00917	0.00879
8	0.0153	0.00510	0.00814	0.00765
9	0.0155	0.00517	0.00695	0.00671
10	0.0211	0.00703	0.00777	0.00803
11	0.0221	0.00737	0.00662	0.00683
12	0.0239	0.00797	0.00603	0.00604

f'^* was computed using Eq. 4.60.

The bed shear stress due to skin shear, τ' , is defined as

$$\tau' = \frac{F_s}{L} \quad (4.58)$$

and the bed skin friction factor, f' , is computed from

$$f' = \frac{8 \tau'}{\rho V^2} \quad (4.59)$$

Computed values of τ' and f' are also contained in Table 4.11.

Equation 4.54 may be substituted into Eq. 4.57 and an equation relating F_s to bedform geometry and flow parameters would result. However, since the local skin shear coefficient was found to be related to the Reynolds number only for a given measurement position, the bed skin friction factor should be similarly related to the Reynolds number. In fact, it was found that the equation

$$f' = \frac{0.106}{R_N^{0.25} \frac{D_c}{D}} \quad (4.60)$$

fit the measured f' values very well. The values of bed skin friction factor as computed by Eq. 4.60 are included in Table 4.11. The measured values of f' are compared to Eq. 4.60 in Figure 4.22.

In the uniform, smooth bedform experiment, the total force, the skin shear, and the form drag acting on the test bedform were each independently measured. The values of each of these force quantities have been presented in Tables 4.2, 4.9 and 4.11, respectively. The total force is shown compared to the sum of the skin shear and form drag for each experimental run of the uniform smooth bedform study in Figure 4.23. The present data indicates that the practice of separating flow resistance into the skin and form components is valid, and that these two components together account for the total resistance to flow of modeled alluvial bedforms.

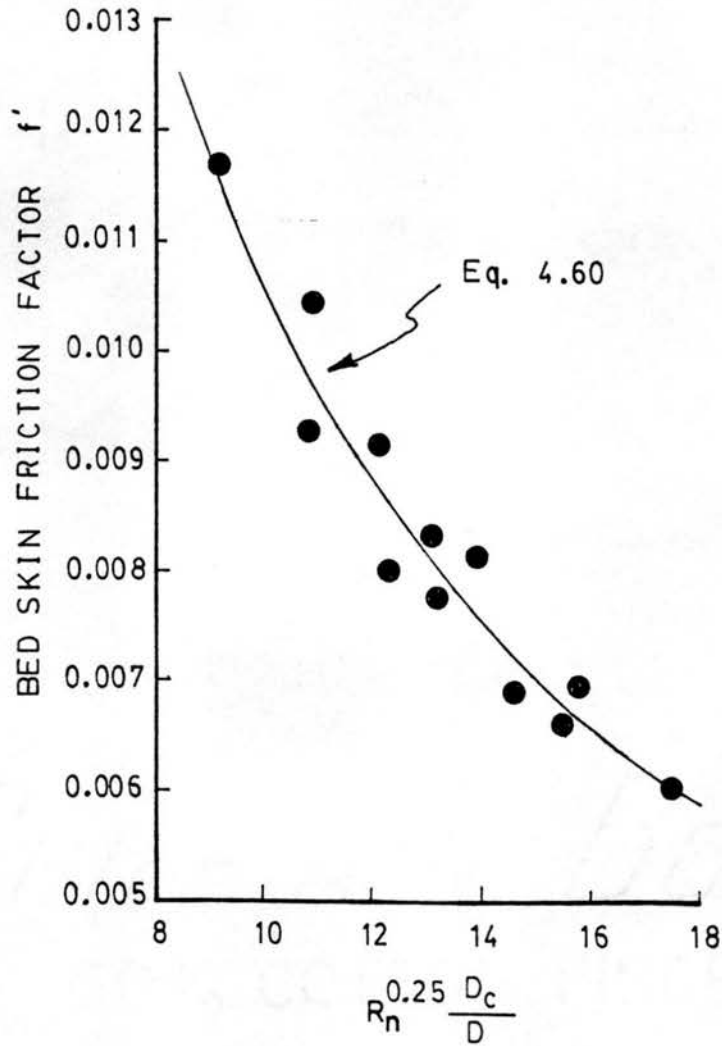


Figure 4.22. Comparison of Measured Bed Skin Friction Factor with Equation 4.60 for Uniform, Smooth Bedform Experiment

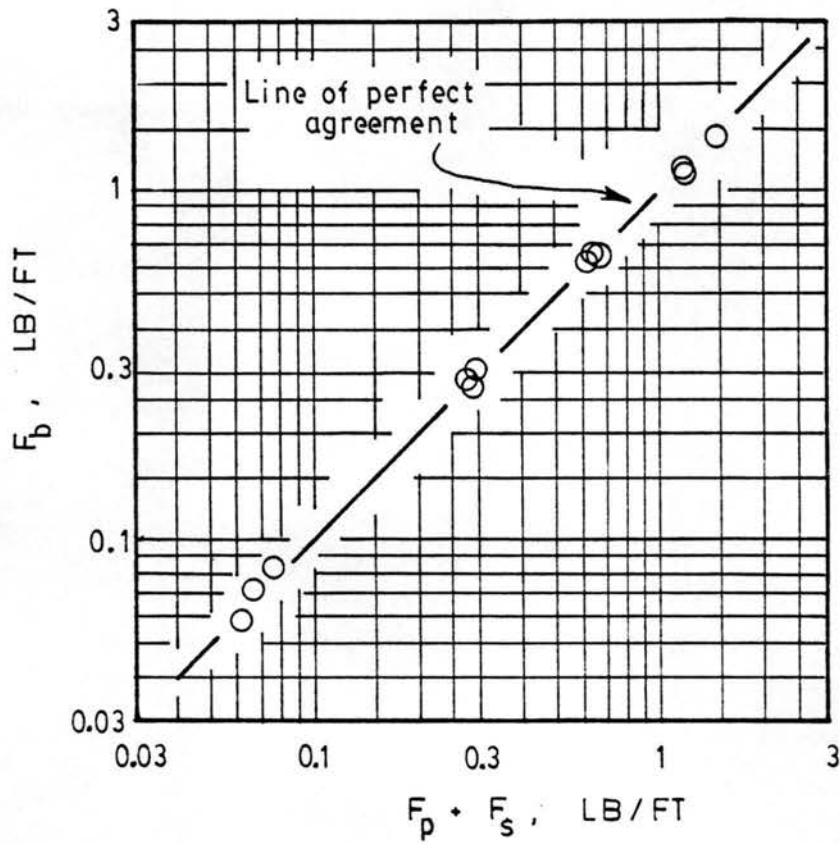


Figure 4.23. Comparison of Measured Total Force with the Sum of the Measured Skin Shear and Measured Form Drag for Uniform, Smooth Bedform Experiment

4.5.2 Nonuniform, Smooth Bedform Experiment

For each experiment run in this study, the differential pressure head was measured along the test bedform surface using the same shear probe as for the uniform, smooth bedform study. Equation 4.45 was used to convert these measurements to local shear stress. A summary of the shear stress distributions for each experimental run of the nonuniform, smooth bedform study is presented in Table 4.12. Using these local shear stress values and the corresponding average velocities for each position, the local skin shear coefficient, C_f , was determined using Eq. 4.46. The variation of C_f with Reynolds number was plotted for each position along the test bedform surface. Figures 4.24 and 4.25 illustrate this variation for six different measurement positions for experimental runs using the small upstream bedform and large upstream bedform, respectively. The Blasius equation is shown in each section of both figures for comparison, and, as determined for the uniform, smooth bedform experiment, it was observed that the local skin shear coefficient may be related to the Reynolds number by Eq. 4.52. The variable B of Eq. 4.52 was determined for 17 of the measurement locations for the experimental runs using the small upstream bedform, and five of the measurement locations for the experimental runs using the large upstream bedform. The variation of B with position on the test bedform is illustrated for both the uniform and nonuniform smooth bedform experiments in Figure 4.26. It may be observed that B varies linearly with longitudinal distance from the toe of the test bedform for the lower portion of each curve illustrated in Figure 4.26, and the slope of each line is approximately equal to the slope determined previously for the uniform, smooth bedform study. It may also be noted

Table 4.12. Summary of Shear Stress Distributions for Nonuniform, Smooth Bedform Experiment

x ft	τ_x , lb/ft ²					
	Run 1S	Run 2S	Run 3S	Run 7S	Run 8S	Run 9S
2.182	0.00513	0.00448	0.00462	0.0301	0.0295	0.0302
2.082	0.00445	0.00394	0.00420	0.0255	0.0249	0.0253
1.982	0.00440	0.00375	0.00380	0.0241	0.0246	0.0236
1.882	0.00398	0.00367	0.00364	0.0216	0.0214	0.0232
1.782	0.00371	0.00327	0.00324	0.0196	0.0208	0.0218
1.682	0.00355	0.00323	0.00312	0.0176	0.0194	0.0203
1.582	0.00282	0.00798	0.00314	0.0159	0.0168	0.0191
1.482	0.00286	0.00278	0.00258	0.0152	0.0154	0.0186
1.382	0.00270	0.00245	0.00254	0.0146	0.0140	0.0147
1.282	0.00249	0.00211	0.00237	0.0124	0.0141	0.0154
1.182	0.00215	0.00206	0.00212	0.0112	0.0128	0.0133
1.082	0.00198	0.00172	0.00181	0.00994	0.0103	0.0105
0.982	0.00176	0.00145	0.00150	0.00953	0.00859	0.00923
0.882	0.00154	0.00154	0.00130	0.00845	0.00610	0.00839
0.782	0.00108	0.00103	0.00113	0.00550	0.00672	0.00590
0.682	0.00117	0.00103	0.00069	0.00501	0.00345	0.00564
0.582	0.00074	0.00089	0.00064	0.00290	0.00345	0.00311
0.482	0.00043	0.00064	0.00032	0.00153	0.00098	0.00203

Table 4.12. Summary of Shear Stress Distributions for Nonuniform, Smooth Bedform Experiment (continued)

x ft	τ_x , lb/ft ²					
	Run 1B	Run 2B	Run 3B	Run 7B	Run 8B	Run 9B
2.18	0.00364	0.00360	0.00351	0.0291	0.0268	0.0252
2.082	0.00224	0.00245	0.00274	0.0202	0.0173	0.0155
1.982	0.00198	0.00207	0.00215	0.0184	0.0115	0.0118
1.882	0.00108	0.00172	0.00172	0.0105	0.0103	0.00959
1.782	0.00079	0.00127	0.00154	0.00720	0.00687	0.00737
1.682	---	0.00069	0.00074	0.00547	0.00592	0.00431
1.582	---	0.00064	0.00074	0.00327	0.00240	---

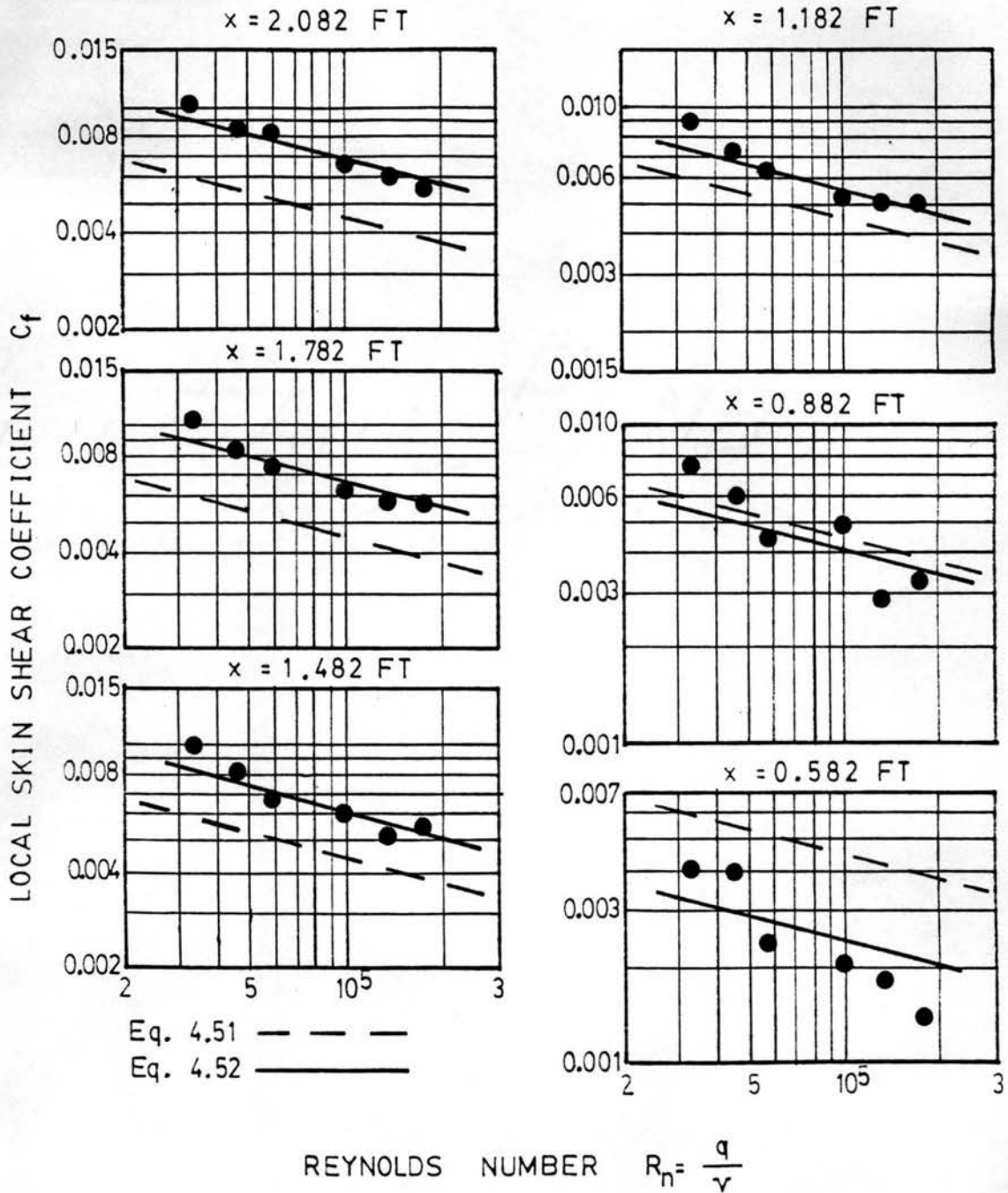


Figure 4.24. Variation of Skin Shear Coefficient with Reynolds Number and Position for Nonuniform, Smooth Bedform
 Experiment: Small Bedform Upstream

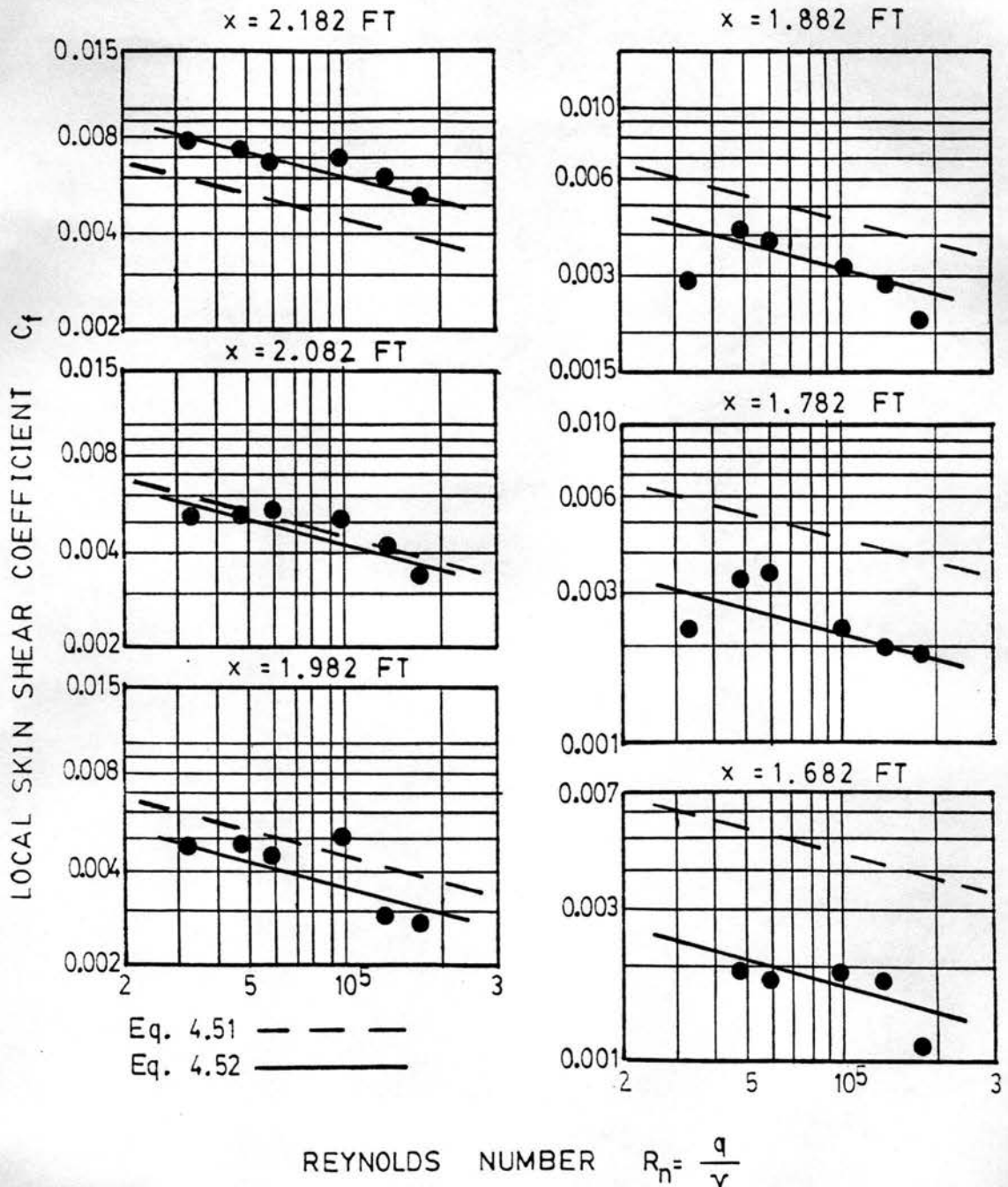


Figure 4.25. Variation of Skin Shear Coefficient with Reynolds Number and Position for Nonuniform, Smooth Bedform Experiment: Large Bedform Upstream

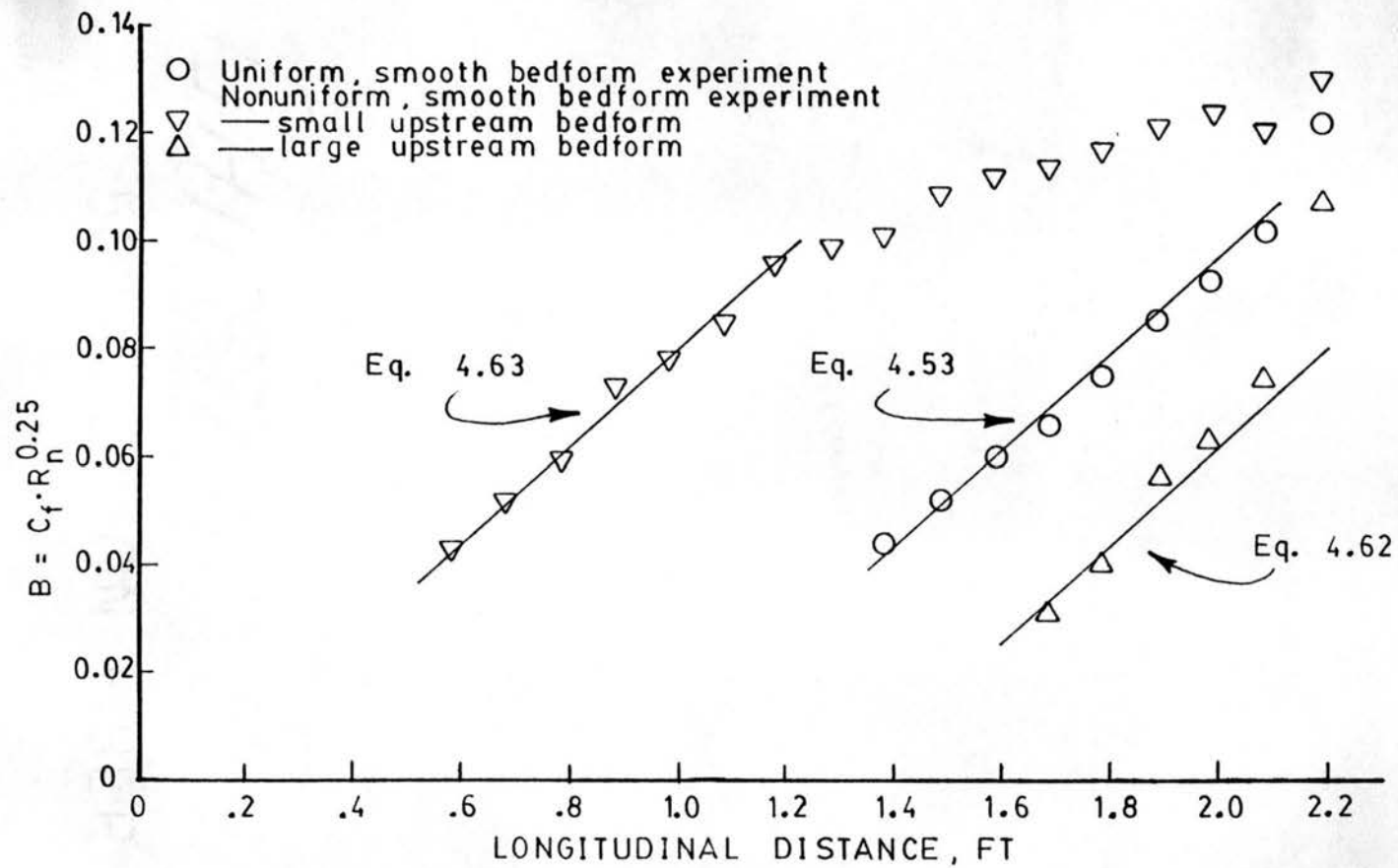


Figure 4.26. Variation of B with Position along the Bedform Surface for Uniform and Nonuniform, Smooth Bedform Experiments

that each curve contains a data point which seems discontinuous with the trend of the majority of the data, and the location of this point is very near the crest of the bedform in each case. This discontinuity is most likely due to the disturbance of flow caused by the sharp edge of the bedform at the crest. The data from the nonuniform smooth bedform experiment with the small bedform upstream indicates that the linear variation of B with position on the bedform surface does not continue indefinitely, but tends to level off to some maximum value.

It was noted in the previous section that the equation

$$B = 0.091x - 0.085 \quad (4.61)$$

may be used to describe the variation of B with longitudinal position along the bedform, and that this equation implies a zero shear stress value at a location approximately equal to the location of maximum piezometric head. A straight line of the same slope may be fitted through the data from the large bedform upstream study, and the equation of this line was determined to be

$$B = 0.091x - 0.12 \quad (4.62)$$

as shown in Figure 4.26. This equation implies a zero shear stress value at a position 1.32 feet downstream of the test bedform toe, or 2.42 feet downstream of the immediately upstream crest. This latter distance corresponds to a distance of 3.8 times the large bedform height, again agreeing well with the location of peak piezometric head, and the location of the reattachment point proposed by Engel (1981). A straight line of the same slope of Eqs. 4.53 and 4.62 may also be fitted through the data from the small bedform upstream study, and the equation of this line was determined to be

$$B = 0.091x - 0.012 \quad (4.63)$$

as shown in Figure 4.26. This equation implies a zero shear stress value at a position 0.132 feet downstream of the test bedform toe, or 0.682 feet downstream of the immediately upstream crest. This latter distance corresponds to a distance of 2.1 times the small bedform height which does not agree well with the location of peak piezometric head nor the location of reattachment proposed by Engel (1981). It is concluded that the placement of the smaller bedform within the series of larger bedforms had a disruptive effect on the flow pattern causing the separation length downstream of the smaller bedform to be significantly less than that commonly observed for uniform bedforms. No explanation is given for the lack of agreement noted for the zero shear stress and peak piezometric head locations.

The shear stress distributions for the nonuniform, smooth bedform experiment are illustrated in Figure 4.27-4.29. The data contained in Table 4.12, plotted in these figures, and Eq. 4.57 was used to compute the longitudinal force due to skin shear stress acting on the test bedform for each experimental run of the nonuniform study. The results of these integrations are summarized in Table 4.13, and data from the uniform smooth study is included for comparison. The skin shear force observed for experimental runs with the small bedform upstream of the test bedform was an average of 1.9 times larger than the skin shear force measured for the comparable run over uniform bedforms. This factor was reduced to 0.52 or 1/1.9 for comparable experimental runs with the large bedform placed upstream. The multiplying factors, 1.9 and 0.52 are comparable to those obtained for drag force, as discussed in Section 4.4.

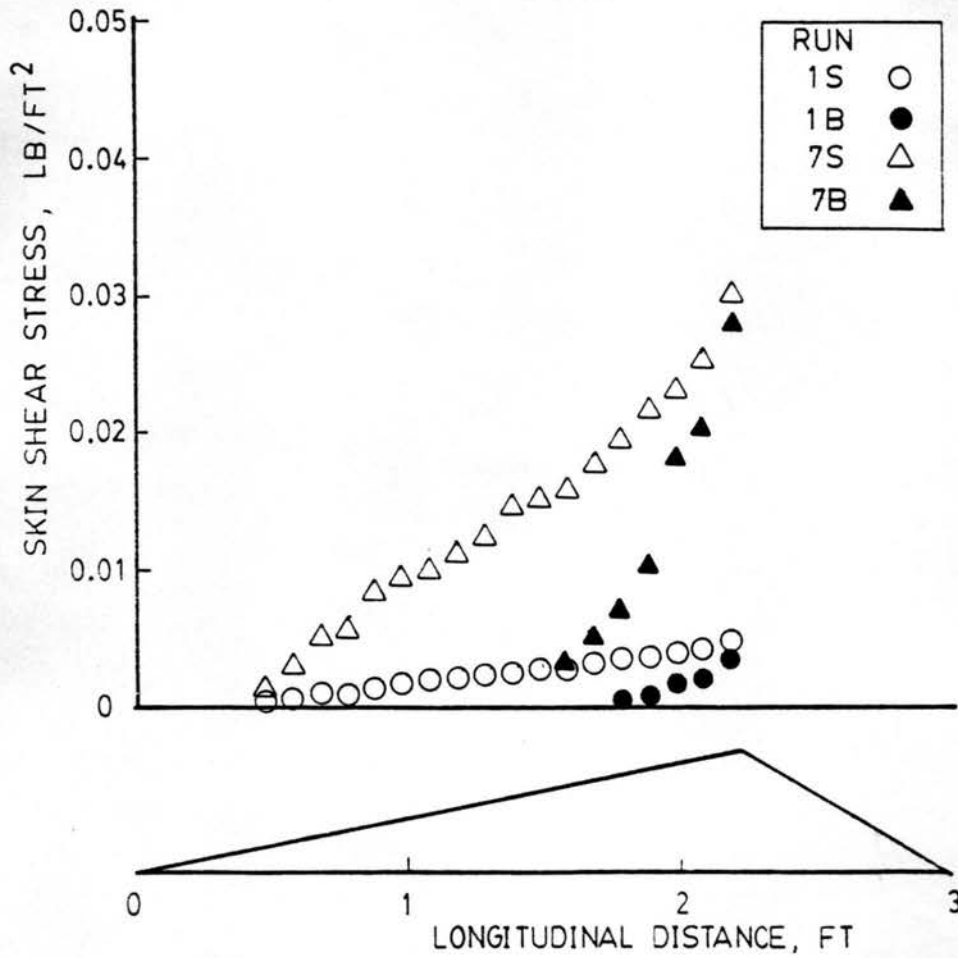


Figure 4.27. Shear Stress Distribution for Nonuniform, Smooth Bedform Experiment: Runs 1S, 1B, 7S, 7B

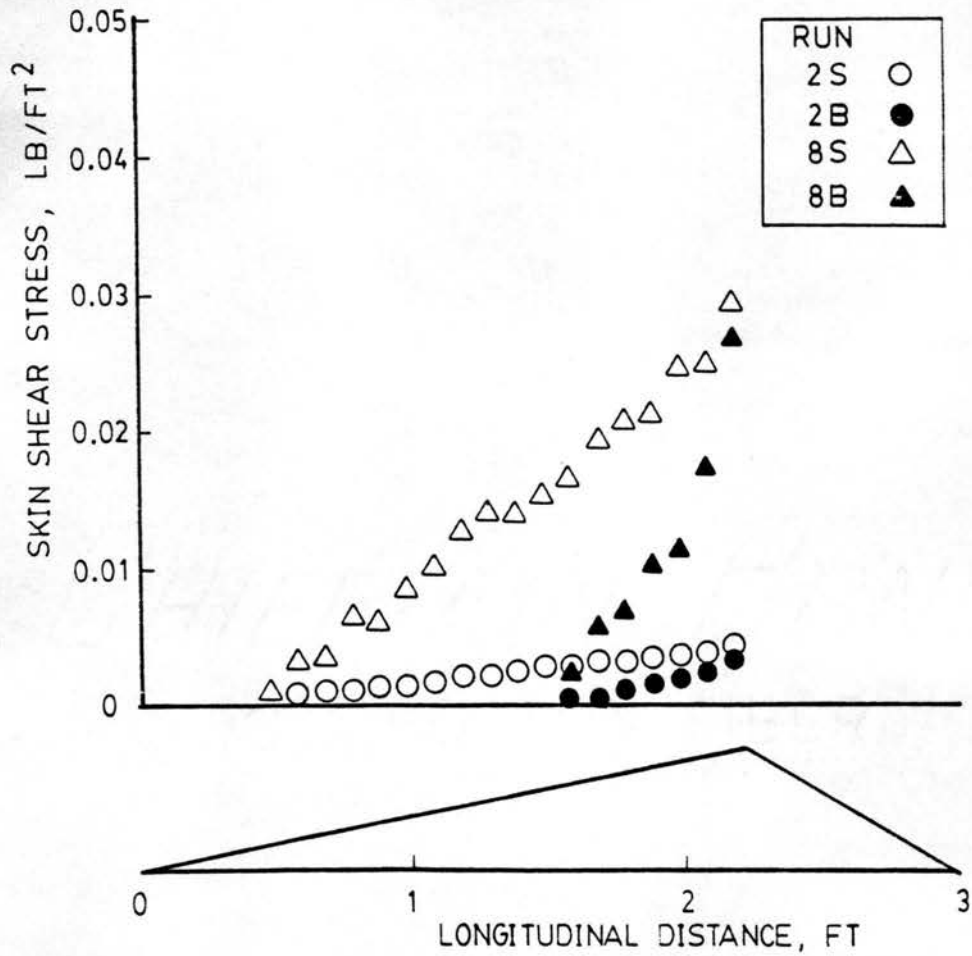


Figure 4.28. Shear Stress Distribution for Nonuniform, Smooth Bedform Experiment: Runs 2S, 2B, 8S, 8B

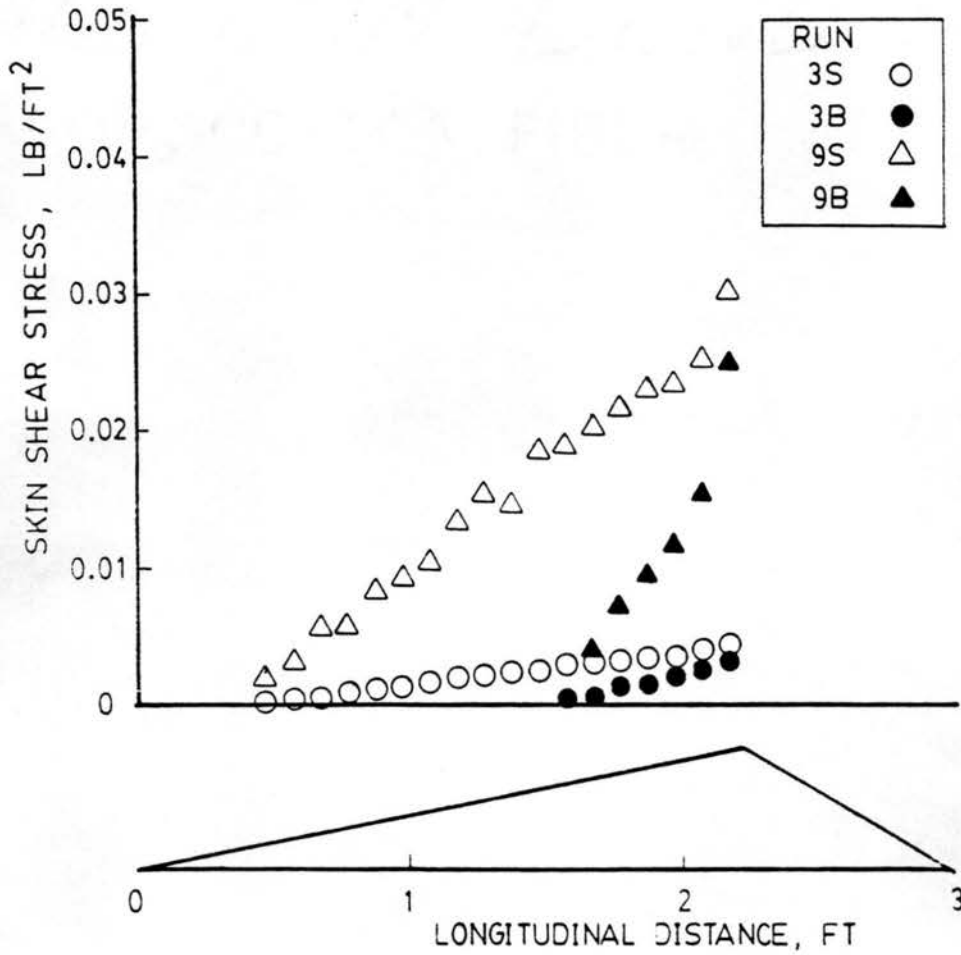


Figure 4.29. Shear Stress Distribution for Nonuniform, Smooth Bedform Experiment: Runs 3S, 3B, 9S, 9B

Table 4.13. Skin Resistance Parameters for Smooth Bedform Studies

Small Bedform Upstream		Uniform Bedforms		Large Bedform Upstream	
Run No.	F_s lb/ft	Run No.	F_s lb/ft	Run No.	F_s lb/ft
1S	0.00452	1	0.00197	1B	0.00086
2S	0.00416	2	0.00194	2B	0.00114
3S	0.00412	3	0.00199	3B	0.00120
7S	0.00242	7	0.0140	7B	0.00861
8S	0.0245	8	0.0153	8B	0.00741
9S	0.0262	9	0.0155	9B	0.00764

4.5.3 Uniform, Rough Bedform Experiment

For fully rough flow, the velocity distribution is generally stated as a logarithmic law. However, it is also recognized that over a limited range, a power law may be used of the form

$$\frac{u}{u_*'} = C_1 \left(\frac{y}{k_s} \right)^{1/\eta} \quad (4.64)$$

where C_1 and η are variables, and k_s is a representative roughness height. Ippen et al. (1960) have shown that the differential pressure measured using a pitot tube placed on a boundary where Eq. 4.64 is valid is directly proportional to the shear stress at that location. That is

$$\tau_x = C_2 \cdot \Delta H_x \quad (4.65)$$

where C_2 is a variable whose value depends on the size of the pitot probe used, the roughness size, and the value of C_1 and η in Eq. 4.64. For the present study, Eq. 4.64 was assumed valid, and the differential pressure heads were measured using a 0.25 inch diameter pitot tube placed at an average of 12 locations along the upstream face of the roughened test bedform. A summary of the differential head measurements is presented in Table 4.14.

Integrating both sides of Eq. 4.65 and combining with Eq. 4.57 yields

$$F_s = \int_{x_r}^{x_c} \tau_x dx = C_2 \int_{x_r}^{x_c} \Delta H_x dx \quad (4.66)$$

Since the total force acting on the bedform has been shown to equal the sum of the form drag and the skin shear, F_s may also be determined by

Table 4.14. Summary of Shear Probe Differential Head Measurements
For the Uniform, Rough Bedform Experiment

x ft	ΔH_x , ft					
	Run 1R	Run 2R	Run 3R	Run 7R	Run 8R	Run 9R
2.182	0.00750	0.00583	0.00550	0.0533	0.0528	0.0508
2.082	0.00542	0.00450	0.00467	0.0411	0.0383	0.0358
1.982	0.00500	0.00450	0.00383	0.0375	0.0335	0.0357
1.882	0.00442	0.00367	0.00317	0.0308	0.0313	0.0295
1.782	0.00358	0.00350	0.00283	0.0276	0.0258	0.0238
1.682	0.00292	0.00325	0.00250	0.0227	0.0245	0.0230
1.582	0.00258	0.00242	0.00217	0.00187	0.0173	0.0190
1.482	0.00225	0.00233	0.00133	0.0148	0.0148	0.0150
1.382	0.00183	0.00175	0.00125	0.00683	0.0109	0.00967
1.282	0.00125	0.00117	0.00083	0.00692	0.00658	0.00458
1.182	0.00083	0.00100	0.00025	0.00450	0.00350	0.00175
1.082	---	0.00025	---	0.00342	0.00208	0.00250

$$F_s = F_b - F_p \quad (4.67)$$

Values of F_b and F_p have been presented for each experimental run of the roughened bedform study in Tables 4.2 and 4.9, respectively.

Combining Eqs. 4.66 and 4.67 yields

$$C_2 = \frac{F_b - F_p}{x_c \int_{x_r} \Delta H_x dx} \quad (4.68)$$

A summary of the integrated differential head measurements, the longitudinal skin shear forces computed using Eq. 4.67, and the computed values of C_2 are presented in Table 4.15. The values of C_2 determined using Eq. 4.68 range between 5.1 and 8.2, and have a mean value of 6.5. This range may seem quite large, but considering that each C_2 value thusly determined is the result of 32 separate measurements using various measurement devices, each with its own potential for error, and considering the highly turbulent and nonsteady characteristic of flow over the size of bedform models used, perhaps this range of uncertainty is not unreasonable. Verification of the local shear stress values determined using the above analysis will be presented in the velocity profile section of this report.

Using the average value of $C_2 = 6.5$, the differential head data contained in Table 4.14 was converted to shear stress using Eq. 4.65. The shear stress distributions along the surface of the test bedform for each experimental run of the uniform, rough bedform study are illustrated in Figures 4.30-4.32. The shear stress distributions have the same form as those measured over the smooth test bedform. However, the maximum shear stress is an order of magnitude larger than that

Table 4.15. Skin Resistance Parameters for Uniform, Rough Bedform Experiment

Run No.	$F_T - F_p$ lb/ft	$\int_{x_r}^{x_c} \Delta H_x dx$	C_2	F_s^* lb/ft	τ' lb/ft ²	f'
1R	0.0206	0.00369	5.6	0.0240	0.00800	0.142
2R	0.0267	0.00338	7.9	0.0220	0.00733	0.105
3R	0.0176	0.00279	6.3	0.0181	0.00603	0.0729
7R	0.214	0.0262	8.2	0.170	0.0567	0.111
8R	0.132	0.0259	5.1	0.168	0.0560	0.0894
9R	0.145	0.247	5.9	0.161	0.0537	0.0722

$$\bar{C}_2 = \overline{6.5}$$

* F_s is computed from $\bar{C}_2 \cdot \int_{x_r}^{x_c} \Delta H_x dx$

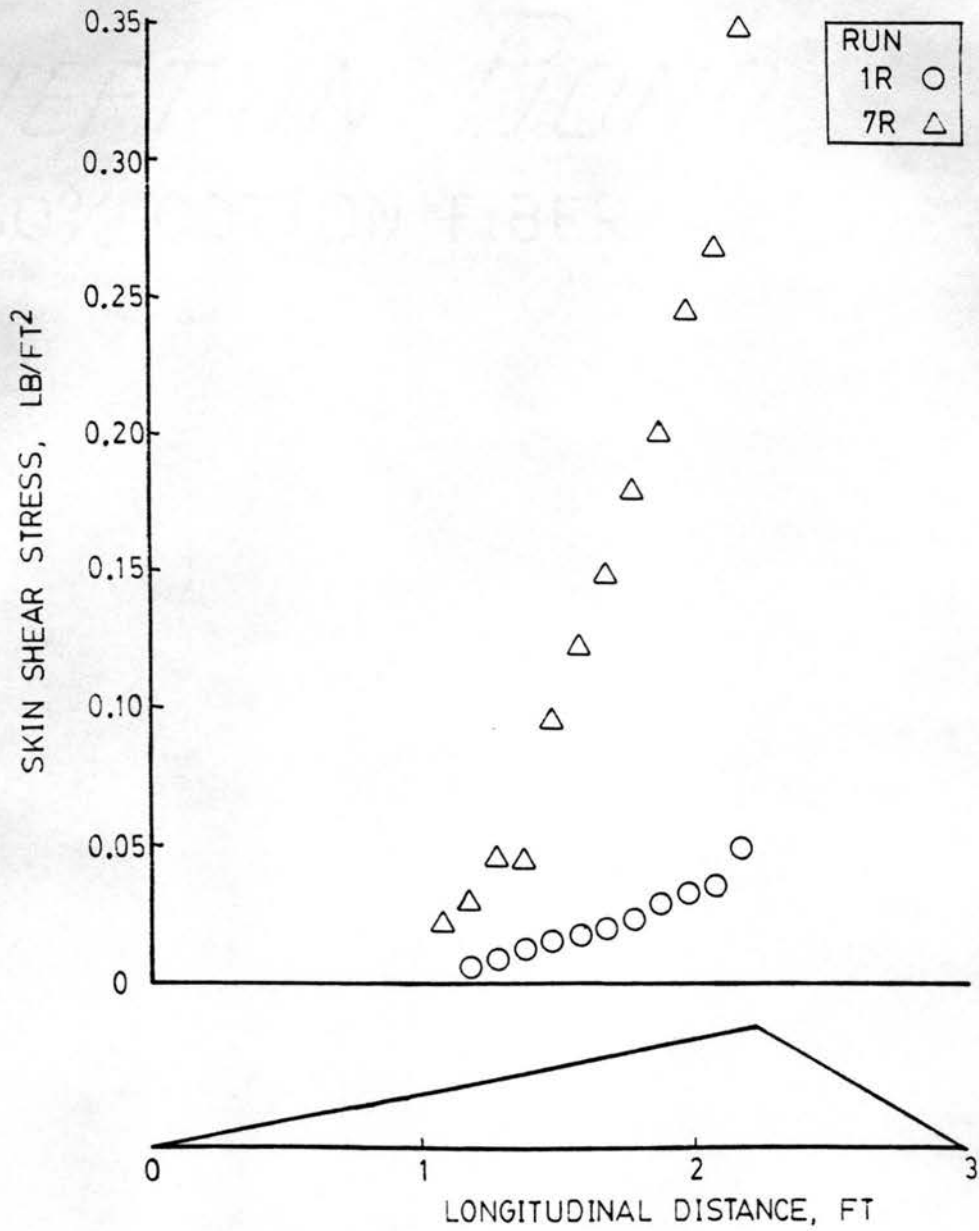


Figure 4.30. Shear Stress Distribution for Uniform, Rough Bedform
Experiment: Depth at Crest = 6 in

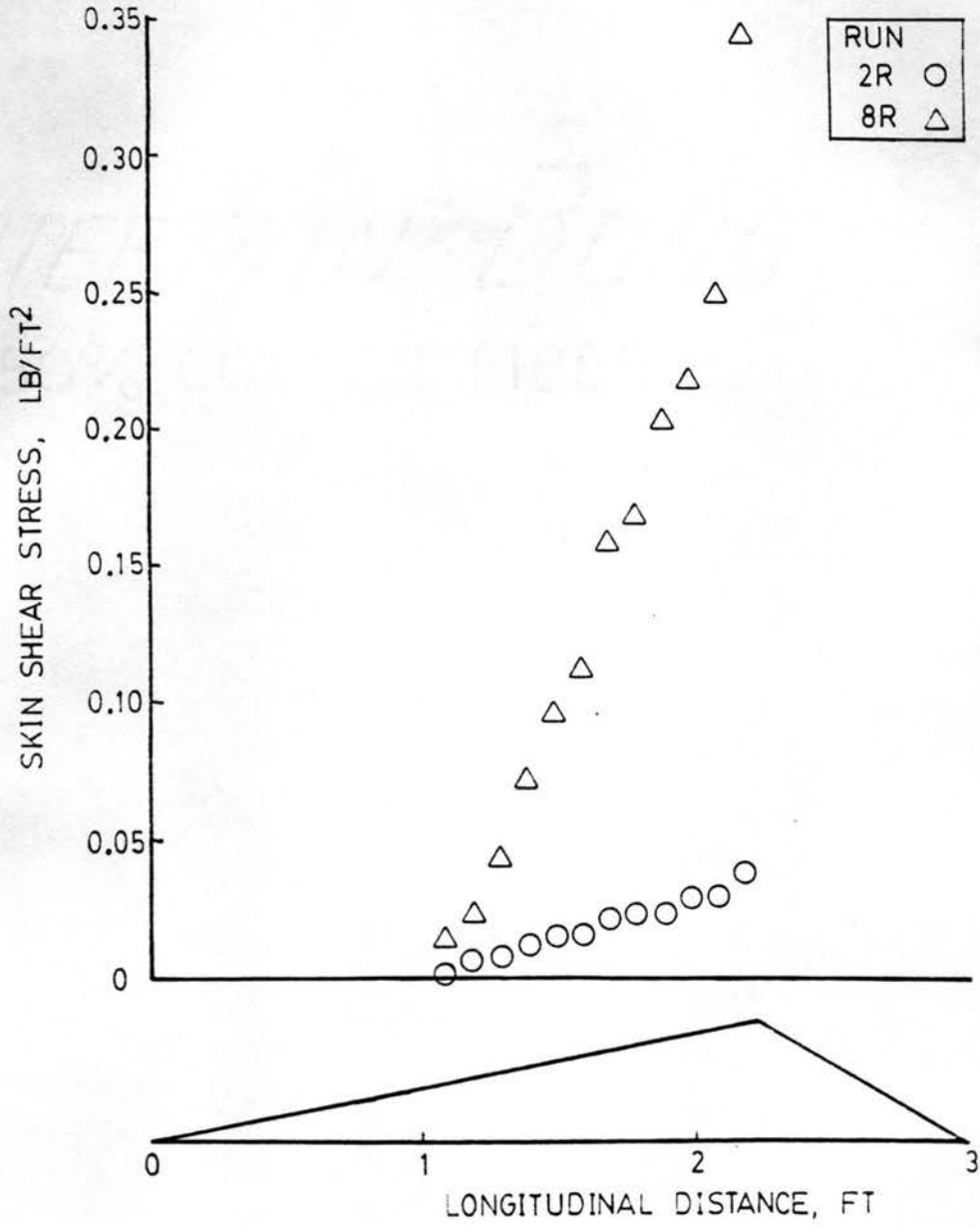


Figure 4.31. Shear Stress Distribution for Uniform, Rough Bedform
Experiment: Depth at Crest = 8 in

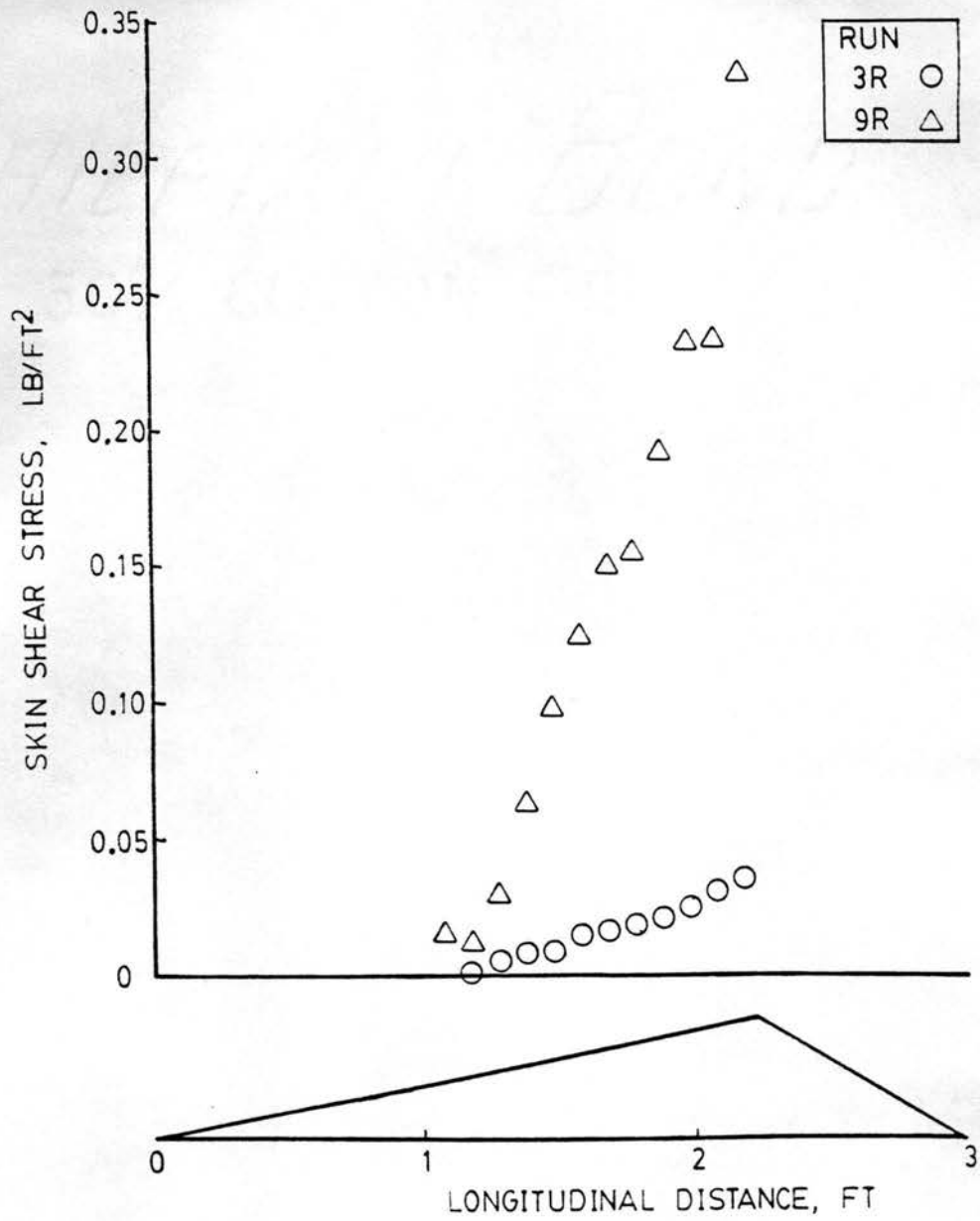


Figure 4.32. Shear Stress Distribution for Uniform, Rough Bedform
Experiment: Depth at Crest = 10 in

measured for comparable experimental runs of the uniform, smooth bedform study. Although the presence of roughness had no significance effect on the pressure drag of the test bedform, the skin shear and therefore, total flow resistance was significantly increased.

The local skin shear coefficient, C_f , was computed for each shear stress value illustrated in Figures 4.30-4.32 using Eq. 4.46. The local skin friction factor, fx' , which is related to C_f by a constant (see Eq. 4.50), has been shown to be dependent on a relative roughness, such as the ratio of pipe diameter to roughness size, for fully rough pipe flow. However, because both separation and reattachment are characteristic to flow over bedforms at Froude numbers less than one, the flow over the upstream face of each bedform is actually transitional in nature. Thus the Reynolds number would be expected to be an additional parameter governing the skin shear on the sand coated bedforms. The relative roughness parameter chosen for the analysis of the local skin shear coefficient was D_x/d_{50} , where D_x is the local depth at location x , and d_{50} is the median grain size of the roughness. In computing the Reynolds number, the hydraulic radius of the bed, R_b , was used for the characteristic depth, calculated using a procedure suggested by Vanoni and Brooks (1957). Values of R_b for each experimental run of the uniform studies are presented in Table 4.2. The Reynolds number thusly computed is given the symbol R_e , that is

$$R_e = \frac{R_b V}{\nu} \quad (4.69)$$

The local skin shear coefficient was found to be related to the product of D_x/d_{50} and $\log R_e$, as shown in Figure 4.33. The measurement positions were identical to those used for the uniform, smooth

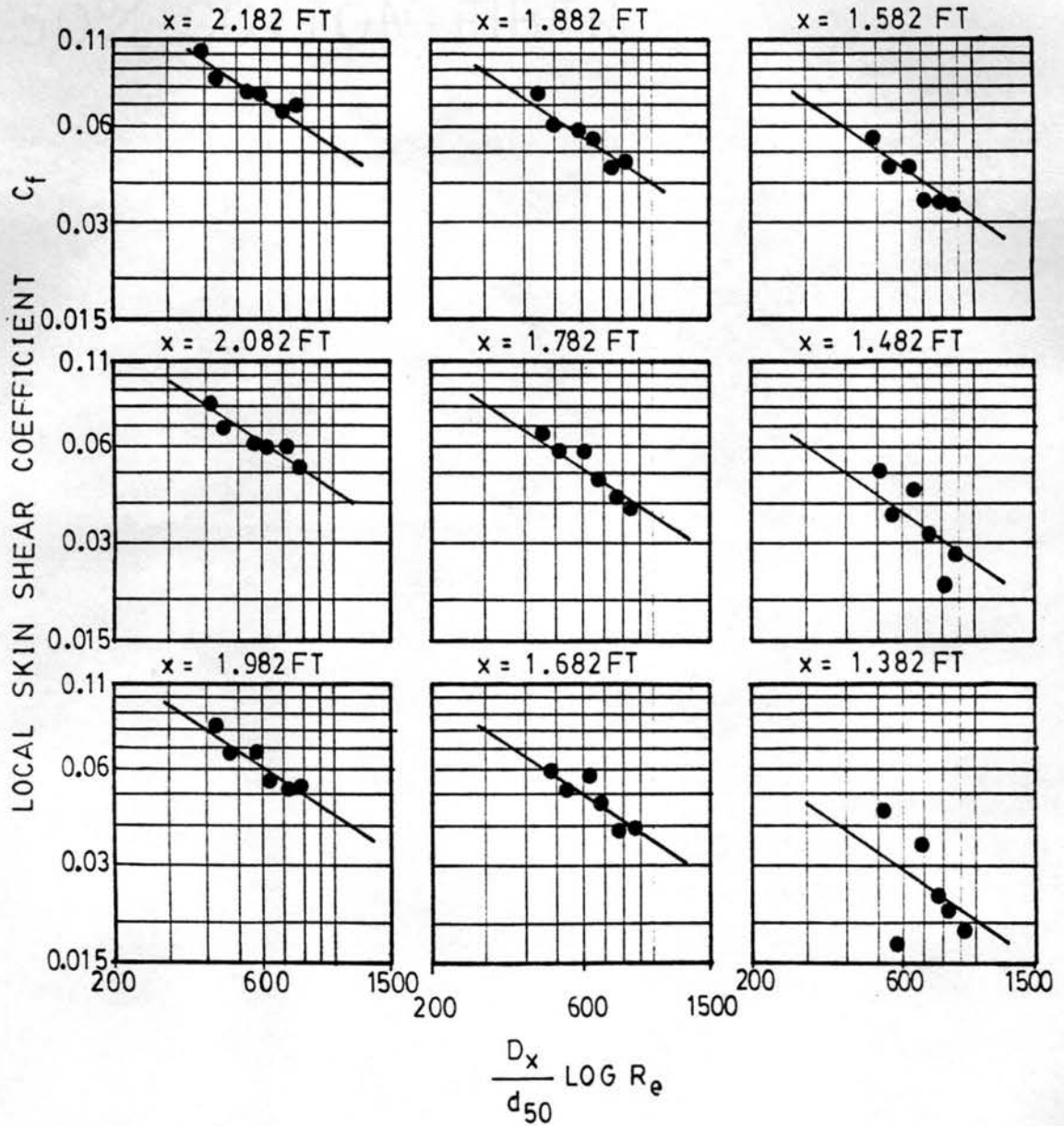


Figure 4.33. Variation of Local Skin Shear Coefficient with $\frac{D_x}{d_{50}} \text{ LOG } R_e$ and Position for Uniform, Rough Bedform Experiment

study, and each section of this figure represents a different position along the surface of the bedform. Thus the six data points in each section represent the C_f values computed for each run of the uniform, rough experiment at the given location on the test bedform. Figure 4.33 illustrates that C_f is related to the same power of $D_x/d_{50} \log R_e$ for each of the position shown, although this relationship is less clear near the reattachment point. In general, the data fit the following equation:

$$C_f = \frac{B_R}{\left[\frac{D_x}{d_{50}} \log R_e\right]^{2/3}} \quad (4.70)$$

where B_R is a variable whose value depends on the position along the bedform surface. Parallel lines representing the same power relationship as in Eq. 4.70 were drawn through the data points in each section of Figure 4.34, and the values of B_R were determined. These values of B_R are illustrated in Fig. 4.34. As found for the variation of B in Eq. 4.52 for the smooth bedform studies, the variable B_R in Eq. 4.70 varies linearly with x in the lower portion of the curve, and a seemingly discontinuous point is observed at the measurement location near the crest. Extending the linear region of the curve downward yields a zero B_R value, or zero shear stress value, at a location one foot downstream of the toe of the bedform, which corresponds to a distance 3.9 bedform heights downstream from the immediately upstream crest. This location is in good agreement with the zero shear stress location observed for the uniform, smooth bedform study.

The bed shear stress due to skin shear, τ' , and the bed skin friction factor, f' , was computed for each experimental run of the

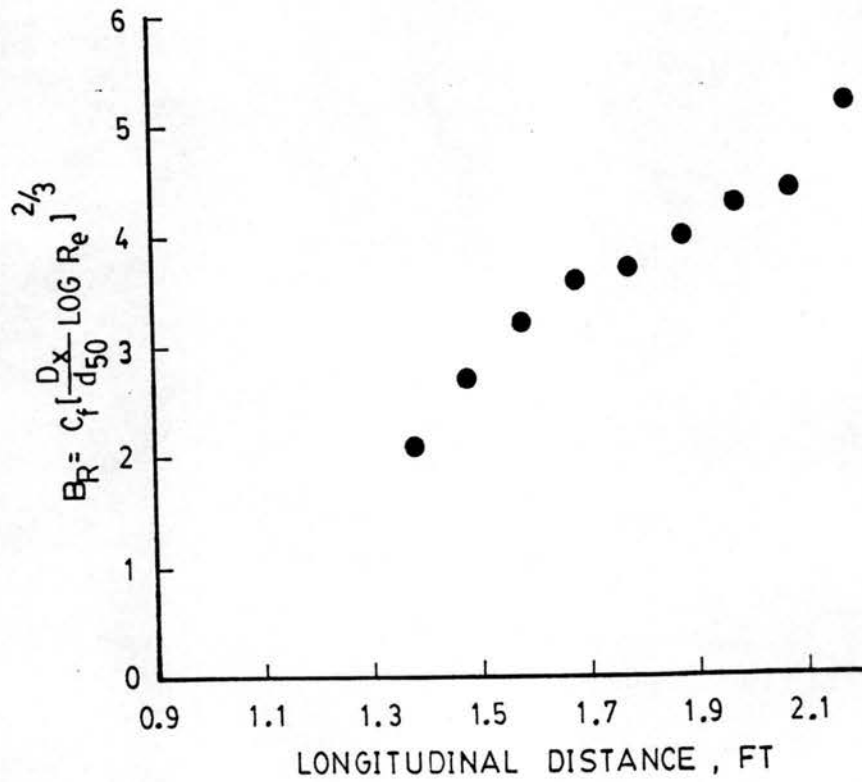


Figure 4.34. Variation of B_R with Position along the Bedform Surface for Uniform, Rough Bedform Experiment

uniform, rough bedform experiment, using Eqs. 4.58 and 4.59, respectively. The values are summarized in Table 4.15. Since the local skin shear coefficient was determined to be related to the product of a relative roughness and $\log R_e$, this product should also be an important parameter governing the bed skin friction factor. The ratio of R_b/d_{50} was selected to represent the relative roughness in the analysis of the bed skin friction factor, and f' was plotted against the parameter $R_b/d_{50} \log R_e$, as shown in Figure 4.35. A smooth curve was determined for this plot, and the equation

$$f' = 772 \left[\frac{R_b}{d_{50}} \log R_e \right]^{-1.37} \quad (4.71)$$

fit the data well.

In order to verify Eq. 4.71, data obtained from Vittal et al. (1977) and Engel and Lau (1980) was also analyzed. The study by Vittal et al. (1977) investigated skin friction factors for modeled triangular bedforms with steepness ratios of 0.05, 0.067, 0.098, and 0.20. A sand grain roughness with 0.6 mm median grain size was used in their study. The study by Engel and Lau (1980) involved the measurement of total friction factor for open channel flow over bedforms with steepness ratios of 0.02, 0.033, 0.05 and 0.07. Sand grain roughnesses with median grain size of 0.65, 1.2, 2.6 and 3.5 mm were used in their study. The bed skin friction factors were estimated from the reported total friction factors by subtracting from the estimated form friction factors given by Eqs. 4.41, 4.42 and 4.43. It should be noted that the data from their study for bedforms with a steepness ratio of 0.07 did not agree with other data analyzed in this report, and was not included in the forthcoming analysis.

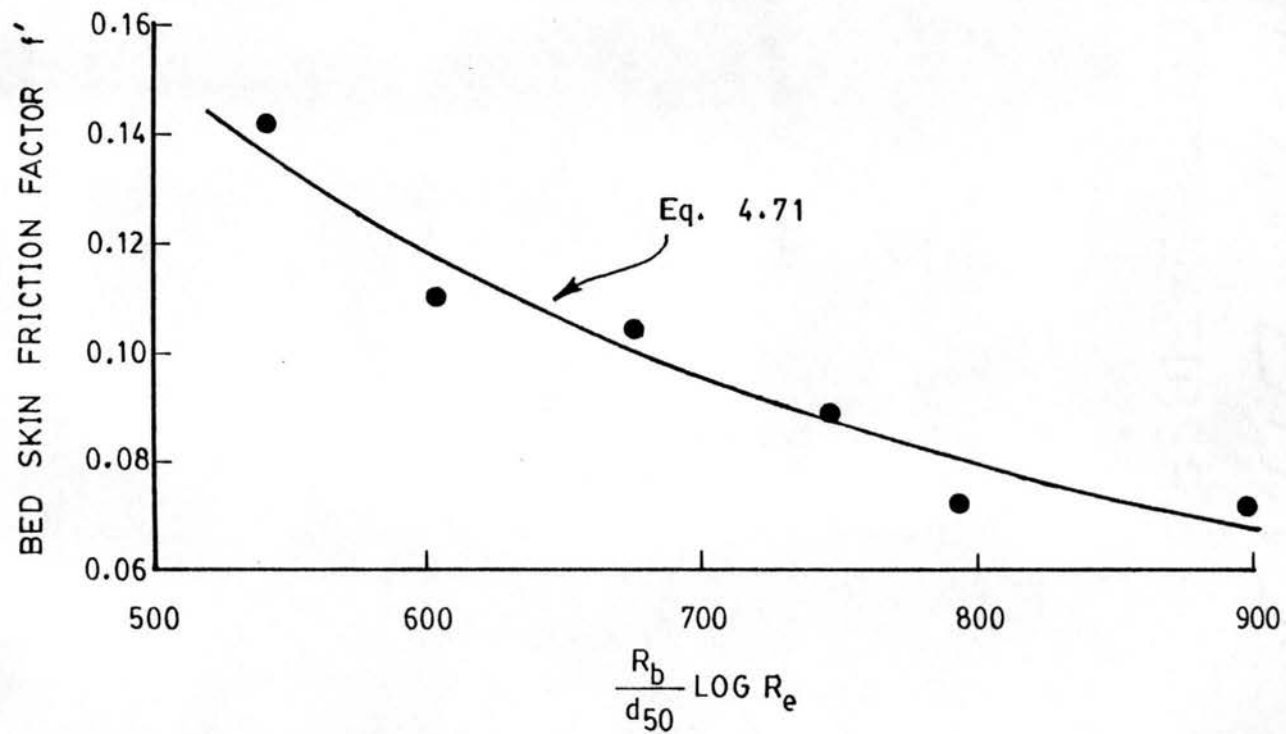


Figure 4.35. Variation of Bed Skin Friction Factor with R_b/d_{50}
 $\text{Log } R_e$ for Uniform, Rough Bedform Experiment

The data from Vittal et al. (1977), Engel and Lau (1980) and the present study is shown plotted in Figure 4.36. It was observed that by multiplying the parameter $R_b/d_{50} \log R_e$ by the square of the bedform steepness ratio, the bed skin friction factors from the studies by Vittal et al. (1977) and Engel and Lau (1980) were condensed into a single curve. The bed skin friction factors obtained in the present study are an order of magnitude larger than those from the outside studies. In Figure 4.36, $1/\sqrt{f'}$ is shown plotted against $R_b/d_{50} \log R_e [A/L]^2$, in order to compare the data from Vittal et al. (1977), Engel and Lau (1980) and the present study in the same figure.

It may be observed that the trend of the data from the present study is parallel to the trend of the data from the outside studies. The studies by Vittal et al. (1977) and Engel and Lau (1980) used bedforms of the same height (0.098 ft) although a large number of other parameters were varied (i.e., A/D, A/L, R_b/d_{50} , d_{50}/A , D/L). Thus, for a given bedform height, the bed skin friction factor seems to be completely controlled by the parameter $R_b/d_{50} [A/L]^2 \log R_e$.

It was observed that by plotting $\frac{1}{\sqrt{f'}} + 18.5A$ vs. $\frac{R_b}{d_{50}} \left[\frac{A}{L}\right]^2 \log R_e$, where A is in feet, it was possible to consolidate all the data from Figure 4.36 to a single curve, as shown in Figure 4.37. The data from this plot was fitted to a power relation given by

$$\frac{1}{\sqrt{f'}} + 18.5 A = 7.5 \left[\frac{R_b}{d_{50}} \left(\frac{A}{L}\right)^2 \log R_e \right]^{0.15} \quad (4.72)$$

The adjustment factor 18.5 A, is not as desirable as a dimensionless parameter, and it is necessary to justify it using other laboratory data. It was considered possible that, due to some unknown calibration

Source	d_{50} , mm	A, FT	A/L
○ Present study	1.75	0.451	0.150
△ Vittal et al (1977)	0.60	0.098	0.05, 0.067, 0.098, 0.20
□ Engel and Lau (1980)	0.65, 1.2, 2.6, 3.5	0.098	0.02, 0.033, 0.05

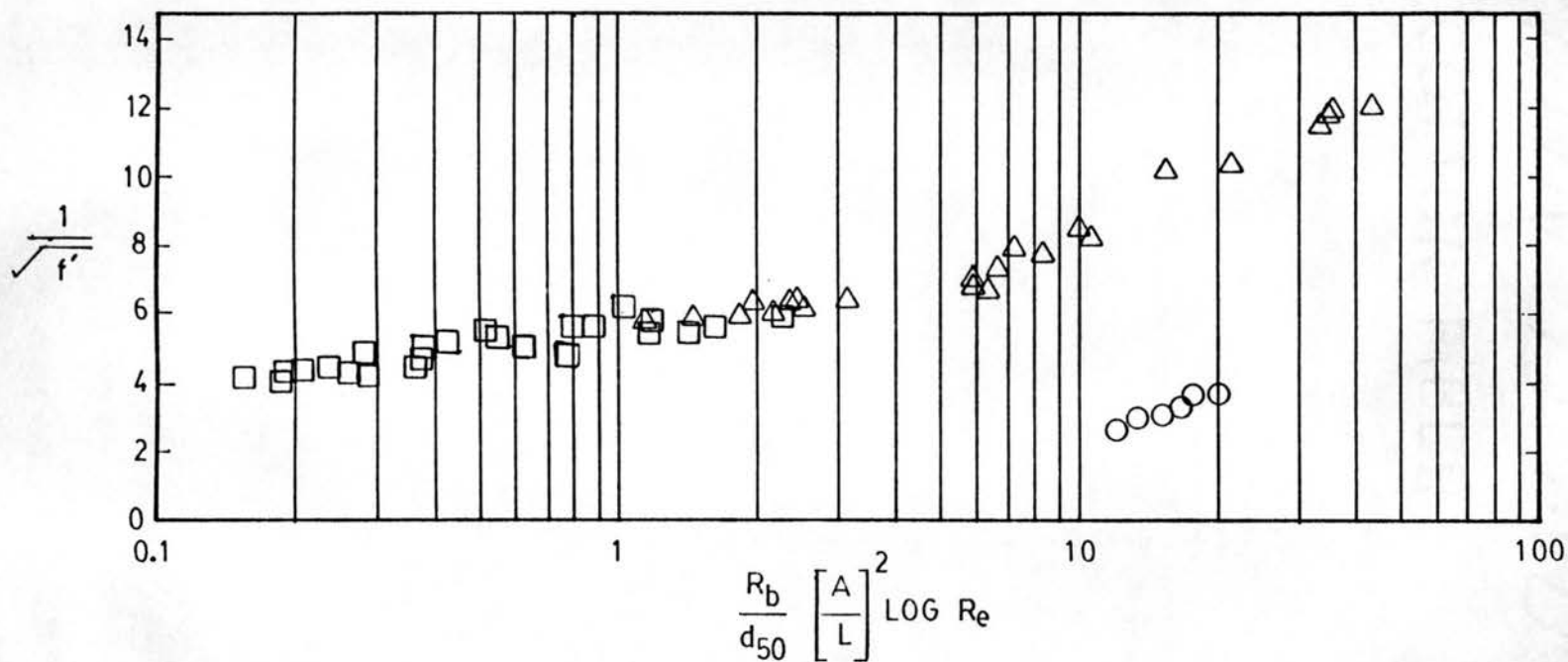


Figure 4.36. Relation between $\frac{1}{\sqrt{f'}}$ and $R_b d_{50} \left[\frac{A}{L} \right]^2 \text{Log } R_e$ for Rough Modeled Bedform Data

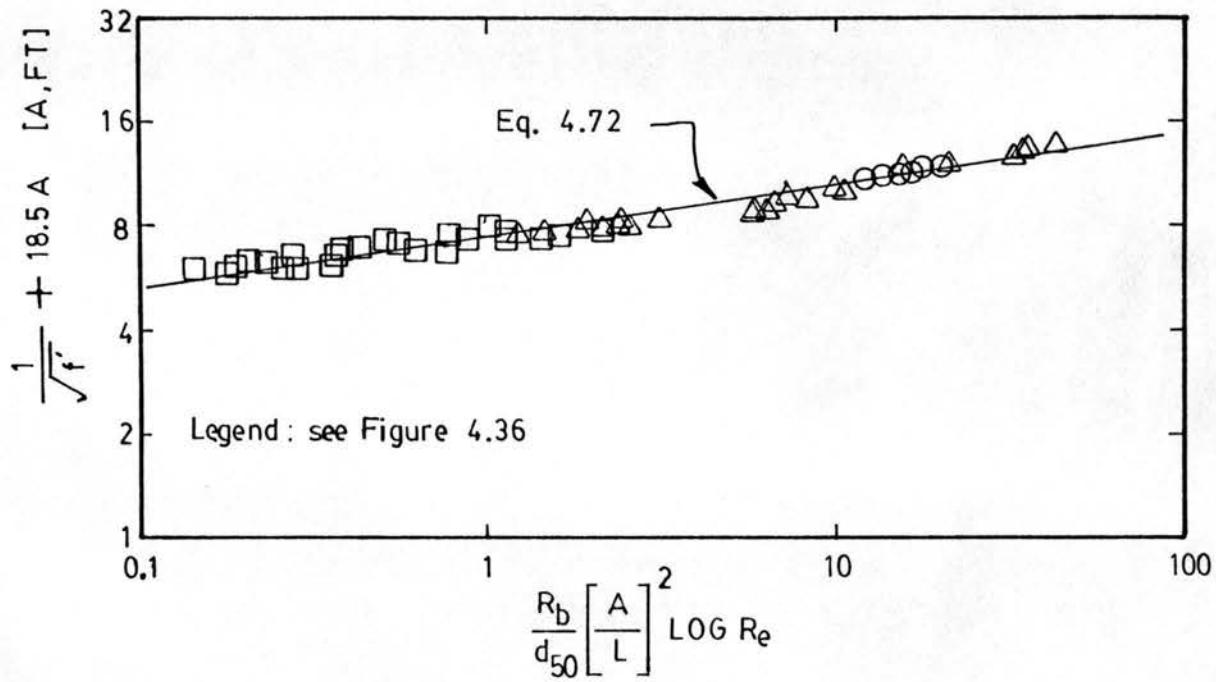


Figure 4.37. Relation between $[\frac{1}{\sqrt{f'}} + 18.5A]$ and $R_b d_{50} \left[\frac{A}{L}\right]^2 \text{Log } R_e$ for Rough Modeled Bedform Data

error, the results of the uniform, rough bedform experiments of the present study were invalid, considering the close agreement of all the data from two independent outside studies. Therefore, a single curve was fitted to the data from the outside studies without the adjustment factor—the data from Figure 4.36. The equation of this curve was determined to be

$$\frac{1}{\sqrt{f'}} = 5.63 \left[\frac{R_b}{d_{50}} \left[\frac{A}{L} \right]^2 \log R_e \right]^{0.181} \quad (4.73)$$

Equations 4.72 and 4.73 were then plotted with data from flume studies by Guy et al. (1966) and Tsubaki et al. (1953) as shown in Figure 4.38. This alluvial flume data is as reported by Wang (1983), and represents studies using median grain sizes of 0.93, 1.03, 1.26, 1.46 and 2.28 mm. In Figure 4.38, f'_e is defined as

$$f'_e = f_r - f'' \quad (4.74)$$

where f_r is the reported total friction factor, f'' is the form friction factor estimated using Eqs. 4.41, 4.42, and 4.43, and f'_e is the estimated bed skin friction factor. As can be seen from Figure 4.38, Eq. 4.72 best represents the trend of the data, lending support to the use of the adjustment for bedform height contained in this equation.

Further verification of Eq. 4.72 is illustrated in Figure 4.39. For the ranges of bedform heights illustrated in this figure, the quantity

$$\varepsilon = \frac{f'_p - f'_e}{f'_e} \quad (4.75)$$

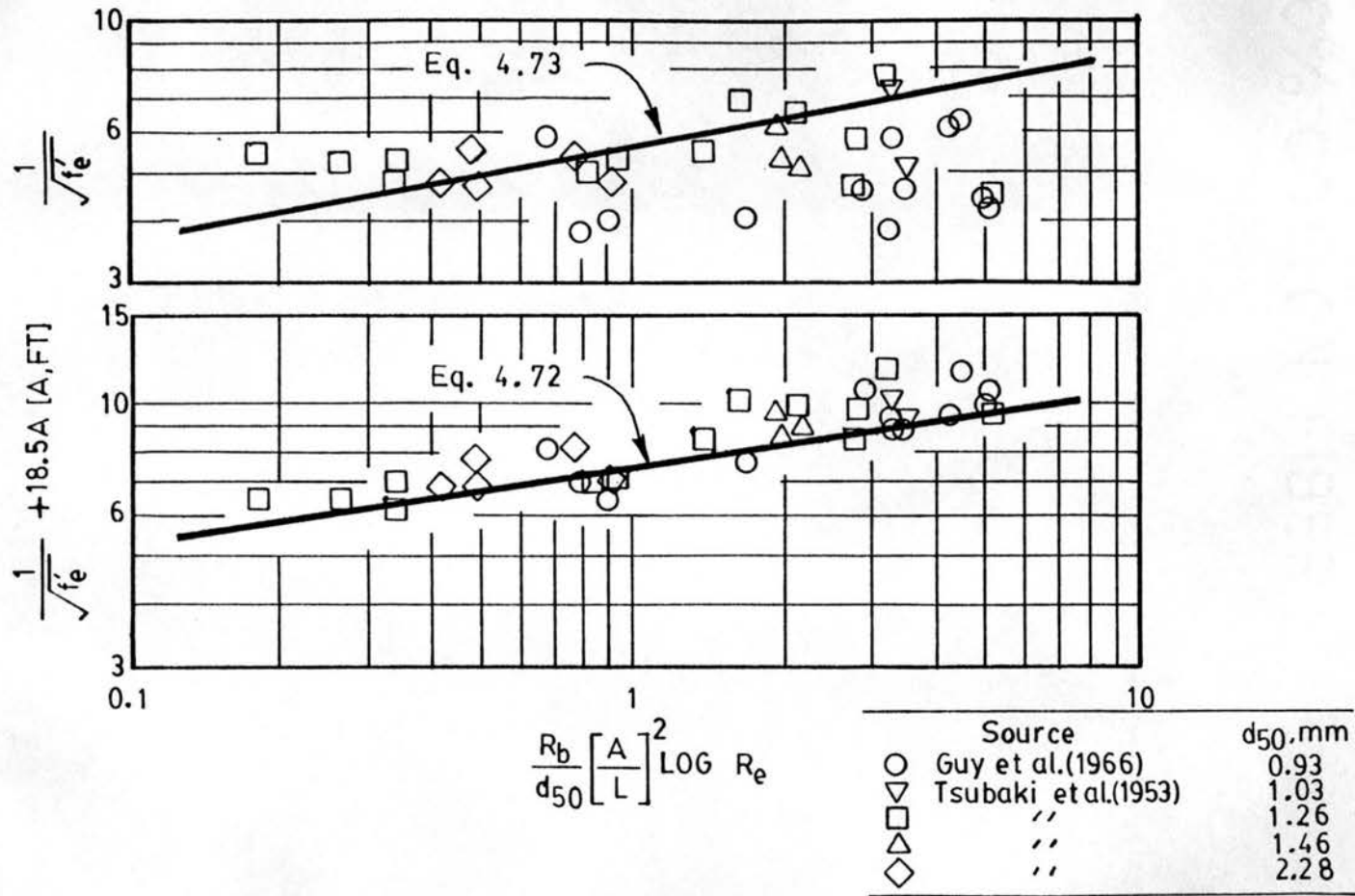


Figure 4.38. Comparison of Equations 4.72 and 4.73 Using Reported Alluvial Data

was determined, where f'_p is the skin friction factor determined using either Eq. 4.72 or 4.73, and ε represents the deviation of the predicted bed skin friction factor from f'_e . Values of ε were determined for the data shown in Figure 4.38. If the value of ε thusly determined was greater than 100 percent, the data point was considered an outlier and not included further analysis. The values of ε were summed and averaged over various ranges of bedform heights, and the results are illustrated in Figure 4.39. Note that using Eq. 4.72, a fairly constant positive error is observed over each range of bedform heights. However, using Eq. 4.73 results in consistently larger negative errors as the bedform height increases. Thus, the adjustment factor in Eq. 4.72 seems to be justified.

Using Eq. 4.72 results in consistently larger values of f' than f'_e . Recall that

$$f'_e = f_r - f'' \quad (4.74)$$

Equations 4.41 and 4.42 were derived for stable, two-dimensional or immobilized alluvial bedforms, and were based on centerline pressure measurements which were assumed to apply over the entire width of the bedform. Alluvial bedforms, however, are three-dimensional objects, somewhat streamlined with the flow. It is expected that the form drag due to a true three-dimensional dune would be less than that estimated using Eqs. 4.41 and 4.42, and this would result in larger values of f'_e in Eqs. 4.74 and 4.75. Thus, Eq. 4.72 may predict the bed skin friction factor for alluvial bedforms even better than indicated by Figures 4.38 and 4.39.

For given values of A , R_e , and L/R_b , the bed skin friction factor computed using Eq. 4.72 is a function of A/L and d_{50}/A only. Using

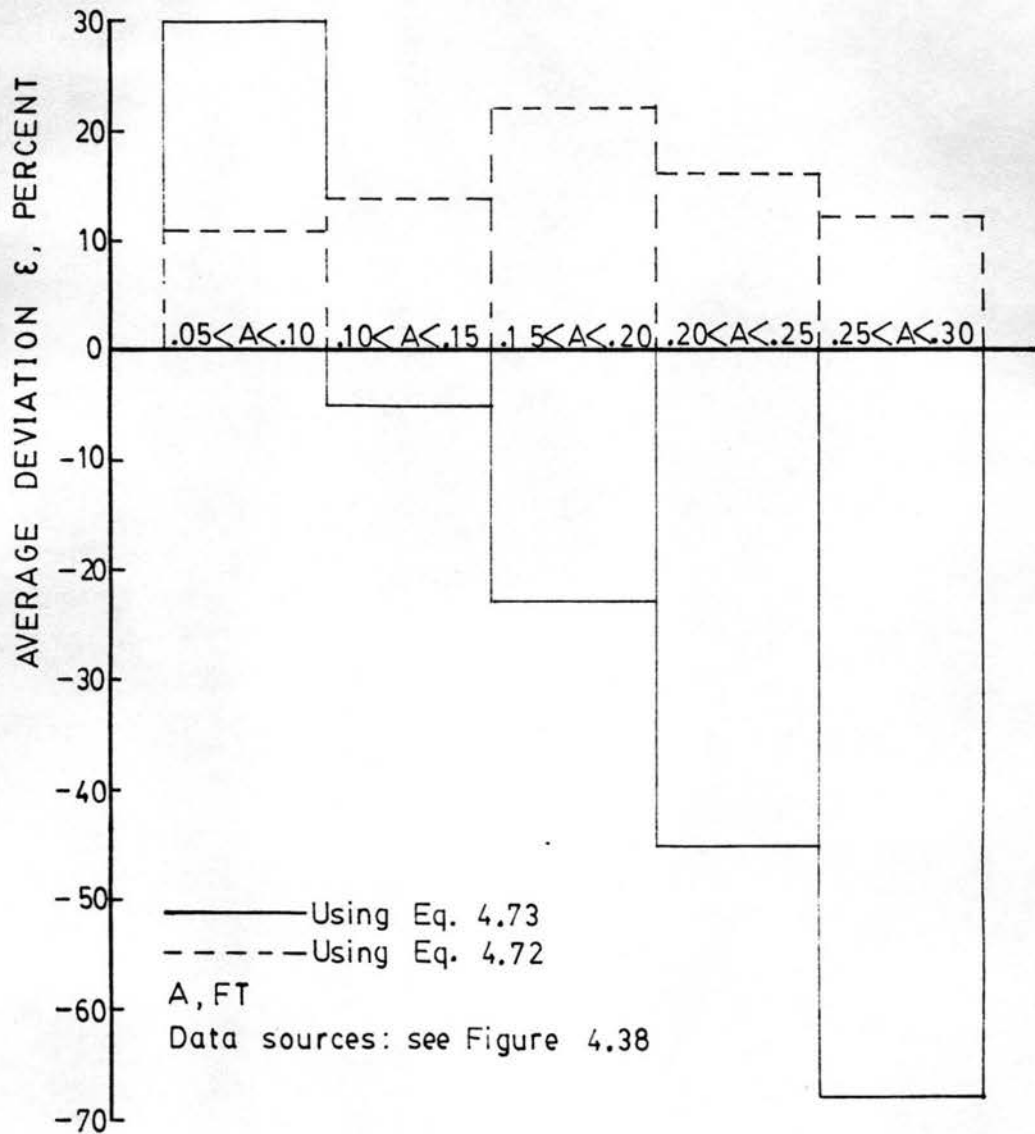


Figure 4.39. Average Deviation of Predicted f' from f'_e for Different Ranges of Bedform Heights Using Reported Alluvial Data

the same bedform height as in the studies by Engel and Lau (1980) and Vittal et al. (1977) with an R_e value of 100,000 and $L/R_b = 5$, the variation of the predicted f' with d_{50}/A was plotted for various values of A/L as shown in Figure 4.40. Notice that the parameter d_{50}/A has a large effect on the predicted bed skin friction factor for bedforms with small steepness ratios, but becomes relatively unimportant as the steepness ratio increases. This observation agrees with that made by Engel and Lau (1980). For the same values of A and R_e , the predicted bed skin friction factor was also plotted against the parameter R_b/d_{50} for various values of A/L , as illustrated in Figure 4.41. Included in this figure is the relationship given by Yalin (1977) for plane bed:

$$f' = 1.3 \left[\ln \left(11 \frac{D}{k_s} \right) \right]^{-2} \quad (4.76)$$

using $D = R_b$ and $k_s = 2 d_{50}$. It is observed that Eq. 4.76 overestimates the value of predicted bed skin friction factor for bedforms with A/L greater than about 0.05. Similar results were obtained by Vittal et al. (1977) where measured values of f' were compared to those estimated from the Moody Diagram.

Figures 4.40 and 4.41 are valid for the particular values of A , R_e , and R_b/L . However, similar figures may be drawn for various values of these parameters. The value of bedform height has a dramatic effect on the bed skin friction factor computed using Eq. 4.72. This effect is illustrated in Figure 4.42. Using $R_e = 100,000$, $L/R_b = 5$, $A/L = 0.05$, and $d_{50} = 1$ mm, the value of f' was computed using Eq. 4.72. As seen in Figure 4.42, the computed bed friction factor increases rapidly with bedform height for values of A larger than

Assumptions :

$A = 0.098 \text{ FT}$

$Re = 1 \times 10^5$

$R_b = L / 5$

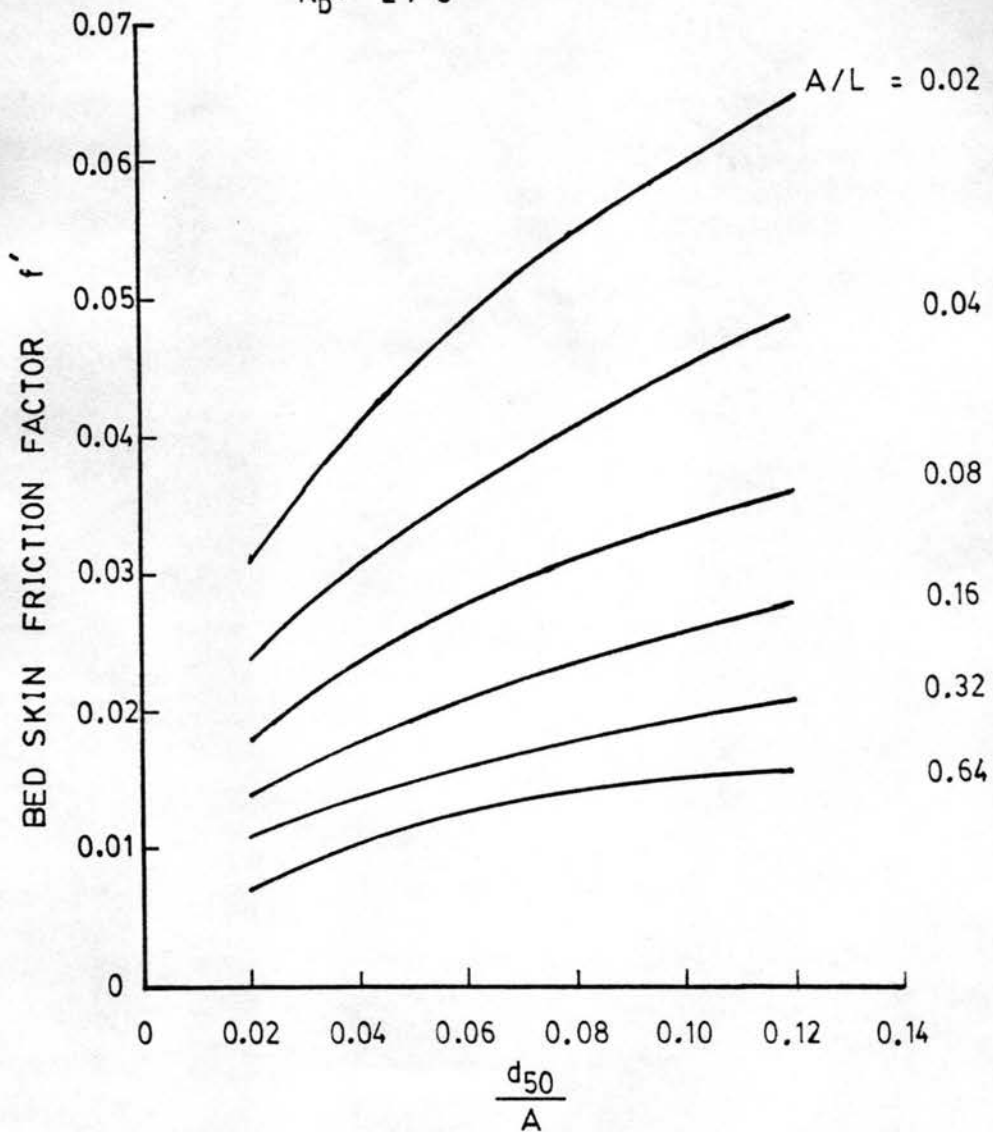


Figure 4.40. Variation of Bed Skin Friction Factor with $\frac{d_{50}}{A}$ and Bedform Steepness Using Equation 4.72

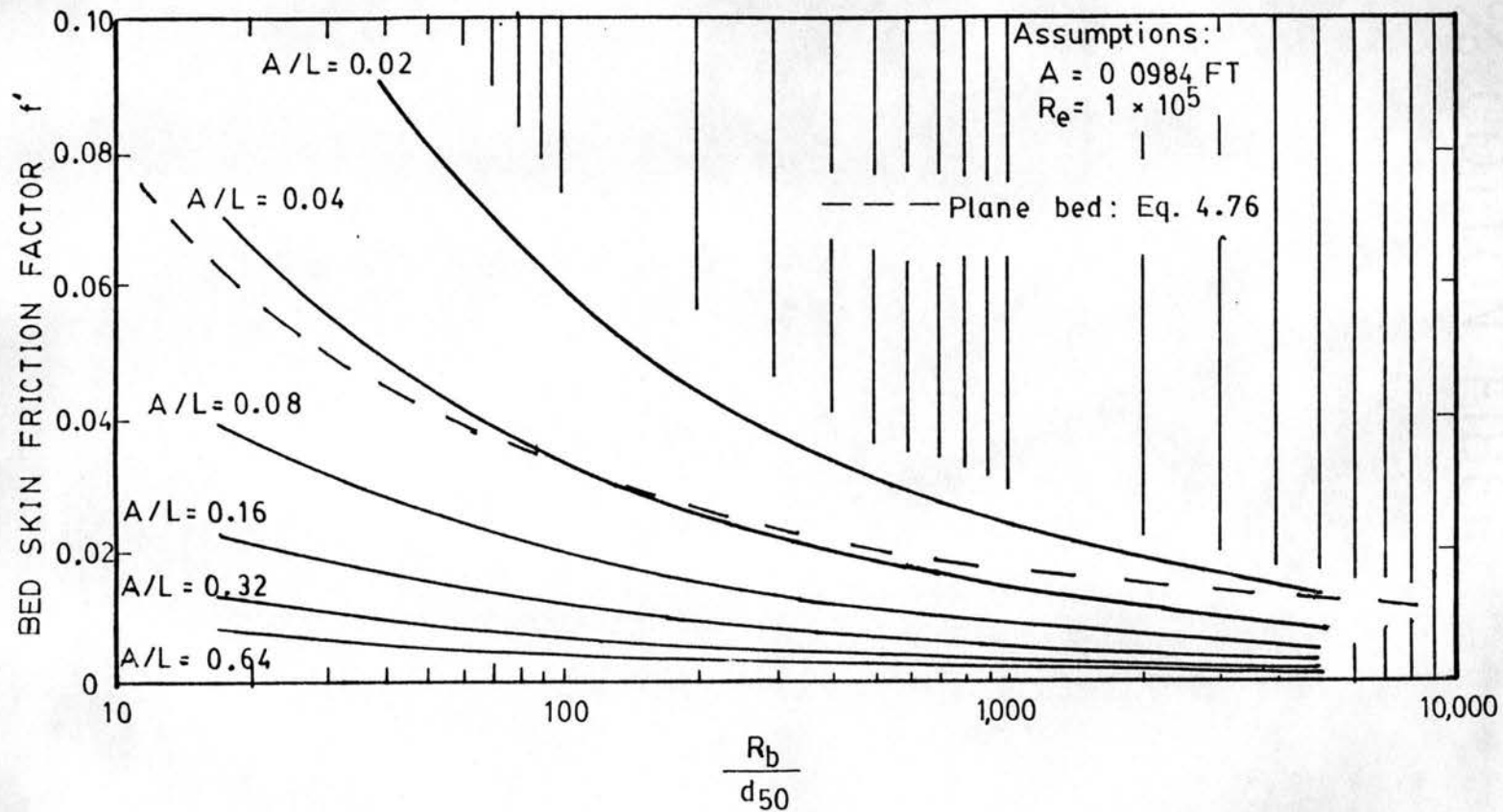


Figure 4.41. Effect of R_b/d_{50} on Bed Skin Friction Factor Using Equation 4.72

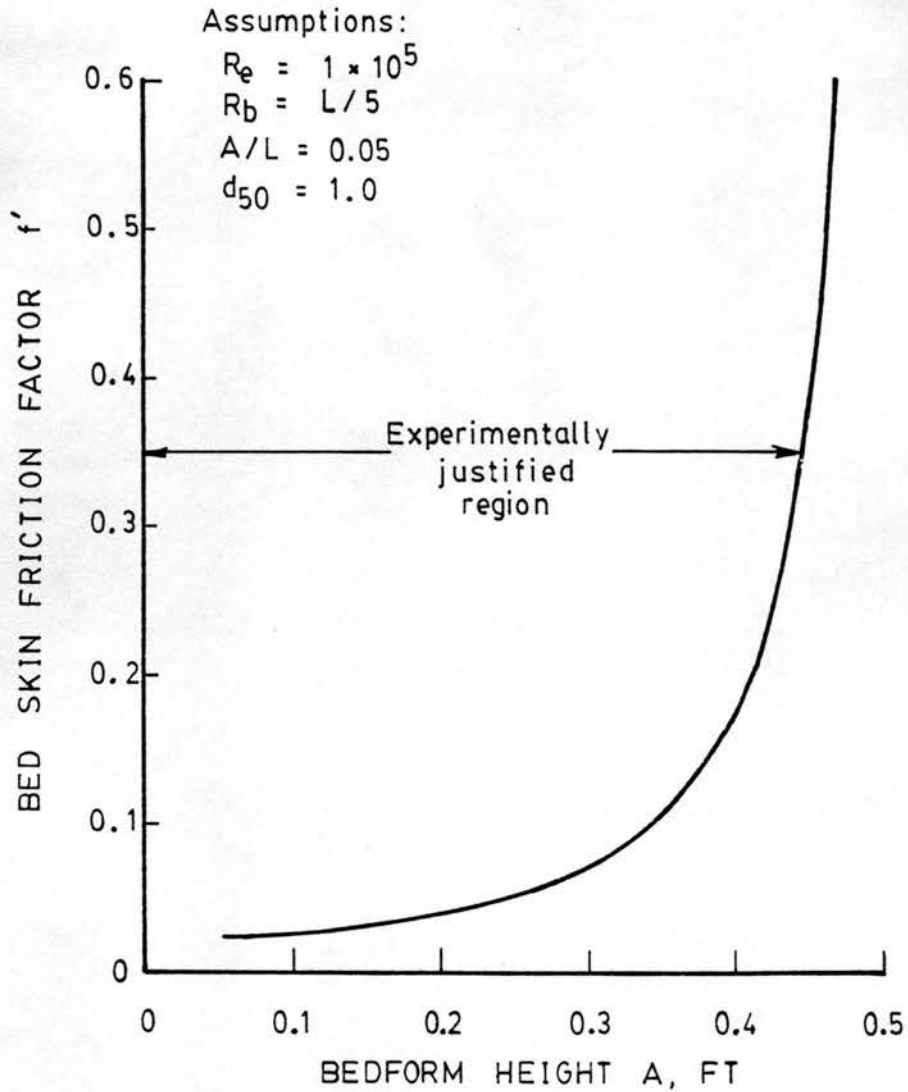


Figure 4.42. Effect of Bedform Height on Bed Skin Friction Factor Computed Using Equation 4.72

about 0.45 ft. Further experimentation is required to justify Eq. 4.72 for values of bedform height larger than those used in the present study.

4.6 Velocity Distributions

Free stream and boundary layer velocity distributions were measured at various locations over the length of the test bedform for selected experimental runs of the smooth and rough uniform bedform studies. Point velocities were measured using a small pitot tube 0.065 in. in diameter. The boundary layer region under study was the region extending from the bedform surface to a height of 0.25 in., corresponding to the diameter of the pitot tube used for local shear stress measurement. A summary of the boundary layer and free stream velocity data measured is presented.

4.6.1 Boundary Layer Velocity Distribution Over Smooth Bedform

The assumed boundary layer velocity equation for the smooth study was

$$\frac{u}{u_*'} = 8.61 \left(\frac{u_*' y}{\nu} \right)^{1/7} \quad (4.44)$$

In order to verify this assumption, and to confirm the smooth shear stress data presented in Section 4.5, the boundary layer velocity distribution was measured at three locations along the test bedform upstream surface for six of the 12 smooth uniform bedform experimental runs. This data is summarized in Tables 4.16-4.18. The dimensionless quantities of Eq. 4.44 were computed for each measured point velocity, using the local shear velocity computed from the measured shear stress distributions presented previously, and using the appropriate value for

Table 4.16. Boundary Layer Velocity Measurements for Uniform, Smooth Bedform Experiment

y	x = 1.465 ft			x = 1.240 ft		
	Run 1 u	Run 2 u	Run 3 u	Run 7 u	Run 8 u	Run 9 u
0.003	0.207	0.164	0.104	0.553	0.617	0.687
0.006	0.220	0.284	0.243	0.553	0.758	0.639
0.009	0.284	0.264	0.264	0.687	0.806	0.861
0.012	0.302	0.408	0.207	0.722	0.710	0.775
0.015	0.336	0.366	0.274	0.663	0.799	0.845
0.017	0.359	0.408	---	---	---	---
0.018	---	---	0.254	0.695	0.819	0.822
0.020	0.302	0.351	---	---	---	---
0.021	---	---	0.274	0.634	0.775	0.832

Units: y = ft
u = ft/s

Table 4.17. Boundary Layer Velocity Measurements for Uniform, Smooth Bedform Experiment

y	x = 1.690 ft					
	Run 1 u	Run 2 u	Run 3 u	Run 7 u	Run 8 u	Run 9 u
0.003	0.274	0.311	0.207	1.118	1.232	1.260
0.006	0.351	0.395	0.366	1.256	1.353	1.296
0.009	0.421	0.452	0.401	1.301	1.400	1.385
0.012	0.408	0.440	0.381	1.319	1.421	1.430
0.015	0.433	0.395	0.414	1.369	1.449	1.436
0.018	0.457	0.433	0.433	1.343	1.483	1.505
0.021	0.421	0.538	0.446	1.426	1.510	1.486

Units: y = ft
u = ft/s

Table 4.18. Boundary Layer Velocity Measurements for Uniform, Smooth Bedform Experiment

y	x = 2.190 ft					
	Run 1 u	Run 2 u	Run 3 u	Run 7 u	Run 8 u	Run 9 u
0.003	0.634	0.718	0.609	2.120	2.228	2.066
0.006	0.733	0.775	0.695	2.186	2.369	2.352
0.009	0.751	0.761	0.740	2.274	2.413	2.366
0.012	0.768	0.835	0.736	2.305	2.402	2.387
0.015	0.761	0.822	0.758	2.285	2.441	2.395
0.018	0.754	0.758	0.765	2.254	2.392	2.447
0.021	0.758	0.729	0.722	2.343	2.387	2.420

Units: y = ft
u = ft/s

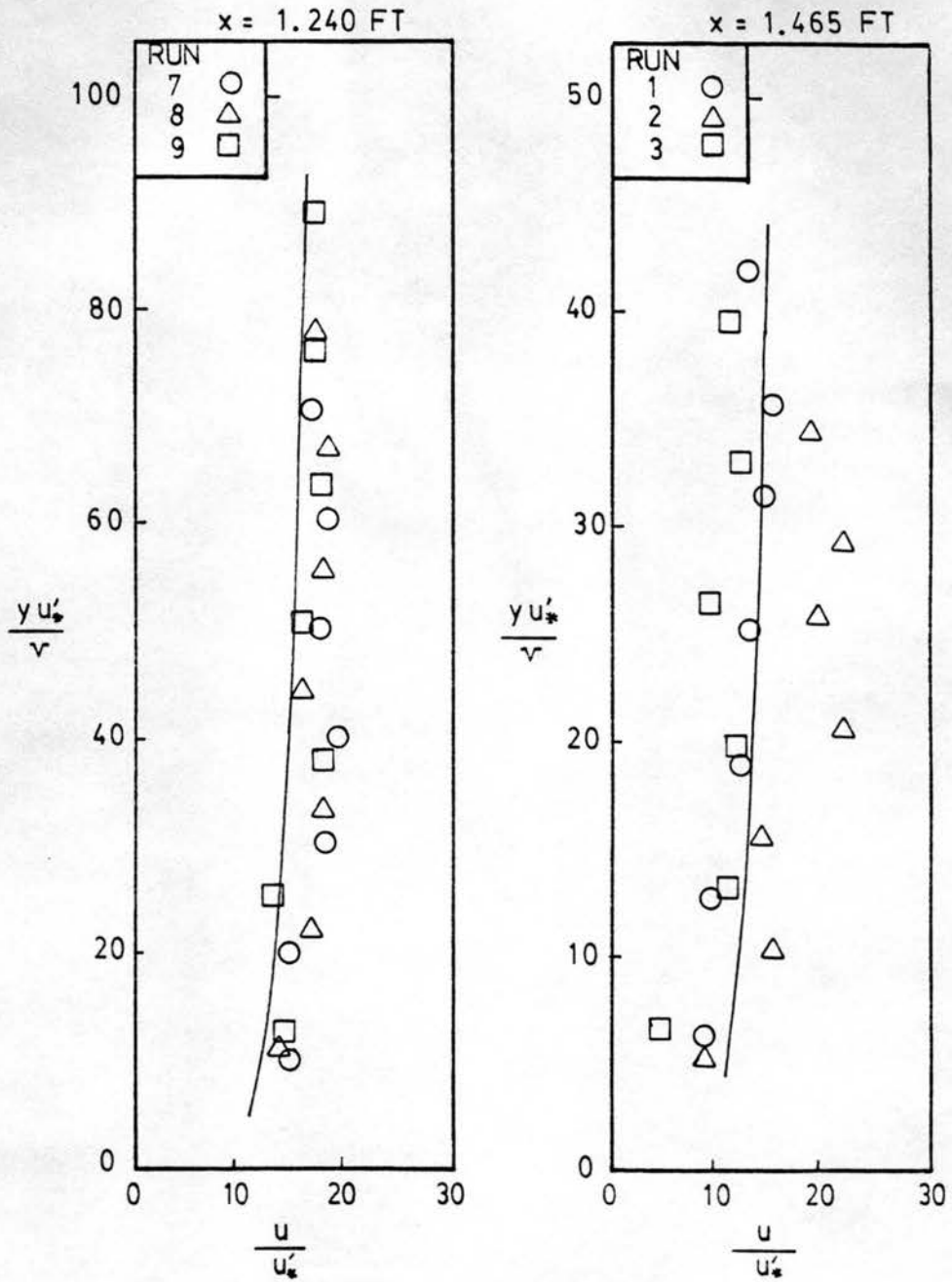
the kinematic viscosity. The velocity distributions at each measurement location are presented in dimensionless form in Figures 4.43-4.45. The data exhibits considerable scatter at measurement locations near the reattachment point, yet follows the trend of Eq. 4.44 quite well for measurement locations further downstream. On the basis of these figures, Eq. 4.44 was considered to adequately represent the boundary layer velocity distribution along the upstream face of the bedform downstream of the separation region, and the previously presented shear stress data was deemed valid.

4.6.2 Boundary Layer Velocity Distribution Over Rough Bedform

A power law of the form

$$\frac{u}{u_*'} = C_1 \left(\frac{y}{k_s} \right)^{1/\eta} \quad (4.64)$$

was assumed for the boundary layer velocity profile for the rough bedform study. Boundary layer velocity distributions were measured at two locations on the test bedform surface in order to validate the above assumption. These measurements were made for each experimental run of the uniform, rough bedform study. A summary of the data is contained in Tables 4.19 and 4.20. The measured data is presented in nondimensional form in Figure 4.46. The median grain size of the roughness material was used to nondimensionalize the quantity y , and the local shear velocity, computed from the previously presented shear stress distributions, was used to nondimensionalize the point velocity u . As indicated by Fig. 4.46, the data exhibits a general trend. The scatter of the data is understandable, due to the inability to place the measurement probes (shear and velocity) in exactly the same place with respect to the roughness grains in the course of each measurement.



————— Eq. 4.44

Figure 4.43. Variation of yu'_*/ν with u/u'_* for Uniform, Smooth Bedform Experiment: $x = 1.240$ and 1.465 ft

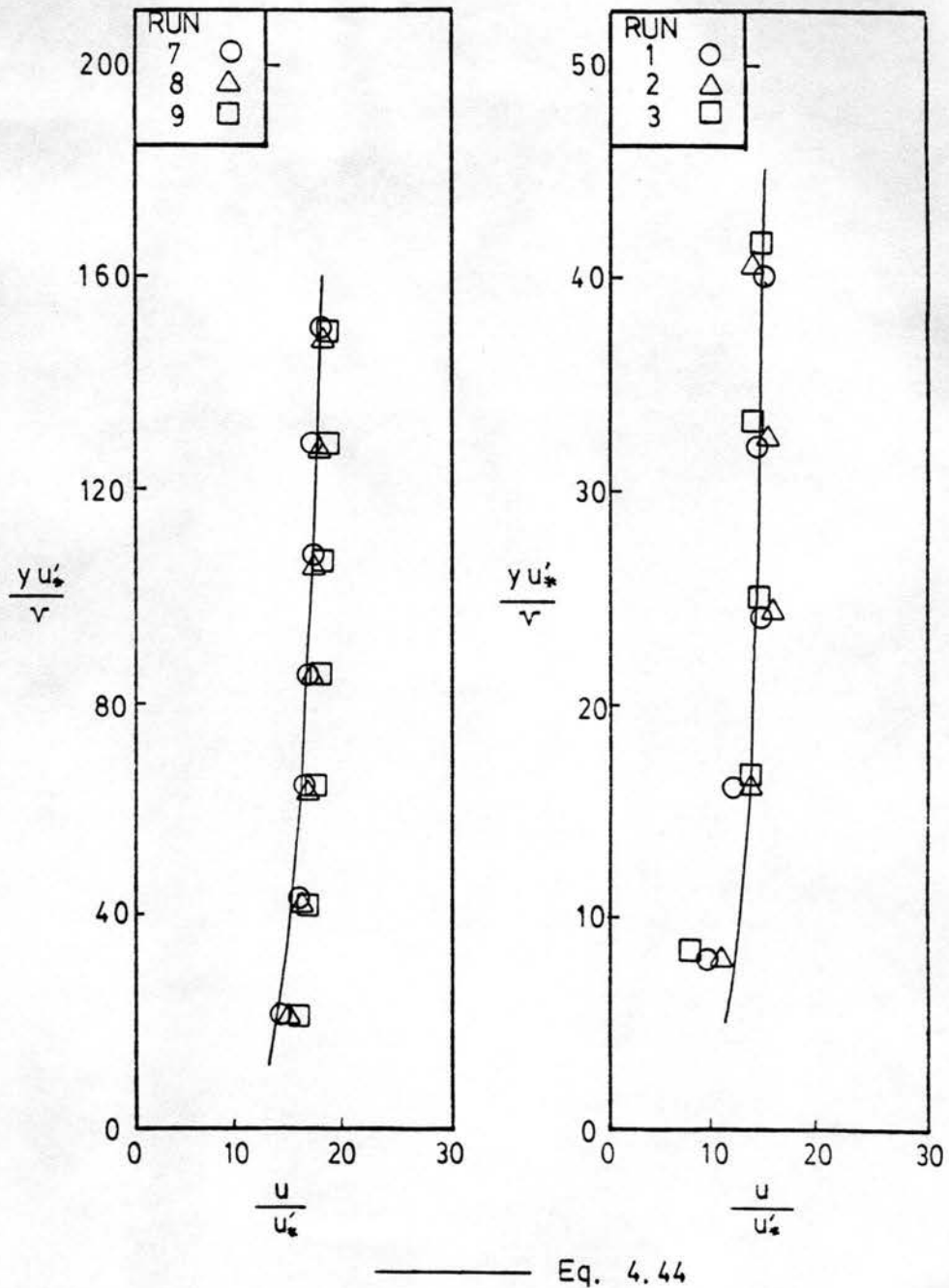


Figure 4.44. Variation of $y u'_*/\nu$ with u/u'_* for Uniform, Smooth Bedform Experiment: $x = 1.690$ ft

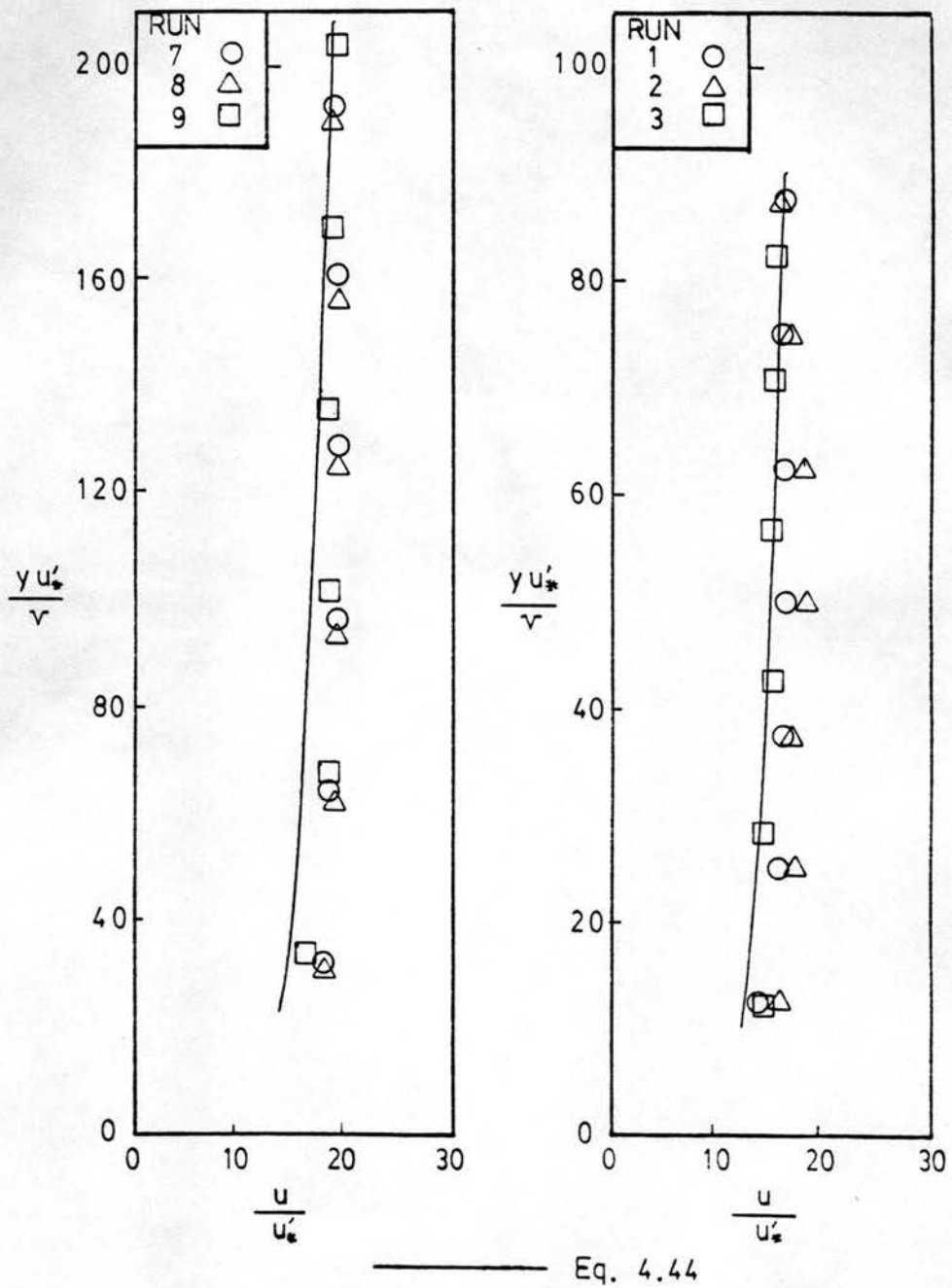


Figure 4.45. Variation of yu'_x/v with u/u'_x for Uniform, Smooth Bedform Experiment: $x = 2.190$ ft

Table 4.19. Boundary Layer Velocity Measurements for Uniform,
Rough Bedform Experiment

$x = 1.682 \text{ ft}$						
y	Run 1R u	Run 2R u	Run 3R u	Run 7R u	Run 8R u	Run 9R u
0.003	0.254	0.254	0.250	0.796	0.845	0.835
0.004	0.274	0.284	0.254	0.829	0.906	0.932
0.005	0.311	0.311	0.311	0.882	0.972	0.964
0.006	0.344	0.319	0.319	0.927	0.996	1.028
0.007	0.336	0.328	0.336	1.007	1.054	1.069
0.009	0.366	0.359	0.351	1.015	1.101	1.104
0.013	0.408	0.414	0.401	1.172	1.190	1.215
0.021	0.440	0.446	0.452	1.275	1.292	1.333

Units: $y = \text{ft}$
 $u = \text{ft/s}$

Table 4.20. Boundary Layer Velocity Measurements for Uniform,
Rough Bedform Experiment

y	x = 2.182 ft					
	Run 1R u	Run 2R u	Run 3R u	Run 7R u	Run 8R u	Run 9R u
0.003	0.232	0.344	0.302	1.449	1.228	1.186
0.004	0.366	0.408	0.319	1.510	1.277	1.378
0.005	0.469	0.502	0.310	1.641	1.415	1.552
0.006	0.513	0.502	0.366	1.715	1.535	1.662
0.007	0.553	0.543	0.427	1.806	1.667	1.723
0.009	0.609	0.604	0.553	1.876	1.787	1.781
0.013	0.663	0.630	0.609	2.031	1.940	1.949
0.021	0.706	0.687	0.679	2.076	2.108	2.037

Units: y = ft
u = ft/s

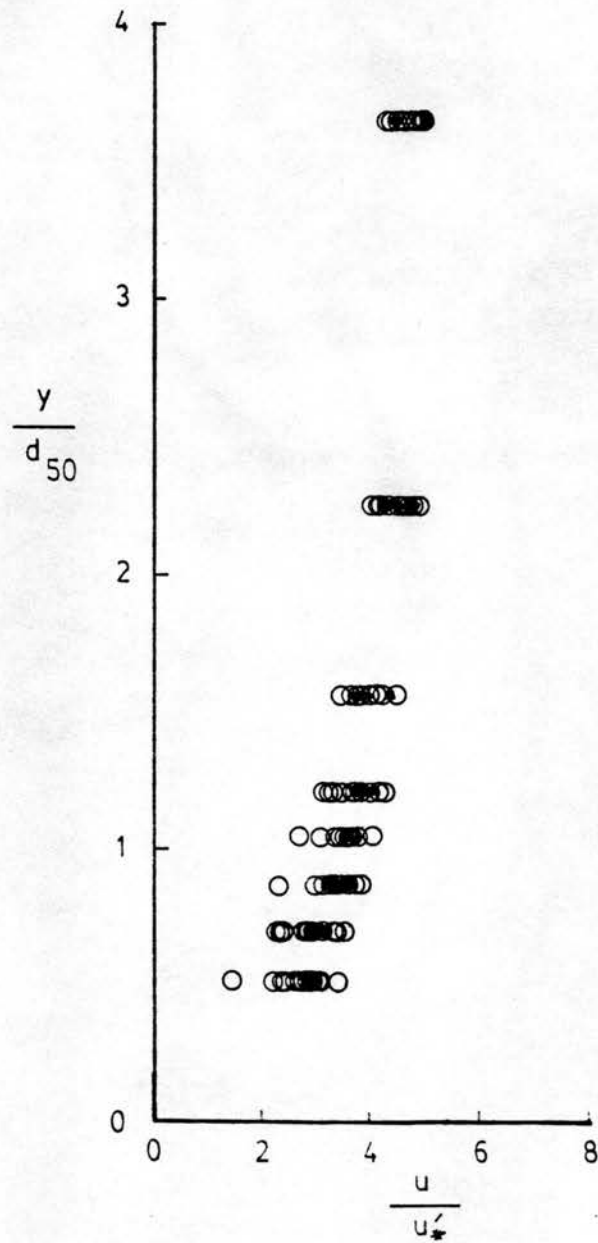


Figure 4.46. Nondimensional Boundary Layer Velocity Profiles for Uniform, Rough Bedform Experiment

The trend of the data in Fig. 4.46 may be further illustrated by plotting the average u/u_*' value for each value of y/d_{50} , as shown in Figure 4.47. The data from this figure was shown to fit the equation

$$\frac{u}{u_*'} = \frac{10}{3} \left(\frac{y}{d_{50}}\right)^{3/10} \quad (4.77)$$

which is of the same form as Eq. 4.64 with $k_s = d_{50}$, and $C_1 = \eta = 10/3$. Thus, an equation of the form of Eq. 4.64 was found to adequately represent the boundary layer velocity profile along the upstream face of the roughened bedform, at locations downstream of the separation region.

The data from Fig. 4.48 was found to also fit the equation

$$\frac{u}{u_*'} = 0.40(5.75 \log \frac{y}{d_{50}} + 8.5) \quad (4.78)$$

which is similar to the relation developed by Nikuradse [see Schlichting (1980)] for rough pipe flow. Nikuradse's equation is

$$\frac{u}{U_*} = \frac{2.3}{K} \log \frac{y}{k_s} + 8.5 \quad (2.4)$$

Using $K = 0.40$, $k_s = d_{50}$, and u_*' for U_* this equation differs from Eq. 4.78 by a single constant. A more general form of Eq. 2.4 may be written as

$$\frac{u}{u_*'} = C_3 \left(\frac{2.3}{K} \log \frac{y}{k_s} + 8.5\right) \quad (4.79)$$

where C_3 is a variable whose value may depend on some parameter related to the bedform geometry. For flat bed or pipe flow, C_3 has been found to be equal to 1.0. For flow over bedforms with the geometry used in the present study, C_3 was found to be equal to 0.40. In

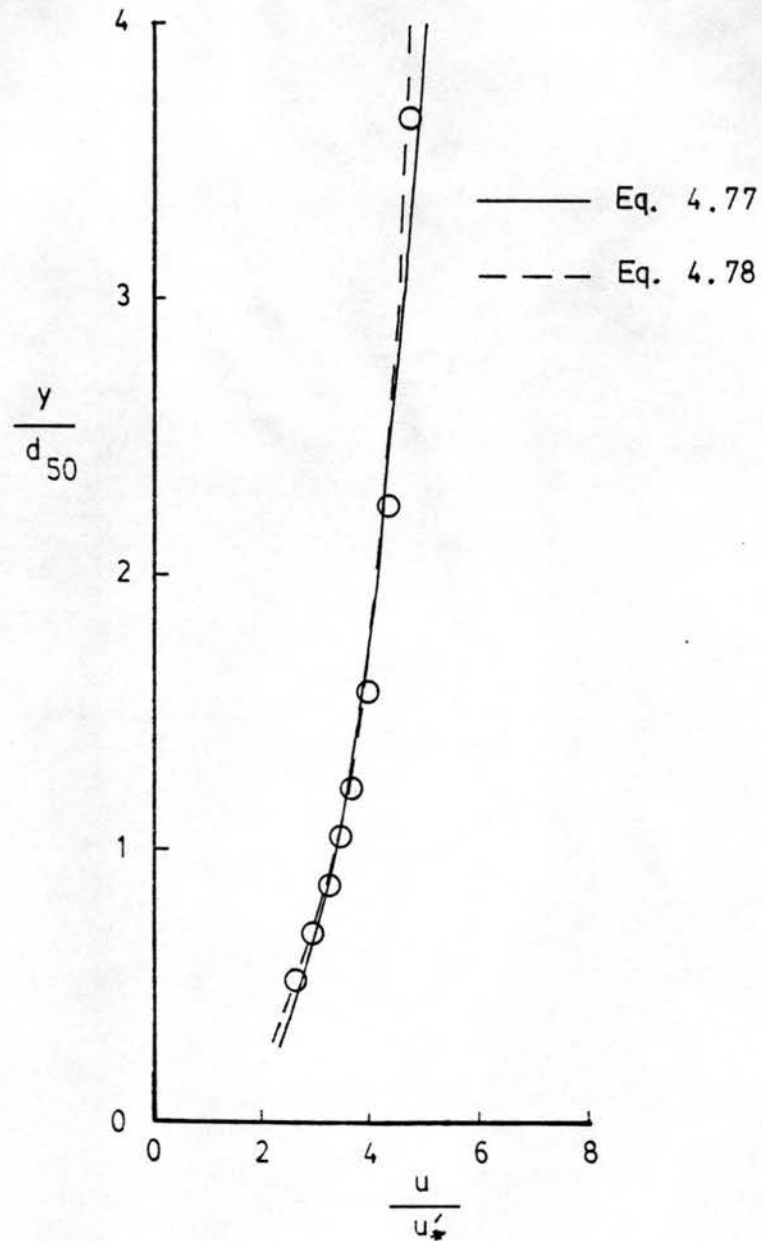


Figure 4.47. Average Nondimensional Boundary Layer Velocity Profile for Uniform, Rough Bedform Experiment

the previous section of this thesis, it was found that the bed skin shear stress was dependent upon the height of the bedform as well as other parameters. In view of this finding, it seems likely that C_3 is also dependent on the bedform height. The gravitational effect on the water as it flows over the crest of an upstream bedform and reattaches on the immediately downstream bedform may in part explain the dependence of bed skin shear stress on bedform height, and may explain the variation of C_3 in Eq. 4.79. Further experimentation is required in order to verify this hypothesis.

4.6.3 Average Velocity Distribution Over Bedform

Free stream velocity distributions were measured at seven locations along the length of the test bedform for six of the 12 experimental runs of the uniform, smooth bedform study. The measured data is summarized in Tables 4.21-4.27. It was found that by plotting y_m/D against u/V_c , all the measured data, representing 42 separate velocity profiles, could be made to follow the same general trend as shown in Figure 4.48. In this figure, u is the measured point velocity at a distance y_m from the mean bed line, and V_c is the average velocity at the bedform crest. The mean bed line is defined as the line parallel to the flume a distance of $A/2$ from the bedform base. The majority of the band of data contained in Fig. 4.48 fit the equation

$$\frac{u}{V_c} = 1.25 + 0.40 \ln \frac{y_m}{D} \quad (4.80)$$

although considerable deviation from the line representing Eq. 4.80 exists for values of u/V_c greater than about 1.0.

Free stream velocity distributions were measured at three locations along the length of the test bedform for all of the experimental runs

Table 4.21. Free Stream Velocity Measurements for Uniform, Smooth Bedform Experiment

x = 0.00 ft											
Run 1		Run 2		Run 3		Run 7		Run 8		Run 9	
y	u	y	u	y	u	y	u	y	u	y	u
0.932	0.768	1.095	0.835	1.245	0.747	0.932	2.198	1.095	2.322	1.245	2.340
0.882	0.779	0.995	0.848	1.145	0.772	0.832	2.340	0.995	2.413	1.145	2.047
0.832	0.809	0.895	0.842	1.045	0.806	0.732	2.379	0.895	2.424	1.045	2.490
0.782	0.812	0.795	0.842	0.954	0.826	0.632	2.385	0.795	2.473	0.945	2.506
0.732	0.826	0.695	0.842	0.845	0.848	0.582	2.293	0.695	2.463	0.845	2.543
0.632	0.802	0.595	0.822	0.745	0.809	0.532	2.053	0.595	2.351	0.745	2.495
0.582	0.740	0.545	0.796	0.645	0.792	0.482	1.447	0.495	1.718	0.645	2.430
0.532	0.679	0.495	0.630	0.545	0.679	0.432	0.882	0.395	0.842	0.545	2.117
0.482	0.502	0.445	0.508	0.495	0.591	0.382	0.655	0.295	0.164	0.445	1.331
0.432	0.311	0.395	0.351	0.445	0.446	0.332	0.220			0.395	0.751
		0.345	0.194	0.395	0.194					0.345	0.401

Units: y = ft
u = ft/s

Table 4.22. Free Stream Velocity Measurements for Uniform, Smooth Bedform Experiment

x = 0.446 ft											
Run 1		Run 2		Run 3		Run 7		Run 8		Run 9	
y	u	y	u	y	u	y	u	y	u	y	u
0.841	0.733	1.004	0.761	1.154	0.725	0.841	2.198	1.004	2.192	1.154	2.258
0.741	0.761	0.904	0.786	1.054	0.743	0.741	2.212	0.904	2.264	1.054	2.287
0.641	0.761	0.804	0.802	0.954	0.747	0.641	2.258	0.804	2.345	0.954	2.385
0.541	0.733	0.704	0.819	0.854	0.799	0.541	2.123	0.704	2.374	0.854	2.457
0.491	0.714	0.604	0.775	0.754	0.802	0.491	1.979	0.604	2.391	0.754	2.468
0.441	0.614	0.504	0.736	0.654	0.816	0.441	1.802	0.504	2.246	0.654	2.473
0.391	0.558	0.454	0.675	0.554	0.740	0.391	1.341	0.404	1.671	0.554	2.311
0.341	0.344	0.404	0.647	0.454	0.667	0.341	1.111	0.304	0.983	0.454	1.979
0.291	0.264	0.354	0.634	0.404	0.543	0.291	0.733			0.354	1.409
		0.304	0.344	0.354	0.463	0.241	0.284			0.304	1.087
		0.254	0.254	0.304	0.284					0.254	0.591
				0.254	0.232						

Units: y = ft
u = ft/s

Table 4.23. Free Stream Velocity Measurements for Uniform, Smooth Bedform Experiment

x = 0.890 ft											
Run 1		Run 2		Run 3		Run 7		Run 8		Run 9	
y	u	y	u	y	u	y	u	y	u	y	u
0.751	0.687	0.914	0.733	1.064	0.687	0.751	1.910	0.914	2.072	1.064	2.142
0.651	0.703	0.814	0.751	0.964	0.699	0.651	1.993	0.814	2.117	0.964	2.204
0.551	0.714	0.714	0.768	0.864	0.722	0.551	2.000	0.714	2.198	0.864	2.317
0.451	0.675	0.614	0.725	0.764	0.754	0.451	1.868	0.614	2.222	0.764	2.357
0.401	0.634	0.514	0.714	0.664	0.768	0.401	1.734	0.514	2.173	0.664	2.374
0.351	0.528	0.414	0.710	0.564	0.753	0.351	1.654	0.414	1.931	0.564	2.305
0.301	0.446	0.364	0.675	0.464	0.714	0.301	1.310	0.314	1.530	0.464	2.085
0.251	0.311	0.314	0.613	0.364	0.586	0.251	0.912	0.214	1.041	0.364	1.853
0.201	0.254	0.264	0.567	0.314	0.548	0.201	0.675	0.114	0.491	0.264	1.290
		0.214	0.381	0.264	0.475	0.151	0.433			0.214	1.147
		0.164	0.336	0.214	0.319					0.164	0.714
		0.114	0.207	0.164	0.194					0.114	0.433
				0.114	0.164						

Units: y = ft
u = ft/s

Table 4.24. Free Stream Velocity Measurements for Uniform, Smooth Bedform Experiment

Run 1		x = 1.465 ft Run 2		Run 3		Run 7		x = 1.240 ft Run 8		Run 9	
y	u	y	u	y	u	y	u	y	u	y	u
0.020	0.302	0.020	0.351	0.021	0.274	0.021	0.634	0.021	0.775	0.021	0.832
0.053	0.359	0.066	0.452	0.066	0.293	0.100	0.802	0.063	0.972	0.063	0.996
0.153	0.388	0.116	0.486	0.116	0.344	0.200	1.181	0.113	1.069	0.113	1.036
0.253	0.543	0.166	0.480	0.166	0.414	0.300	1.537	0.163	1.170	0.163	1.204
0.353	0.604	0.216	0.491	0.216	0.463	0.400	1.749	0.213	1.380	0.263	1.563
0.453	0.613	0.266	0.613	0.266	0.502	0.500	1.868	0.263	1.489	0.363	1.931
0.553	0.600	0.316	0.626	0.316	0.581	0.600	1.831	0.313	1.654	0.463	2.246
0.636	0.604	0.416	0.663	0.416	0.675	0.683	1.779	0.363	1.882	0.563	2.270
		0.516	0.675	0.516	0.706			0.463	2.059	0.663	2.270
		0.616	0.667	0.616	0.706			0.563	2.104	0.763	2.210
		0.716	0.643	0.716	0.683			0.663	2.085	0.863	2.148
		0.806	0.655	0.816	0.647			0.763	2.006	0.963	2.033
				0.916	0.600			0.853	1.882		

Units: y = ft
u = ft/s

Table 4.25. Free Stream Velocity Measurements for Uniform, Smooth Bedform Experiment

x = 1.690 ft											
Run 1		Run 2		Run 3		Run 7		Run 8		Run 9	
y	u	y	u	y	u	y	u	y	u	y	u
0.021	0.421	0.021	0.538	0.021	0.446	0.021	1.426	0.021	1.510	0.021	1.486
0.106	0.518	0.069	0.528	0.069	0.480	0.106	1.437	0.069	1.537	0.069	1.607
0.206	0.567	0.119	0.528	0.119	0.497	0.206	1.622	0.119	1.622	0.119	1.669
0.306	0.604	0.169	0.600	0.169	0.543	0.306	1.794	0.169	1.757	0.169	1.824
0.406	0.647	0.219	0.613	0.219	0.609	0.406	1.868	0.219	1.861	0.219	1.889
0.506	0.613	0.269	0.634	0.269	0.617	0.506	1.868	0.269	1.945	0.269	2.022
0.589	0.595	0.369	0.675	0.369	0.710	0.589	1.853	0.369	2.079	0.369	2.224
		0.469	0.725	0.469	0.710			0.469	2.148	0.469	2.287
		0.569	0.679	0.569	0.722			0.569	2.111	0.569	2.305
		0.669	0.671	0.669	0.695			0.669	2.026	0.669	2.282
		0.759	0.655	0.769	0.675			0.759	1.986	0.769	2.167
				0.869	0.639					0.869	2.098

Units: y = ft
u = ft/s

Table 4.26. Free Stream Velocity Measurements for Uniform, Smooth Bedform Experiment

x = 2.190 ft											
Run 1		Run 2		Run 3		Run 7		Run 8		Run 9	
y	u	y	u	y	u	y	u	y	u	y	u
0.021	0.758	0.021	0.729	0.021	0.722	0.021	2.343	0.021	2.387	0.021	2.420
0.071	0.733	0.060	0.751	0.060	0.758	0.071	2.262	0.060	2.315	0.060	2.322
0.147	0.710	0.110	0.751	0.110	0.722	0.147	2.113	0.110	2.194	0.110	2.299
0.197	0.710	0.160	0.743	0.160	0.725	0.197	2.123	0.160	2.259	0.160	2.282
0.297	0.683	0.260	0.743	0.260	0.768	0.297	2.117	0.260	2.305	0.260	2.357
0.397	0.683	0.360	0.733	0.360	0.761	0.397	2.098	0.360	2.311	0.360	2.430
0.480	0.655	0.460	0.714	0.460	0.751	0.480	2.098	0.460	2.264	0.460	2.424
		0.560	0.695	0.560	0.736			0.560	2.179	0.560	2.357
		0.650	0.675	0.660	0.671			0.650	2.123	0.660	2.230
				0.760	0.643					0.760	2.182

Units: y = ft
u = ft/s

Table 4.27. Free Stream Velocity Measurements for Uniform, Smooth Bedform Experiment

x = 2.612 ft											
Run 1		Run 2		Run 3		Run 7		Run 8		Run 9	
y	u	y	u	y	u	y	u	y	u	y	u
0.708	0.754	0.871	0.751	1.021	0.675	0.708	2.216	0.871	2.264	1.021	2.252
0.608	0.743	0.771	0.772	0.921	0.710	0.608	2.210	0.771	2.276	0.921	2.322
0.508	0.733	0.671	0.786	0.821	0.733	0.508	2.142	0.671	2.334	0.821	2.391
0.408	0.733	0.571	0.786	0.721	0.796	0.408	2.142	0.571	2.340	0.721	2.435
0.358	0.733	0.471	0.786	0.621	0.802	0.358	2.117	0.471	2.317	0.621	2.457
0.308	0.671	0.371	0.751	0.521	0.782	0.308	2.098	0.371	2.270	0.521	2.374
0.258	0.655	0.321	0.733	0.421	0.747	0.258	2.006	0.271	2.098	0.421	2.317
0.208	0.491	0.271	0.675	0.321	0.736	0.208	1.571	0.171	1.269	0.321	2.204
0.158	0.147	0.221	0.634	0.271	0.714	0.158	1.023	0.071	0.600	0.221	1.824
		0.171	0.344	0.221	0.513	0.108	0.591			0.171	1.483
		0.121	0.127	0.171	0.433					0.121	0.996
										0.071	0.867
										0.021	0.695

Units: y = ft
u = ft/s

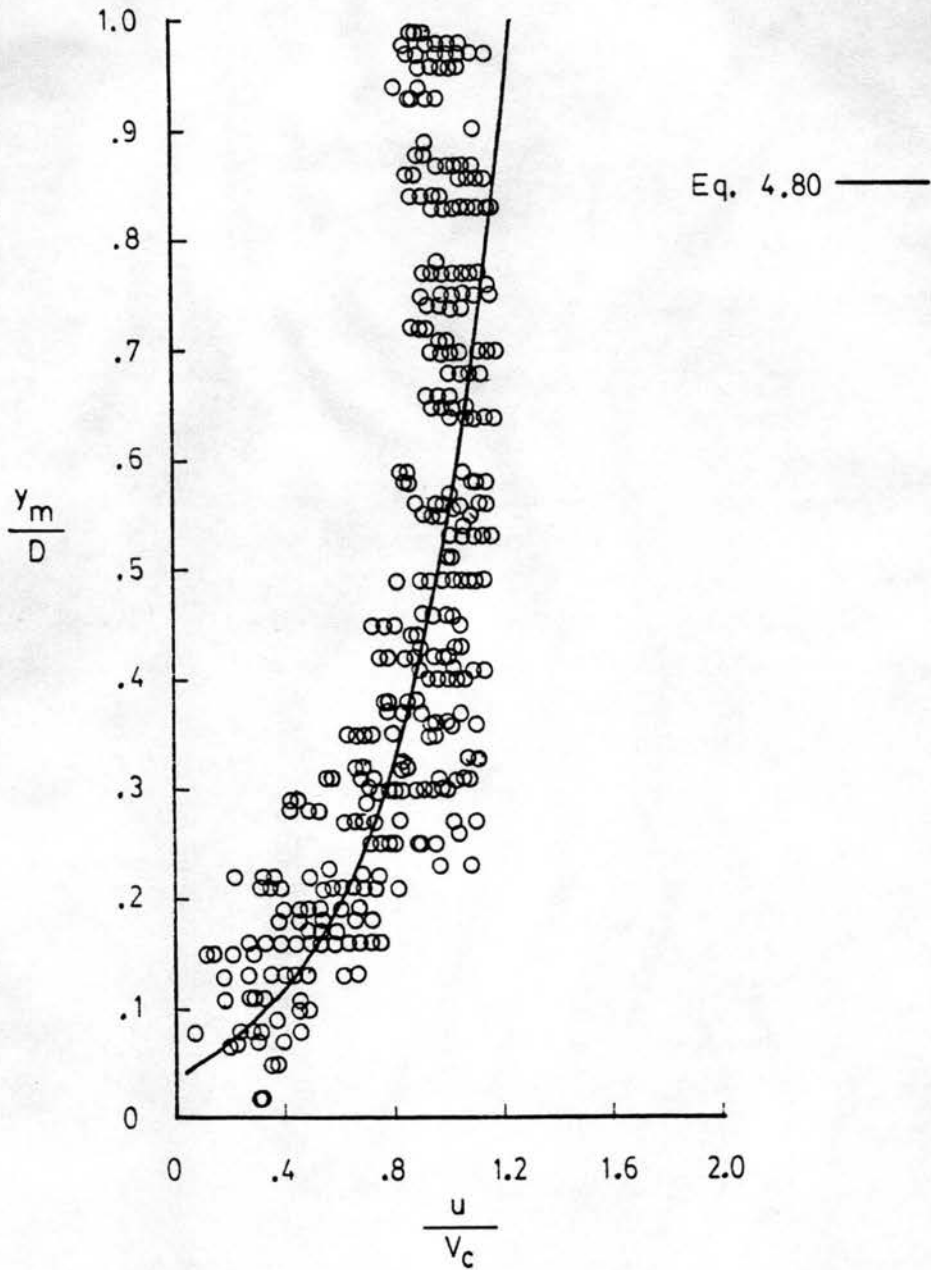


Figure 4.48. Nondimensional Velocity Profiles for Uniform, Smooth Bedform Experiment

of the uniform, rough bedform study. A summary of the measured data is presented in Tables 4.28-4.30. A plot of the measured data, using the same parameters as in Fig. 4.48, is shown in Fig. 4.49. The trend of the data for the rough bedform is identical to that observed for the data using a smooth bedform, indicating that for the size of roughness used in the present study, the average velocity distribution is not dependent on the local roughness.

Jonys (1973) used the hydrogen bubble technique to determine mean dimensionless velocity profiles for 10 different positions along naturally formed bedforms. On the basis of several experimental runs with various flow conditions, he also developed an average dimensionless bedform profile. Using this data and the flow conditions and observed bedform heights from two of his experimental runs (Run 24, Range 2 and Run 17, Range 2) Figure 4.50 was plotted, using the parameters developed in the present study. As indicated by this figure, the data from Jonys (1973) exhibits the same trend as the data in Figs. 4.48 and 4.49.

Haque (1970) made velocity profile measurements at five different locations along the length of a modeled stationary bedform for two different flow conditions. His data is presented in Figure 4.51. This data seems to follow Eq. 4.80 over the entire range of u/V_c . It is possible that the deviation of the data from Eq. 4.80, shown in Figs. 4.48, 4.49 and 4.50, may be caused by the relative depths of flow used in the studies these figures represent. In the present study, experimental runs were made with A/D values of 0.43, 0.51, and 0.62, for both the smooth and rough bedform studies. The mean dimensionless velocity profiles published by Jonys (1973) were developed from

Table 4.28. Free Stream Velocity Measurements for Uniform, Rough Bedform Experiment

x = 1.182 ft											
Run 1R		Run 2R		Run 3R		Run 7R		Run 8R		Run 9R	
y	u	y	u	y	u	y	u	y	u	y	u
0.021	0.104	0.021	0.207	0.021	0.207	0.021	0.491	0.021	0.609	0.021	0.613
0.037	0.127	0.037	0.243	0.037	0.232	0.037	0.543	0.037	0.647	0.037	0.639
0.069	0.179	0.069	0.284	0.069	0.261	0.069	0.722	0.069	0.743	0.069	0.809
0.133	0.293	0.133	0.311	0.133	0.296	0.133	0.845	0.133	0.950	0.133	0.994
0.233	0.440	0.233	0.480	0.261	0.493	0.233	1.361	0.233	1.349	0.261	1.489
0.333	0.553	0.333	0.651	0.411	0.696	0.333	1.796	0.333	1.747	0.411	2.076
0.433	0.643	0.433	0.659	0.561	0.730	0.433	2.064	0.433	2.187	0.561	2.312
0.533	0.710	0.533	0.740	0.711	0.812	0.533	2.046	0.533	2.221	0.711	2.350
0.633	0.703	0.633	0.754	0.861	0.862	0.633	2.001	0.633	2.266	0.861	2.289
		0.733	0.718	0.961	0.841			0.733	2.193	0.911	2.127
		0.833	0.733					0.833	2.172		

Units: y = ft
u = ft/s

Table 4.29. Free Stream Velocity Measurements for Uniform, Rough Bedform Experiment

$x = 1.682 \text{ ft}$											
Run 1R		Run 2R		Run 3R		Run 7R		Run 8R		Run 9R	
y	u	y	u	y	u	y	u	y	u	y	u
0.021	0.440	0.021	0.446	0.021	0.452	0.021	1.275	0.021	1.292	0.021	1.333
0.037	0.497	0.037	0.480	0.037	0.457	0.037	1.386	0.037	1.345	0.037	1.390
0.069	0.508	0.069	0.523	0.069	0.491	0.069	1.521	0.069	1.476	0.069	1.476
0.133	0.528	0.133	0.563	0.133	0.548	0.133	1.690	0.133	1.603	0.133	1.651
0.233	0.626	0.233	0.595	0.261	0.655	0.233	1.863	0.233	1.863	0.261	1.953
0.333	0.718	0.333	0.675	0.411	0.754	0.333	2.097	0.333	2.127	0.411	2.355
0.433	0.765	0.433	0.740	0.561	0.809	0.433	2.117	0.433	2.250	0.561	2.406
0.533	0.740	0.533	0.743	0.711	0.835	0.533	2.064	0.533	2.273	0.711	2.343
		0.633	0.740	0.861	0.812			0.633	2.333	0.861	2.236
		0.733	0.747					0.733	2.152		

Units: y = ft
u = ft/s

Table 4.30. Free Stream Velocity Measurements for Uniform, Rough Bedform Experiment

x = 2.182 ft											
Run 1R		Run 2R		Run 3R		Run 7R		Run 8R		Run 9R	
y	u	y	u	y	u	y	u	y	u	y	u
0.021	0.706	0.021	0.687	0.021	0.679	0.021	2.076	0.021	2.108	0.021	2.037
0.037	0.754	0.047	0.714	0.037	0.691	0.037	2.137	0.037	2.136	0.037	2.118
0.069	0.740	0.111	0.714	0.069	0.710	0.069	2.188	0.069	2.137	0.069	2.171
0.133	0.751	0.211	0.765	0.133	0.747	0.133	2.197	0.133	2.171	0.133	2.230
0.233	0.796	0.311	0.786	0.261	0.789	0.233	2.343	0.233	2.286	0.261	2.337
0.333	0.819	0.411	0.816	0.411	0.857	0.333	2.306	0.333	2.364	0.411	2.506
0.433	0.816	0.511	0.819	0.561	0.873	0.433	2.284	0.433	2.409	0.561	2.472
		0.611	0.782	0.711	0.854			0.533	2.353	0.711	2.322
				0.811	0.829			0.633	2.272	0.811	2.282

Units: y = ft
u = ft/s

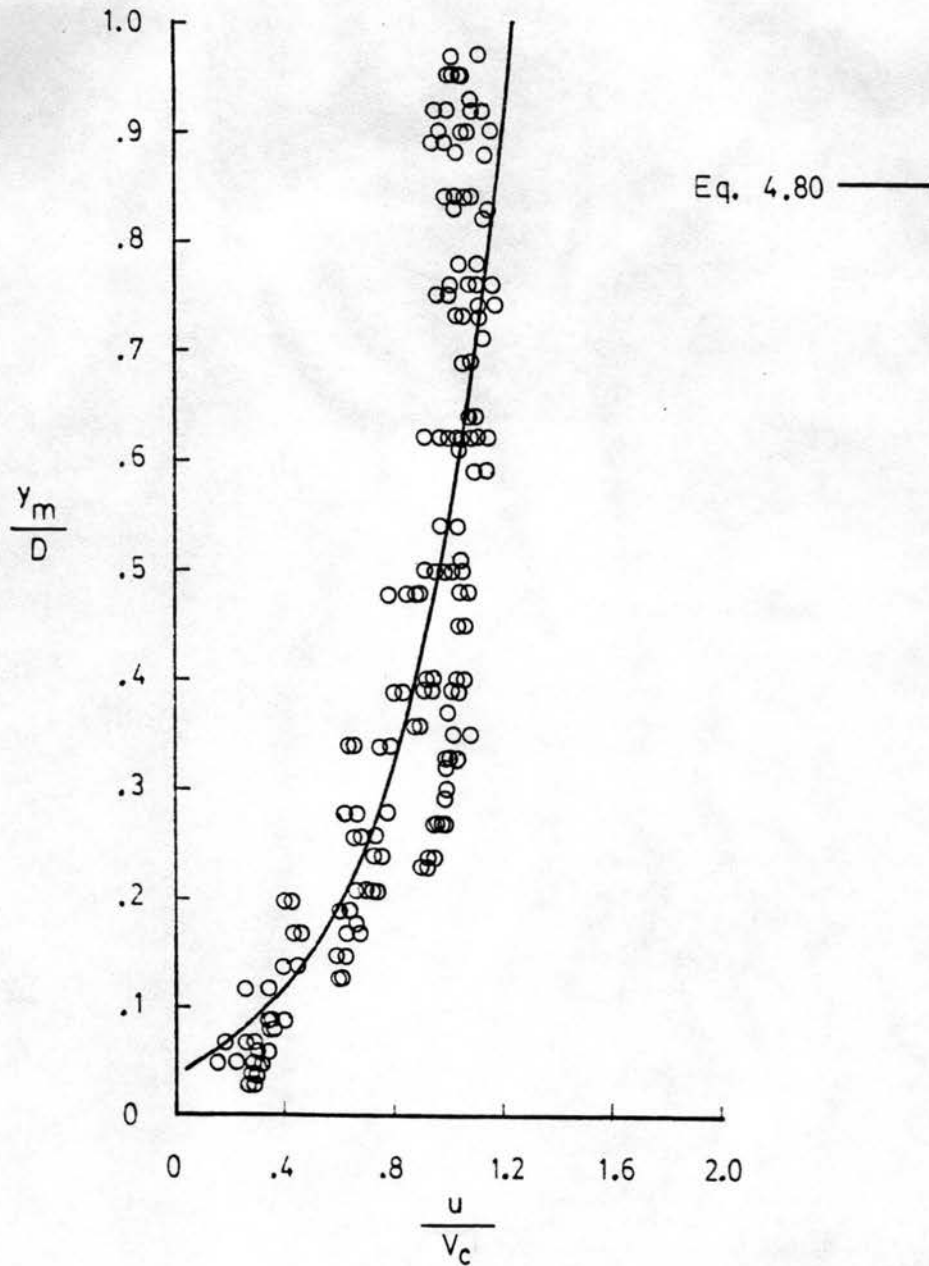


Figure 4.49. Nondimensional Velocity Profiles for Uniform, Rough Bedform Experiment

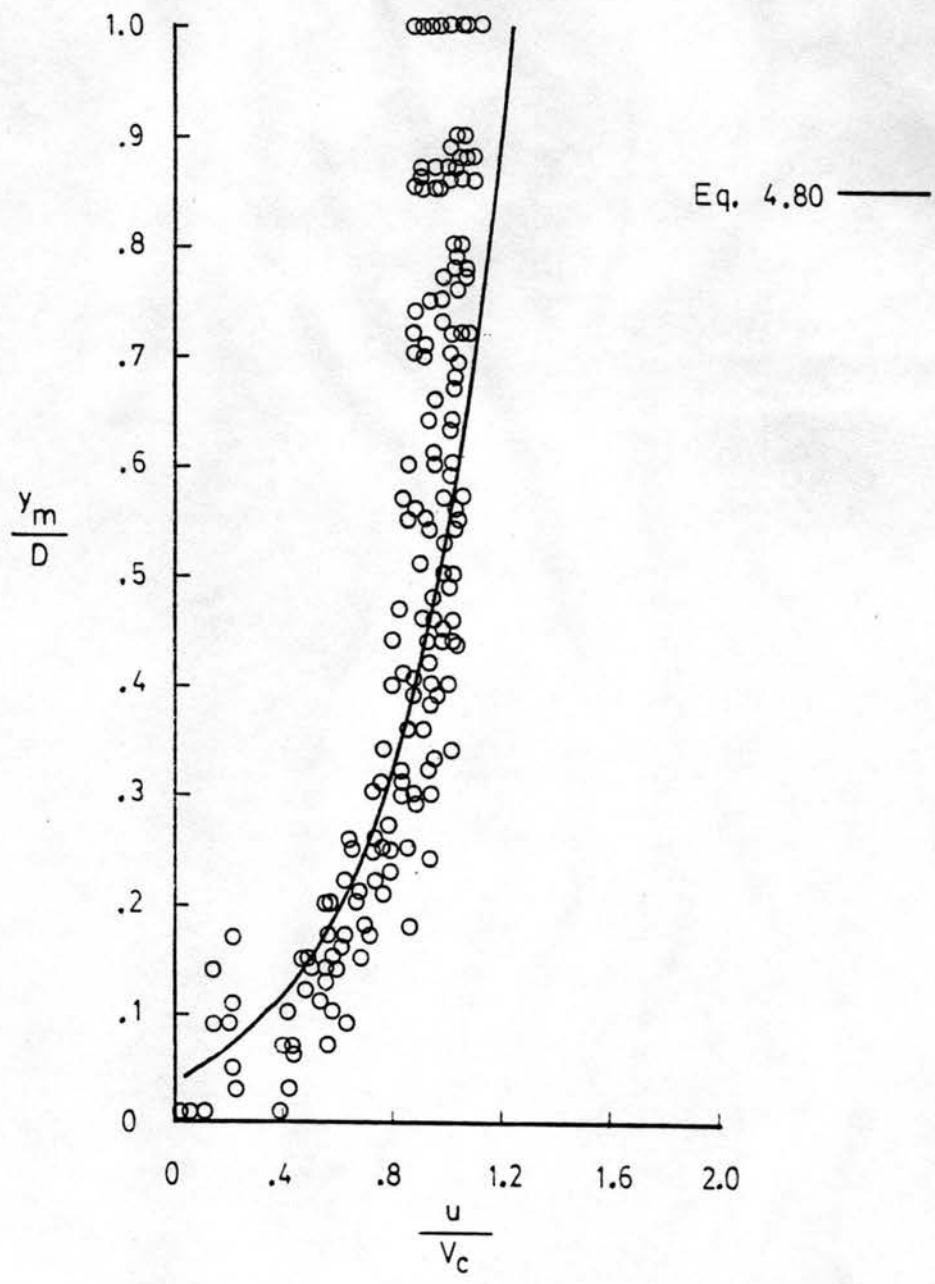


Figure 4.50. Comparison of Equation 4.80 with Data from Jonys (1973)

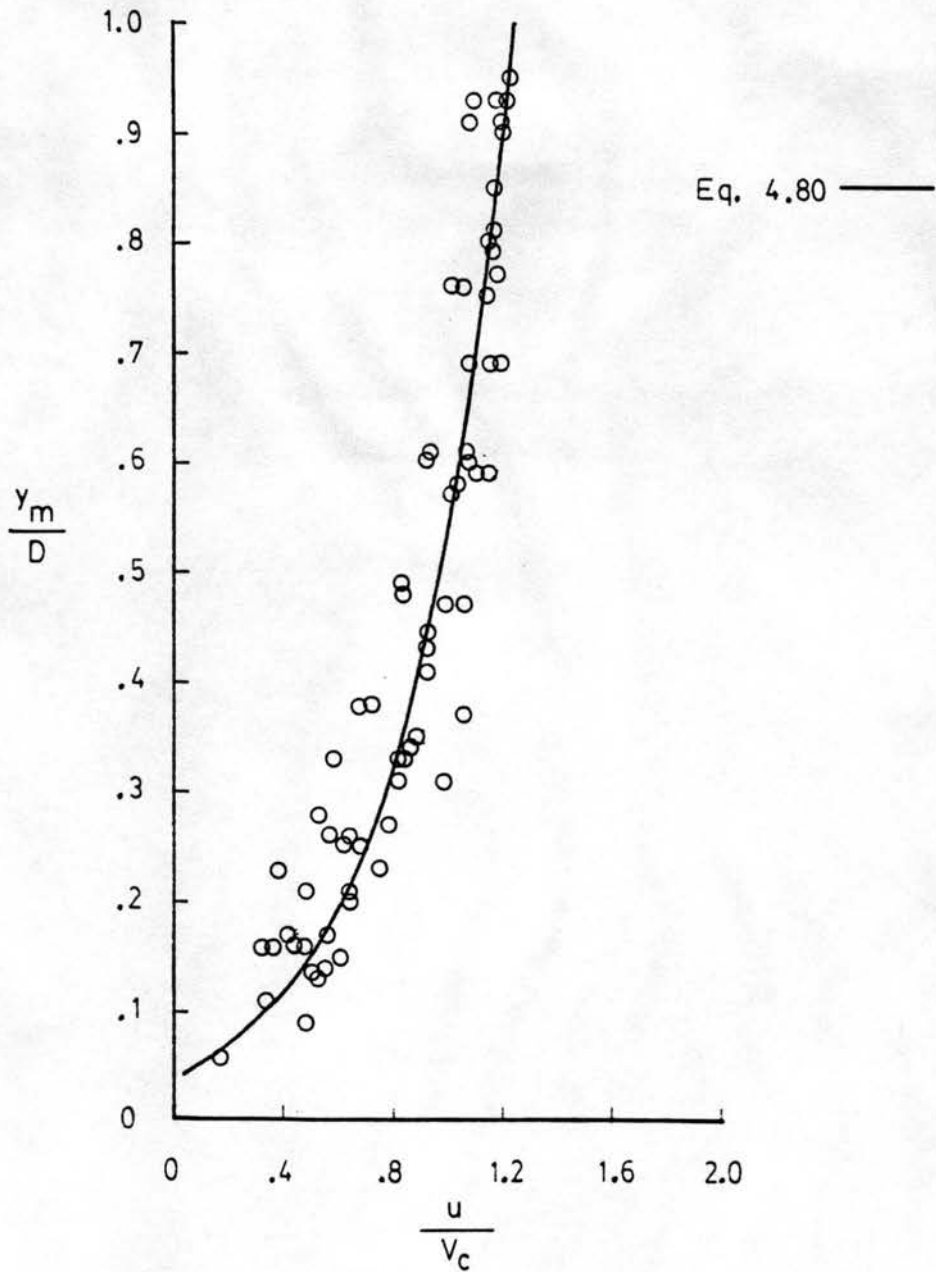


Figure 4.51. Comparison of Equation 4.80 with Data from Haque (1970)

experimental runs with an average A/D value of 0.37. The data from Haque (1970), however, was from experimental runs with A/D values of 0.21 and 0.33. The importance of the parameter A/D may also be seen in Figures 4.52-4.59 where the velocity profiles measured for the smooth, uniform bedform experiment are presented separately for each measurement station. Note that invariably the largest deviation of the measured data from Eq. 4.80 is caused by the experimental runs with the largest A/D value.

On the basis of the present rough and smooth uniform bedform experimental runs, the data from Jonys (1973), and the data from Haque (1970), Eq. 4.80 is a good representation of the average velocity profile over the length of a given bedform, for u/V_c values less than about 1.0. As the value of A/D decreases, Eq. 4.80 becomes valid for the entire velocity profile. Further experimentation is required to determine the limits of validity of Eq. 4.80 for all values of relative roughness.

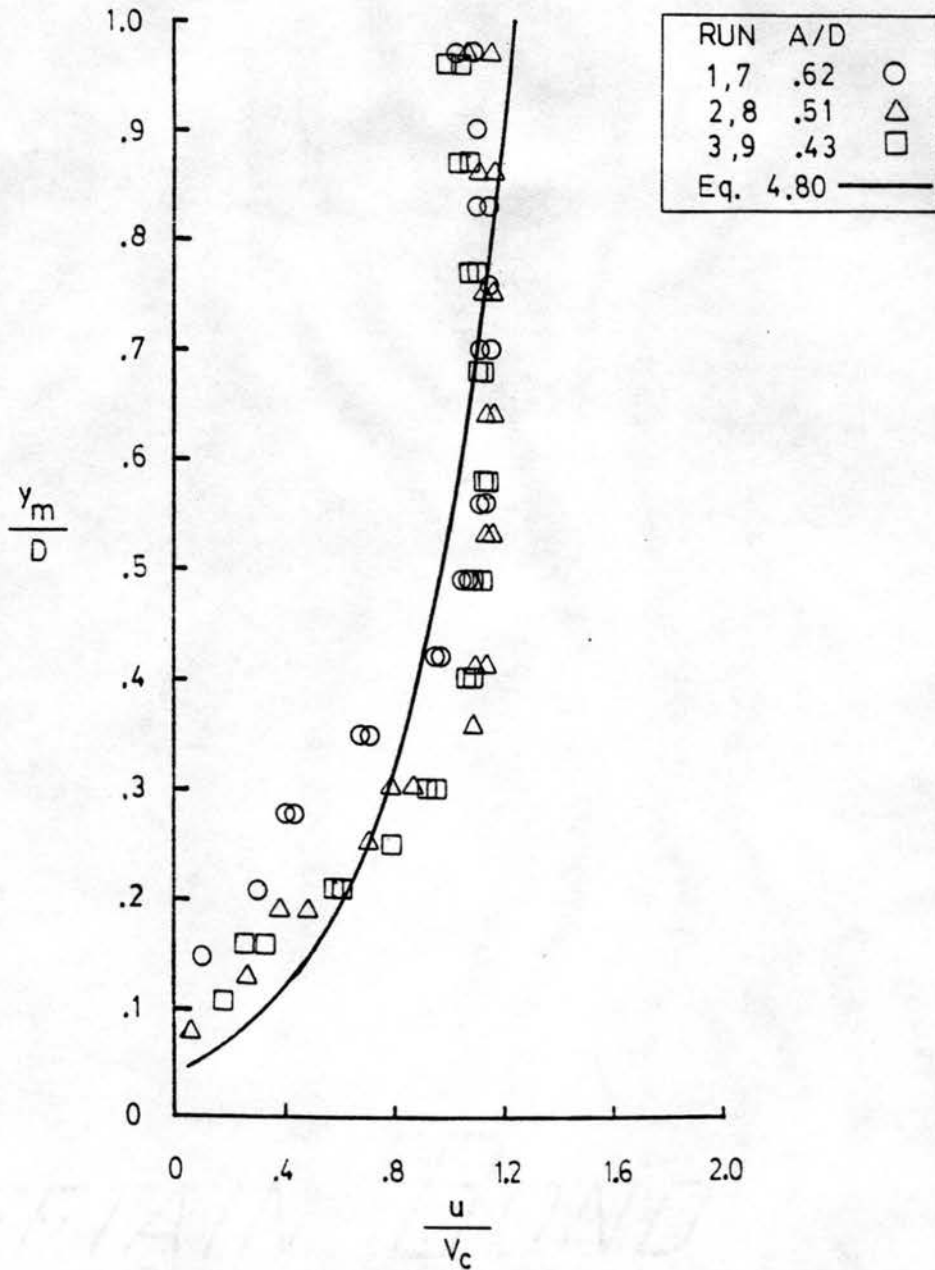


Figure 4.52. Nondimensional Velocity Profiles for Uniform, Smooth Bedform Experiment: $x = 0.000$ ft

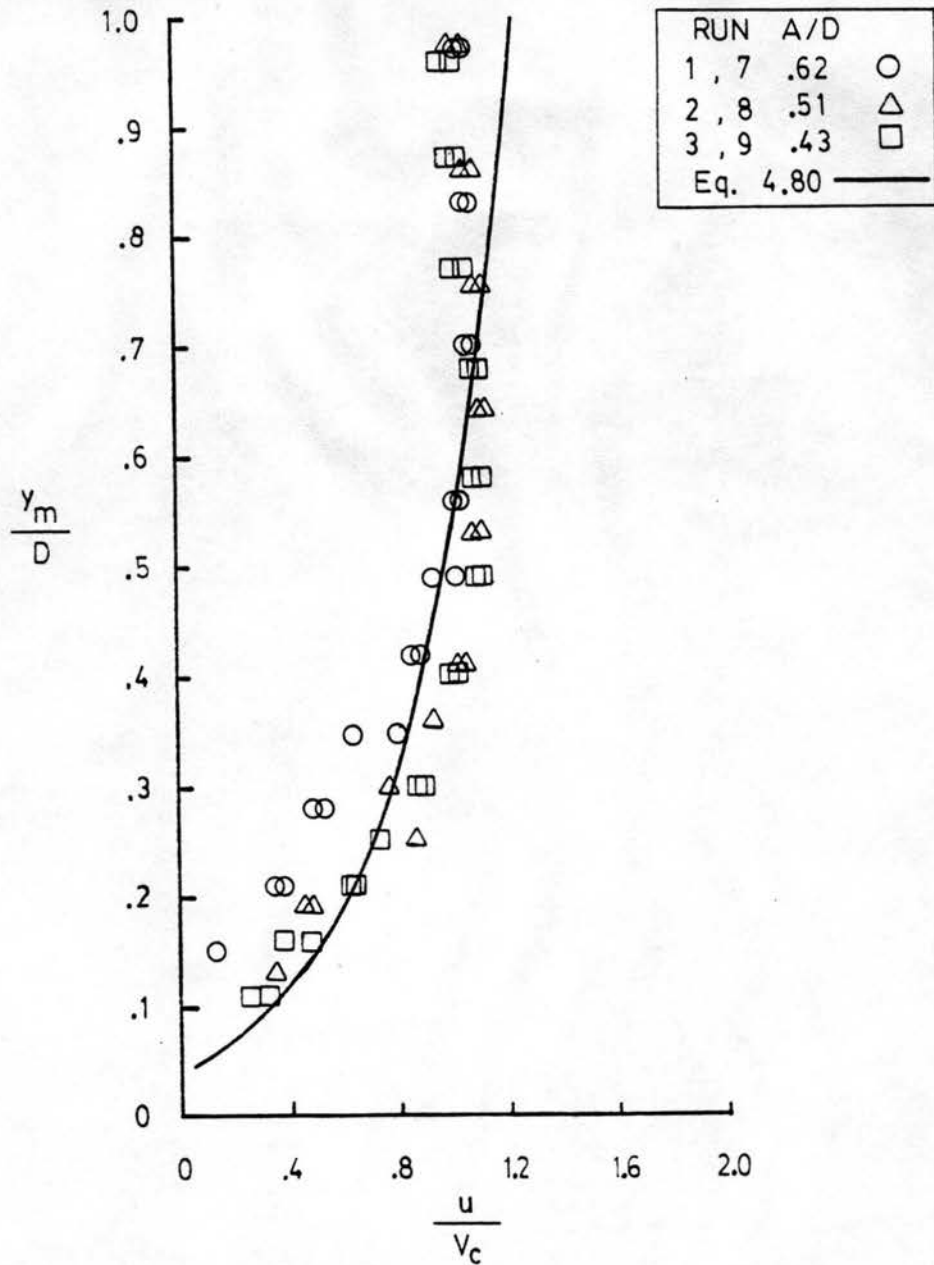


Figure 4.53. Nondimensional Velocity Profiles for Uniform, Smooth Bedform Experiment: $x = 0.446$ ft

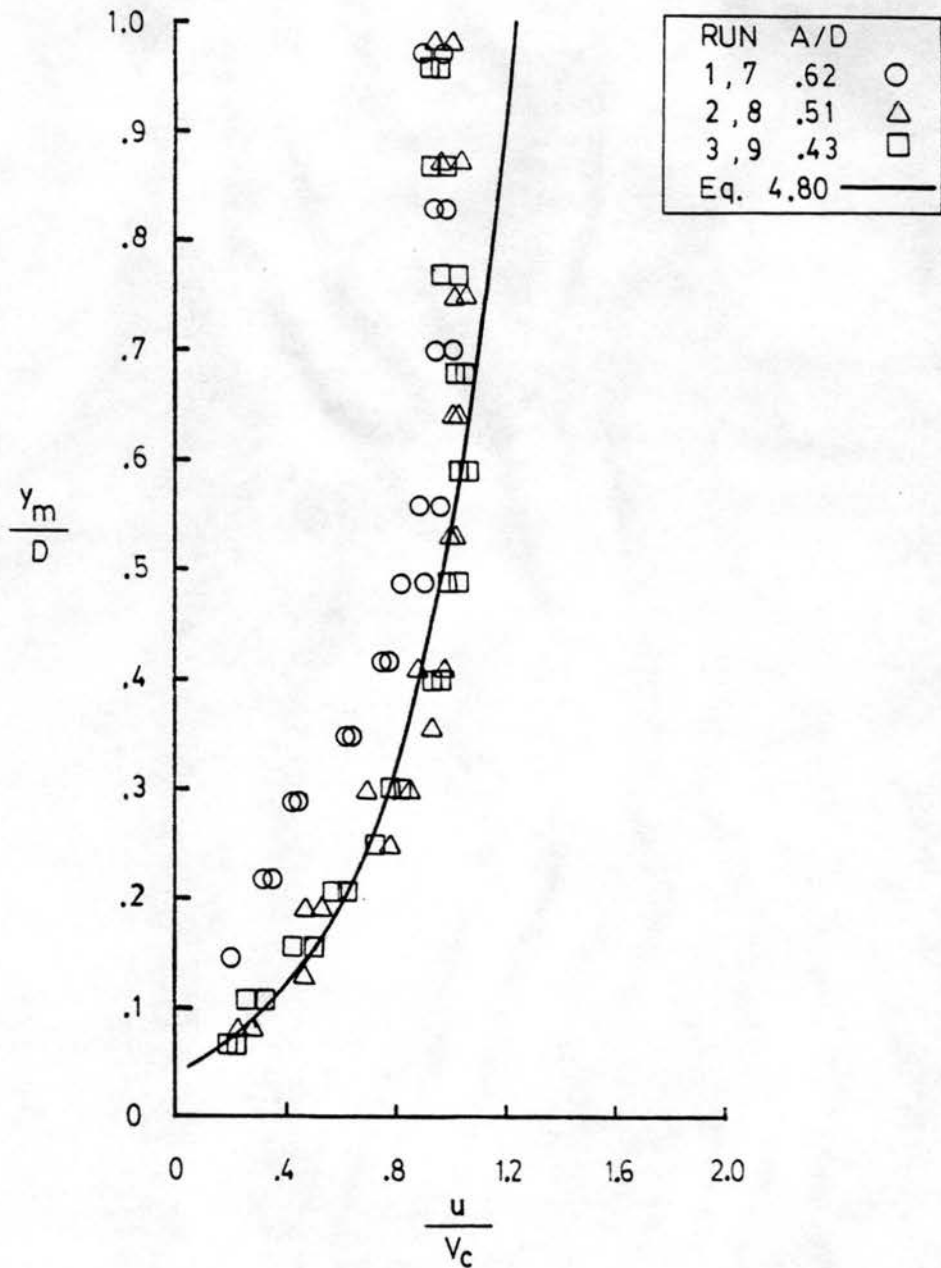


Figure 4.54. Nondimensional Velocity Profiles for Uniform, Smooth Bedform Experiment: $x = 0.890$ ft

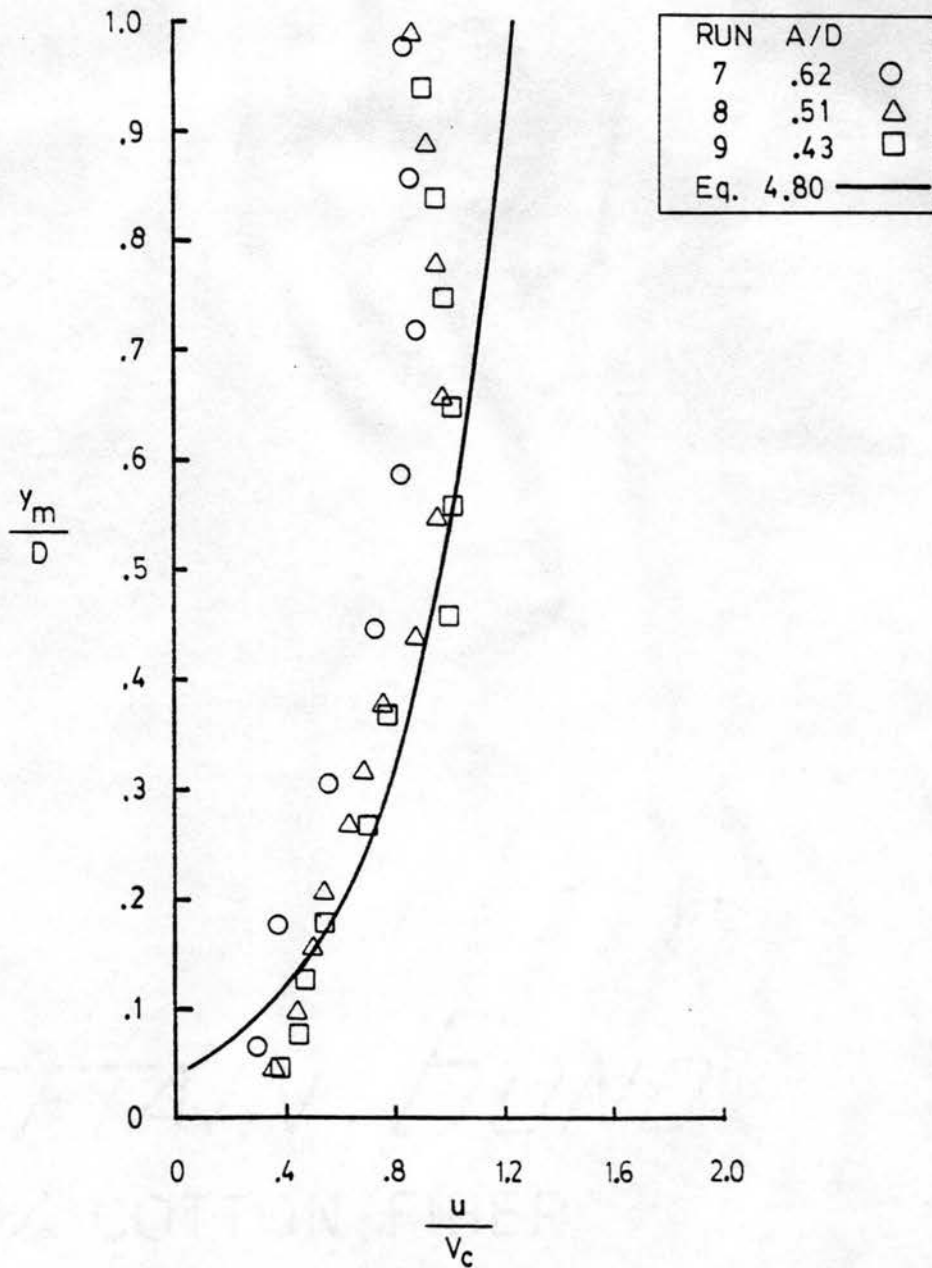


Figure 4.55. Nondimensional Velocity Profiles for Uniform, Smooth Bedform Experiment: $x = 1.240$ ft

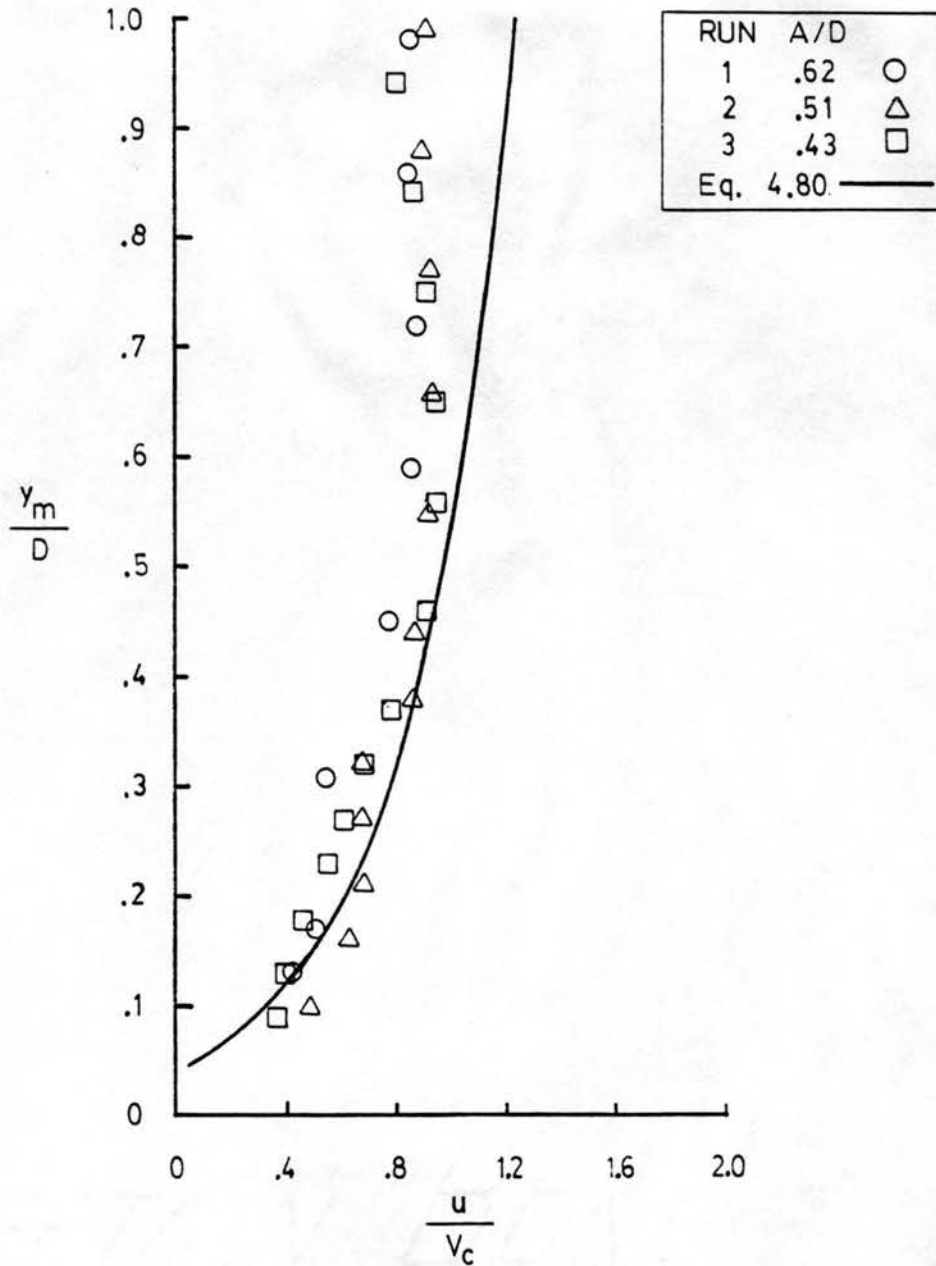


Figure 4.56. Nondimensional Velocity Profiles for Uniform, Smooth Bedform Experiment: $x = 1.465$ ft

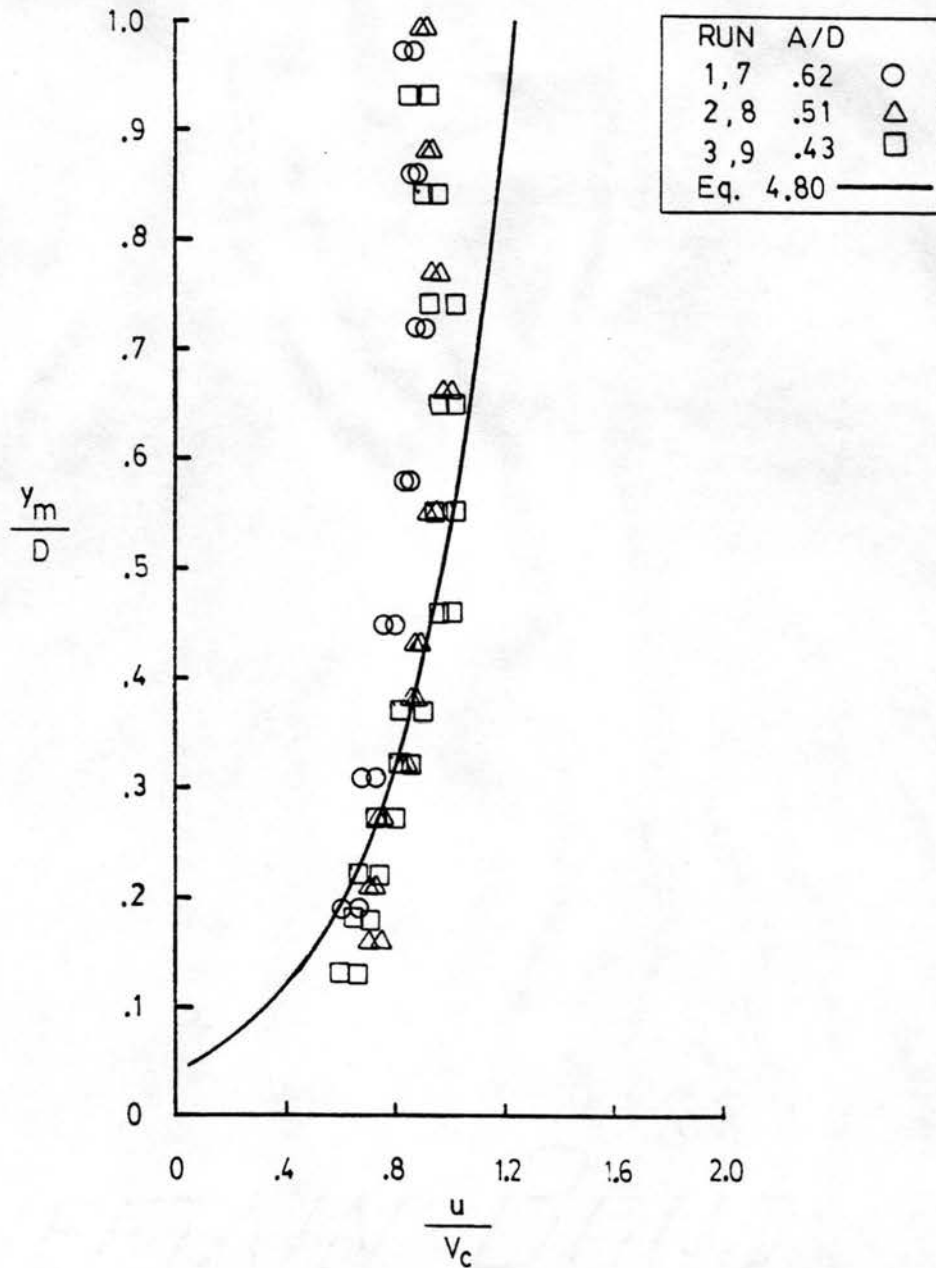


Figure 4.57. Nondimensional Velocity Profiles for Uniform, Smooth Bedform Experiment: $x = 1.690$ ft

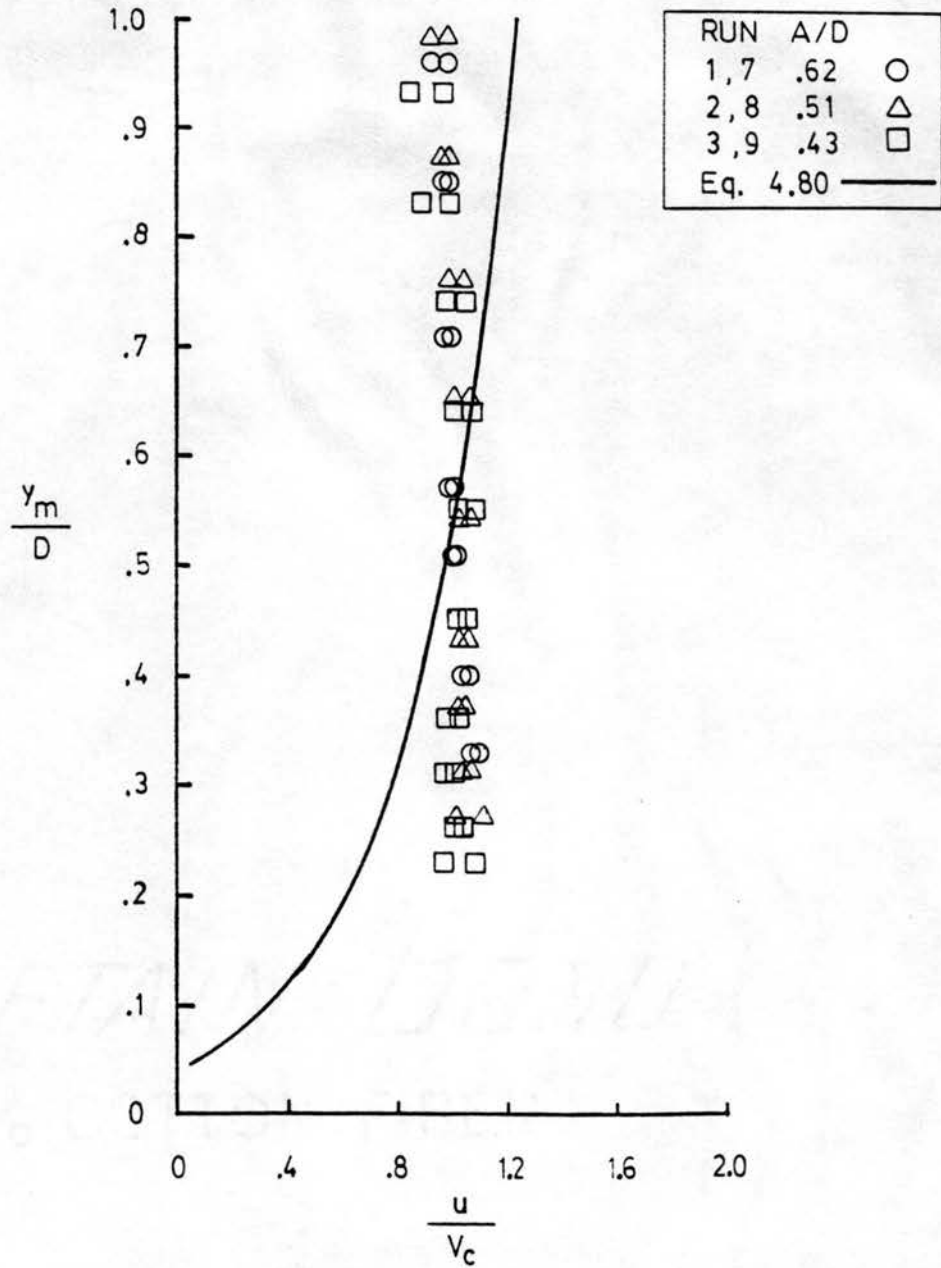


Figure 4.58. Nondimensional Velocity Profiles for Uniform, Smooth Bedform Experiment: $x = 2.190$ ft

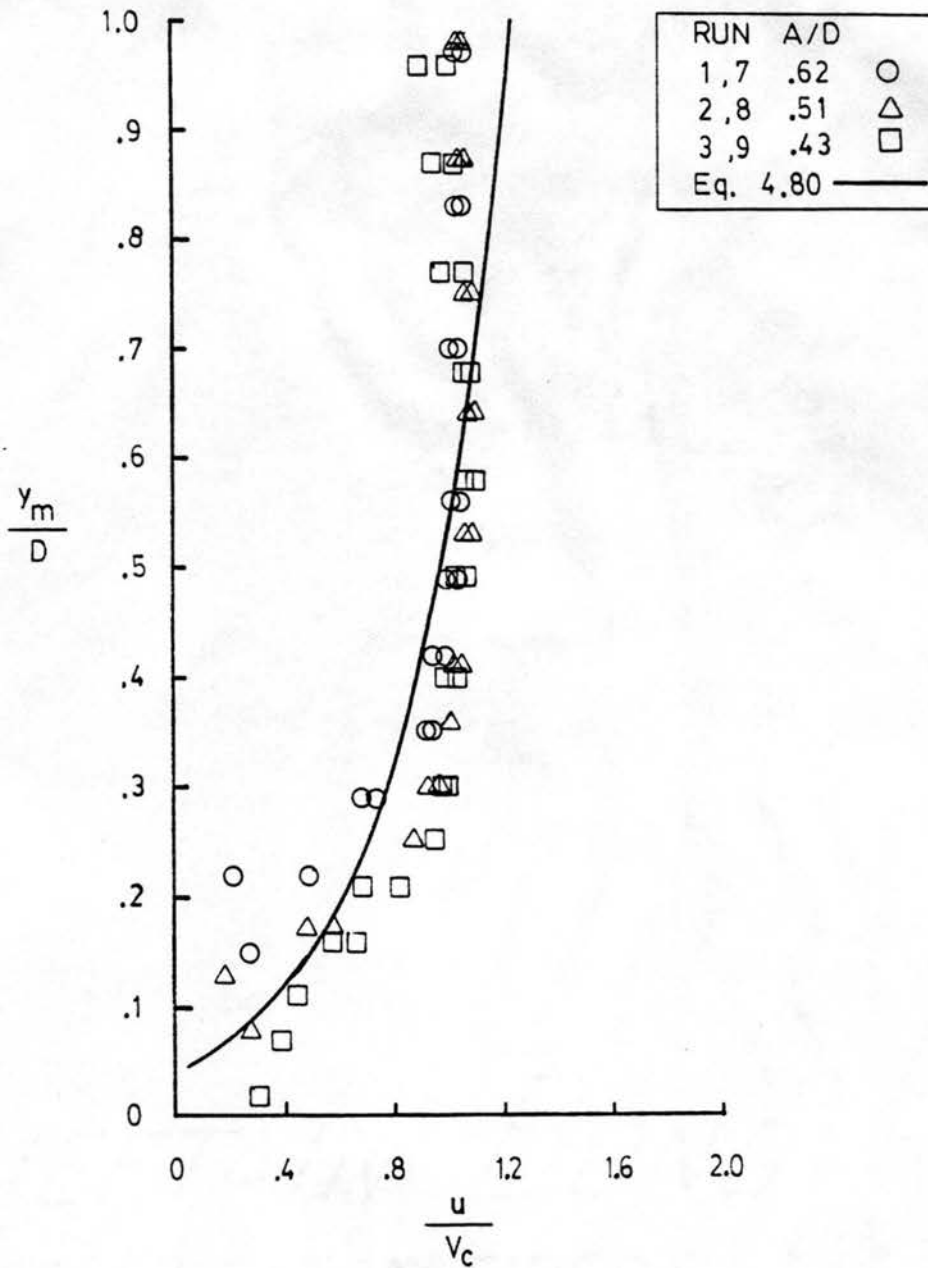


Figure 4.59. Nondimensional Velocity Profiles for Uniform, Smooth Bedform Experiment: $x = 2.612$ ft

Chapter 5

CONCLUSIONS

Resistance and velocity characteristics of open-channel flows over bedforms were investigated in this thesis. The investigation consisted of a uniform, smooth bedform experiment, a nonuniform, smooth bedform experiment, and a uniform, rough bedform experiment. Idealized triangular bedform models were used in each experiment. Local skin shear stress and piezometric head on the bedform surface were measured in each phase of the investigation. Total flow resistance and velocity profiles were measured in the smooth and rough uniform bedform experiments. On the basis of the measurements conducted in this study and the results of other investigators, the following conclusions are presented. A discussion of these conclusions and their application is contained in the closing paragraphs of this chapter.

1. Total Flow Resistance

The directly measured total flow resistance was within 8 percent of the sum of the measured skin and form resistance components for each experimental run of the uniform, smooth bedform study. Thus, skin resistance and form resistance together make up the total resistance to flow of modeled alluvial bedforms for the case of open channel flow with Froude number less than 0.4.

2. Pressure Distribution

The location of peak piezometric head was approximately four bedform heights downstream of the immediately upstream bedform crest. The pressure variation over the bedform increased in amplitude as the Froude number increased. The existence of roughness on the bedform surface had no effect on the pressure distribution. The relative size of the immediately upstream bedform had a drastic effect on the shape of the pressure distribution. The nondimensional pressure distribution was a single curve for Froude numbers ranging between 0.1 and 0.4 at constant flow depth over uniform bedforms.

3. Form Drag

The form drag depended entirely on the relative roughness. Knowing the relative roughness and the bedform steepness, the form friction factor may be computed. The roughness of the bedform surface was found to have no effect on the form drag, for the bedform geometry and roughness size used in this study.

4. Skin Shear Stress--Smooth Bedforms

The measured skin shear stress was 1-3 percent of the total flow resistance of the uniform, smooth bedforms. The local skin shear stress varied with position on the bedform surface, increasing from a zero value at the flow reattachment point to a maximum value at or near the crest. The maximum value increased with Froude number. The local skin shear coefficient on uniform and nonuniform, smooth bedforms was

related to the same power of the Reynolds number as in the Blasius equation for flow through smooth pipes. However, the coefficient in the Blasius equation was found to vary with position along the bedform surface.

5. Skin Shear Stress--Rough Bedforms

The measured form drag was 18-33 percent less than the total flow resistance of the uniform, rough bedforms. The shape of the skin shear stress distribution over the uniform, rough bedform was similar to the distribution over the uniform, smooth bedform. However, the maximum value of local skin shear stress was an order of magnitude larger in the rough case. The local skin shear coefficient was a function of the local depth-to-roughness size ratio and the Reynolds number. The parameter controlling the bed skin friction factor for bedforms of constant height was $R_b/d_{50} [A/L]^2 \text{Log } R_e$. (Each of these symbols are defined in the list of symbols at the beginning of this thesis). A single relation was developed, incorporating a bedform height adjustment factor, enabling the prediction of bed skin friction factor for bedforms with heights of 0.451 ft and less. The developed relationship was verified by alluvial flume data.

6. Boundary Layer Velocity--Uniform, Smooth Bedforms

The boundary layer velocity profile over uniform, smooth bedforms followed the one-seventh power law in the region extending downstream from the flow reattachment point to the bedform crest. The local value of shear velocity was used to normalize the local velocity, and to compute the dimensionless distance above the bedform surface.

7. Boundary Layer Velocity--Uniform, Rough Bedforms

A power law was valid for the boundary layer velocity profile over uniform, rough bedforms in the region extending downstream from the flow reattachment point to the bedform crest. The local value of shear velocity was used to normalize the local velocity, and the median grain size was used to normalize the distance above the sand grains at each measurement location on the bedform surface. The rough boundary layer velocity profile also followed a logarithmic relation which resembled the rough boundary layer velocity equation developed for plane surfaces.

8. Average Velocity Profile

An average free stream velocity profile equation was developed which describes the average flow velocity at locations above and along a bedform element. The local velocity was normalized by the average flow velocity above the crest of the bedform. This parameter was related to the ratio of the distance above the mean bed level to the average flow depth. Negative (upstream) velocities were not included in the development of this average velocity profile. It was determined that the accuracy of the developed equation increases as the relative roughness decreases.

Presented in this thesis are relations enabling the prediction of skin and form resistance of alluvial bedforms which are characteristic to open channel flows in the lower flow regime. These relations were developed from flows with Froude numbers ranging between 0.1 and 0.5, bedforms heights of 0.08-0.451 ft, and relative roughness values

ranging between 0.1 and 0.7. Bedform steepness values ranged from 0.05 to 0.20, and the grain sizes used were 0.06-3.5 mm. Data from studies using stationary, artificial bedforms and naturally formed, immobilized bedforms were used in the development of each relation.

The average velocity profile equation presented in this thesis was verified by studies involving velocity measurements over nontriangular, stationary bedforms and naturally formed, moving bedforms. Outside data allowing the verification of the boundary layer velocity profiles presented in this thesis was not available.

In order to use the resistance and velocity relations presented in this thesis, the bedform geometry and flow conditions of the channel under study must be known. Without relations enabling the prediction of bedforms based on flow parameters, detailed measurements are required before the proposed resistance and velocity relations may be applied.

Chapter 6

RECOMMENDATIONS FOR FUTURE STUDY

Within this report, relations were developed relating the pressure drag coefficient to a single parameter: the relative roughness. The ability to determine the pressure drag coefficient given a single measured parameter enables an investigator to easily separate flow resistance into its two components. Further research should be conducted to verify the proposed pressure drag coefficient relations over a wide range of relative roughness values, bedform geometries, and flow conditions.

The present analysis of skin shear on rough bedforms indicates that the bedform height has a significant effect on the magnitude of local skin shear and bed skin friction factor. Additional laboratory studies are required to verify the skin friction relations proposed in this report, which include bedform height adjustment factors.

REFERENCES

- Alam, A. M. Z. and Kennedy, J. F., "Friction Factors for Flow in Sand Bed Channels," Journal of Hydraulics Division, ASCE, Vol. 95, No. HY6, Proc. Paper 6400, November, 1969.
- ASCE Task Force on Bed Forms in Alluvial Channels, John F. Kennedy, Chmn., "Nomenclature for Bed Forms in Alluvial Channels," Journal of the Hydraulics Division, ASCE, Vol. 92, No. HY3, Proc. Paper 4823, May 1966.
- Einstein, H. A., "The Bed-Load Function for Sediment Transportation in Open Channel Flows," U.S. Department of Agriculture, Soil Conservation Service, Technical Bulletin No. 1026, 1950.
- Einstein, H. A. and Barbarossa, N. L., "River Channel Roughness," Transactions, ASCE, Vol. 117, 1952.
- Engel, P., "Length of Flow Separation over Dunes," ASCE, Journal of Hydraulics Division, Vol. 107, No. HY10, 1981.
- Engel, P. and Lau, Y. L., "Friction Factor for Two-Dimensional Dune Roughness," Journal of Hydraulic Research, Vol. 18, No. 3, 1980.
- Garde, R. J. and Paintal, A. S., "Velocity Distribution in Alluvial Channels," La Houille Blanc, No. 6, 1964.
- Guy, H. P., Simons, D. B., and Richardson, E. V., "Summary of Alluvial Channel Data from Flume Experiments, 1956-1961," Professional Paper 462-I, United States Geological Survey, 1966.
- Haque, M. I., "Analytically Determined Ripple Shapes," Thesis presented to Colorado State University, Fort Collins, CO, in 1970 in partial fulfillment of the requirements for the degree of Master of Science.
- Haque, M. I. and Mahmood, K., "Analytical Determination of Form Friction Factor," ASCE, Journal of Hydraulic Engineering, Vol. 109, No. 4, April, 1983.
- Henderson, F. M., "Open Channel Flow," The MacMillan Co., New York, New York, 1966.
- Hsu, E. Y., "The Measurement of Local Turbulent Skin Friction by Means of Surface Pitot Tubes," U.S. Department of the Navy, Report 957, August, 1955.

- Ippen, A. T., Drinker, P. A., Jobin, W. R., and Noustsopoulos, G. K., "The Distribution of Boundary Shear Stress in Curved Trapezoidal Channels," Technical Report No. 43, Mass. Inst. of Tech., Cambridge, Mass., October, 1960.
- Jonys, C. K., "An Experimental Study of Bed-Form Mechanics," Ph.D. Thesis, The University of Alberta, Edmonton, Alberta, Canada, 1973.
- Keulegan, G. H., "Laws of Turbulent Flow in Open Channels," National Bureau of Standards, Journal of Research 21, 1938.
- Kikkawa, H., and Ishikawa, T., "Resistance of Flow over Dunes and Ripples," Transactions of JSCE, Hydraulic and Sanitary Division, Vol. 11, 1979.
- Lovera, F. and Kennedy, J. F., "Friction Factor for Flat-Bed Flows in Sand Channels," Proceedings of ASCE, Journal of Hydraulics Division, No. HY4, 1969.
- Mahmood, K. and Blinco, P. H., Discussion of "Flow Over Triangular Elements Simulating Dunes," by M. F. Rifai and K. V. H. Smith (ASCE Proc. Paper 8246), ASCE, No. HY3, March, 1972.
- Meyer, S., Personal communication, unpublished report, 1985.
- Patel, U. C., "Calibration of the Preston Tube and Limitations on Its Use in Pressure Gradients," Journal of Fluid Mechanics, Vol. 23, Part 1, 1965.
- Preston, J. H., "The Determination of Turbulent Skin Friction by Mean of Pitot Tubes," Journal of the Royal Aeronautical Society, Vol. 48, 1954.
- Raudkivi, A. J., "Study of Sediment Ripple Formation," ASCE, Journal of Hydraulics Division, Vol. 89, No. HY6, November, 1963.
- Rifai, M. F. and Smith, K. V. H., Discussion of "Pressure Fluctuations in Reattaching Flow," by R. Narayanan and A. J. Reynolds (ASCE, Proc. Paper 6212), ASCE, Vol. 95, No. HY5, 1969.
- Rifai, M. F. and Smith, K. V. H., "Flow Over Triangular Elements Simulating Dunes," ASCE Journal of Hydraulics Division, Vol. 97, No. HY7, 1971.
- Schlichting, H., "Boundary Layer Theory," McGraw-Hill, New York, 1980.
- Shen, H. W., "Development of Bed Roughness in Alluvial Channels," Proceedings of ASCE, Journal of Hydraulics Division, Vol. 88, No. HY3, 1962.
- Simons, D. B. and Richardson, E. V., "Resistance to Flow in Alluvial Channels," U.S. Geological Survey, Professional Paper 422-J, 1966.

- Tsubaki, T., Kawasumi, T. and Yasutomi, T., "On the Influence of Sand Ripples upon the Sediment Transport in Open Channels," Report, Research Institute of Applied Mechanics, Kyushu University, Japan, Vol. II, No. 8, 1953.
- Vanoni, V. A. and Brooks, N. H., "Laboratory Studies of the Roughness and Suspended Load of Alluvial Streams," MRD Sediment Series, No. 11, Corps of Engineers, Missouri River Division, Omaha, 1957.
- Vanoni, V. A. and Hwang, L. S., "Relation Between Bed Forms and Friction in Streams," ASCE, Journal of Hydraulics Division, No. HY3, May, 1967.
- Vittal, N., Ranga Raju, K. G., and Garde, R. J., "Resistance of Two-Dimensional Triangular Roughness," Journal of Hydraulic Research, Vol. 15, No. 1, 1977.
- Wang, W. C., "Flow Characteristics Over Alluvial Bedforms," Ph.D. Dissertation, Colorado State University, Fort Collins, CO, 1983.
- Wang, W. C. and Shen, H. W., "Statistical Properties of Alluvial Bed Forms," Proceedings of Bed International Symposium on Stochastic Hydraulics, Japan, 1980.
- Yalin, M. S., "Mechanics of Sediment Transport," Second Edition, Pergamon Press, 1977.

#149608